Synthesis and study of the self-assembly of linear ABC terpolymers in order to create innovative asymmetric membranes

Hana Bouzit

THÈSE POUR OBTENIR LE GRADE DE DOCTEUR DE L'UNIVERSITÉ DE MONTPELLIER

En Chimie et Physico-chimie des Matériaux

École doctorale Sciences Chimiques Balard- ED459

Institut Européen des Membranes-UMR5635

Synthèse et étude de l'auto-organisation de terpolymères ABC linéaires en vue de réaliser des membranes asymétriques innovantes

Présentée par Hana BOUZIT
Le 08 avril 2022

Sous la direction de Damien QUÉMENER
Et le co-encadrement de Karim AISSOU

Devant le jury composé de

Virginie PONSINET, Directrice de recherche au CNRS, Université de Bordeaux	Rapporteur
Guillaume FLEURY, Professeur des Universités, Université de Bordeaux	Rapporteur
Corine GÉRARDIN, Directrice de recherche au CNRS, Université de Montpellier	Examinateur
Eliane ESPUCHE, Professeur des Universités, Université de Lyon	Examinateur
Mona SEMSARILAR, Chargée de recherche au CNRS, Université de Montpellier	Examinateur
Daniel GRANDE, Directeur de recherche au CNRS, Université Paris-Est	Examinateur
Damien QUÉMENER, Maître de Conférences (HDR), Université de Montpellier	Directeur de thèse
Karim AISSOU, Chargé de recherche au CNRS, Université de Montpellier	Co-encadrant de thèse

UNIVERSITÉ DE MONTPELLIER

THÈSE POUR OBTENIR LE GRADE DE DOCTEUR DE L'UNIVERSITÉ DE MONTPELLIER

En Chimie et Physico-chimie des Matériaux

École doctorale Sciences Chimiques Balard- ED459

Institut Européen des Membranes-UMR5635

Synthesis and study of the self-assembly of linear ABC terpolymers in order to create innovative asymmetric membranes

Présentée par Hana BOUZIT
Le 08 avril 2022

Sous la direction de Damien QUÉMENER
Et le co-encadrement de Karim AISSOU

Devant le jury composé de

Virginie PONSINET, Directrice de recherche au CNRS, Université de Bordeaux	Rapporteur
Guillaume FLEURY, Professeur des Universités, Université de Bordeaux	Rapporteur
Corine GÉRARDIN, Directrice de recherche au CNRS, Université de Montpellier	Examinateur
Eliane ESPUCHE, Professeur des Universités, Université de Lyon	Examinateur
Mona SEMSARILAR, Chargée de recherche au CNRS, Université de Montpellier	Examinateur
Daniel GRANDE, Directeur de recherche au CNRS, Université Paris-Est	Examinateur
Damien QUÉMENER, Maître de Conférences (HDR), Université de Montpellier	Directeur de thèse
Karim AISSOU, Chargé de recherche au CNRS, Université de Montpellier	Co-encadrant de thèse

UNIVERSITÉ DE MONTPELLIER

A la mémoire de ma mère

A mon père

Remerciements

Nombreux sont ceux qui m'ont soutenue et aidée au cours de ces trois années de thèse, je vais essayer d'exprimer toute ma reconnaissance dans les quelques lignes qui vont suivre.

Tout d'abord, je tiens à remercier les membres du jury Dr. Virigine Ponsinet et Dr. Guillaume Fleury d'avoir accepté d'examiner ce manuscrit. Un grand merci au Dr. Corine Gérardin, Dr. Mona Semsarilar, Prof. Eliane Espuche et Dr. Daniel Grande pour l'intérêt porté à mon travail.

Je remercie Dr. Damien Quémener de m'avoir accueillie dans son équipe au sein du département IP2 et de sa confiance tout au long de mon doctorat. Je souhaite également remercier Dr. Karim Aissou de sa disponibilité pour discuter de mes résultats et d'avoir pris le temps de corriger ce manuscrit.

Mes prochains remerciements s'adressent à toutes les personnes de l'IEM qui ont contribué de loin ou de près à la réussite de cette thèse. Tout d'abord, un grand merci au Dr. Mona Semsarilar pour son aide sur différents aspects de mes expériences, notamment sur la polymérisation RAFT. Merci à Christelle Floutier pour la bonne humeur qu'elle apporte au quotidien (grâce à elle j'ai mangé moins de chocolat pendant ma rédaction !).

Je remercie également tous les thésards et post-docs rencontrés au cours de ces 3 ans de thèse avec qui j'ai partagé de très bons moments à la fois sur la paillasse et durant les moments conviviaux : Mingyuen, Rui, Marianne, Hamza, Chaimaa, Marine, Alice, Raphael, Quentin, Sher, Gabi, Bénédicte et tous ceux que j'aurai pu oublier…

Je remercie également mes collègues de bureau : Cyril et toutes les soirées plancha ! Jeanne, arrivée au moment le plus critique de la thèse qui est la rédaction mais qui a toujours su trouver les bons mots et être à l'écoute. Merci pour les soirées/sorties entre filles, je suis contente de t'avoir eu dans mon bureau.

Je remercie toutes les personnes du département DM3 : Sara, Ghenwa, Marleine et Ghadi qui sont maintenant Docteurs ! Mahmoud, Elissa, Fida et Joelle vous êtes les prochains ! Syreina (la plus joyeuse de l'IEM, j'attends avec impatience ton mariage). Carole (tu es la suivante et tu vas assurer). Merci à vous pour tous les bons moments passés ensemble et de m'avoir donné la force quand je venais faire un café chez vous (l'équipe des riches).

Comment ne pas remercier la team espagnole (ou presque) avec qui j'ai partagé le plus de sorties, soirées, randonnées…etc. Dana et Pierre, les premiers parents de la team avec l'arrivée de la petite Anaïs. Octavio et Sylvain, toujours partants pour une randonnée. Carlos et Ryan, qui ont capturé tous les Pikatchus. Quicke, le best pâtissier de l'IEM, reviens à Montpellier ! et enfin Sofia, toujours souriante et avec des histoires à raconter, bonne chance pour ton post-doc (mais ne t'éloignes pas trop).

Un grand merci à mes amies de toujours Valdita et Amira. Vous avez été là depuis le début de cette aventure post-bac. Merci pour votre soutien et d'avoir toujours cru en moi, vous êtes les meilleures !

Finalement, mes remerciements s'adressent aux personnes sans qui je ne serais pas arrivée jusque-là. Ma grande sœur, mon bras droit, ma meilleure amie : Hanane a.k.a Kika. Merci d'avoir toujours été là pour moi et de me soutenir pour que je donne le meilleur de moi-même. Un grand merci « aux petits » Rihane, Rana et Mimi, merci pour votre amour. Enfin, un énorme merci à mon père, mon héros ! Papa, tu es un homme exceptionnel et je ne te remercierai jamais assez pour tout ce que tu as fait pour moi. Merci pour tous tes sacrifices et toutes les valeurs que tu m'as inculquées, tu es mon inspiration au quotidien.

Un dernier remerciement à la personne qui a rendu cette thèse et surtout ces derniers mois plus faciles et agréables, Habib, ça n'aurait pas été pareil sans toi !

Table of contents

Abstract

Fouling-resistant membranes endowed with intelligent isopores in high-areal density are highly-desired to move towards next-generation ultrafiltration (UF) membranes. Indeed, membranes tailored with smart nanochannels, able to adjust their size in response to an external stimulus such as temperature and pH, are appealing materials to efficiently prevent the common problem of fouling, considered as one of the biggest challenges in membrane technology.

In this context, the aim of this thesis work was based on the synthesis and self-assembly of a series of well-defined pH- and temperature-double stimuli responsive amphiphilic triblock terpolymers in membrane configuration. For that purpose, a polystyrene-*block*-poly(2-vinylpyridine)-*block*-poly(*N*-isopropylacrylamide) (PS-*b*-P2VP-*b*-PNIPAM) was first prepared by reversible addition-fragmentation chain transfer (RAFT) polymerization. An original methodology combining the traditional nonsolvent-induced phase separation (NIPS) process with a solvent vapor annealing (SVA) treatment was then used to produce a perforated lamellar structure within double stimuli-responsive PS-*b*-P2VP-*b*-PNIPAM membranes. To improve the membrane wettability as well as its thermo-responsiveness, a block copolymer blend strategy was also used.

A double stimuli-responsive porous nanostructure having an excellent long-range order formed within the terpolymer membranes is highly desired to manufacture high selectivity smart separation-based materials able to transit their pore state from hydrophilic to hydrophobic (and vice versa), thereby leading to much more efficient detachment of foulants during the cleaning process.

Keywords : PS-*b*-P2VP-*b*-PNIPAM, RAFT polymerization, thermo-sensitive, pH-sensitive, thick film.

Résumé

Les membranes résistantes à l'encrassement dotées d'isopores intelligents à haute densité surfacique sont fortement désirées pour générer des membranes d'ultrafiltration de nouvelle génération. En effet, les membranes dotées de nano-canaux intelligents, capables d'ajuster leurs tailles en réponse à un stimulus externe tel que la température et/ou le pH sont des matériaux intéressants pour prévenir efficacement le problème courant de l'encrassement, considéré comme l'un des plus grands défis des technologies membranaires.

Dans ce contexte, l'objectif de ce travail de thèse est basé sur la synthèse de terpolymères ABC linéaires amphiphiles bien définis composés de polystyrène-*bloc*-poly(2-vinylpyridine)-*bloc*-poly(*N*-isopropylacrylamide) (PS-*b*-P2VP-*b*-PNIPAM) sensibles au pH et à la température *via* une polymérisation par transfert de chaîne par addition-fragmentation réversible (RAFT).

Une méthodologie originale combinant le procédé traditionnel de séparation de phase induite par l'intrusion de non-solvant (NIPS) avec un traitement de recuit sous vapeur de solvant (SVA) a été utilisée pour produire une structure lamellaire perforée au sein des films épais de terpolymères ABC linéaires doublement stimulables. Une stratégie de mélange de copolymères à blocs a également été utilisée pour améliorer l'hydrophilicité et la thermosensibilité de la membrane. Cette nanostructure poreuse dotée d'un excellent ordre à longue portée est très recherchée pour fabriquer des membranes intelligentes capables de faire passer leurs pores de l'état hydrophile à l'état hydrophobe (et vice versa), ce qui permet un détachement beaucoup plus efficace des polluants pendant le processus de nettoyage.

Mots clés: PS-*b*-P2VP-*b*-PNIPAM, polymérisation RAFT, thermo-sensible, pH-sensible, film épais.

Titre et résumé en français :

Synthèse et étude de l'auto-organisation de terpolymères ABC linéaires en vue de réaliser des membranes asymétriques innovantes

L'eau, également appelée « or bleu » est une ressource naturelle vitale indispensable au développement de l'humanité et à l'équilibre des écosystèmes aquatiques. Pourtant, sa raréfaction est devenue aujourd'hui l'un des problèmes majeurs de notre siècle. La pollution, le changement climatique, la surpopulation ou encore la mauvaise utilisation des ressources sont les principales causes du déficit mondial en eau douce. Selon l'Organisation des nations unis pour l'éducation, la science et la culture (UNESCO), la demande mondiale en eau de bonne qualité augmentera de 55% en 2050,[1] une proportion inquiétante qui risque de s'aggraver au fil des années. Ainsi, il est urgent de proposer des solutions afin de préserver cette ressource vitale.

Afin d'augmenter les stocks d'eau potable, deux voies peuvent être explorées : le traitement des eaux usées et le dessalement de l'eau de mer. À ce titre, la filtration sur membrane est considérée comme la principale technologie de potabilisation de l'eau.[2] Avec une consommation d'énergie relativement faible sans l'ajout de produits chimiques, la technologie membranaire joue un rôle central dans la purification de l'eau. Cependant, cette technique reste limitée par la dégradation des membranes due au colmatage. Ce phénomène découle de l'accumulation de matières (également appelées retentas) à la surface des membranes ayant comme conséquence la diminution des performances de filtrations dans le temps, accompagnée par une diminution de la vie active de la membrane.

Le développement de membranes résistantes à l'encrassement dotées d'isopores intelligents à haute densité surfacique est fortement souhaité pour générer des membranes d'ultrafiltration de nouvelle génération. En effet, les membranes dotées de nano-canaux intelligents, capables d'ajuster leurs tailles en réponse à un stimulus externe tel que la température et/ou le pH sont des matériaux intéressants pour prévenir efficacement le problème courant de l'encrassement, considéré comme l'un des plus grands défis des technologies membranaires.

Les travaux de recherche de cette thèse s'inscrivent dans cette thématique puisque basés sur le développement de nouvelles membranes innovantes résistantes à l'encrassement. Nous avons

choisi l'incorporation de blocs stimuli-répondants au pH et à la température au sein de membranes terpolymères afin de former des nano-pores intelligents capables d'ajuster leurs tailles en réponse à un stimulus externe et de faciliter l'auto-nettoyage des membranes.

Cette thèse se divise en quatre parties. La première porte sur la synthèse et la caractérisation de terpolymères ABC linéaires par polymérisation radicalaire contrôlée, et plus précisément par polymérisation contrôlée par transfert de chaîne réversible par addition-fragmentation (RAFT). La deuxième partie est dédiée à l'étude de l'auto-assemblage des terpolymères sous forme de membranes asymétriques nano-structurées. Pour ce faire, le procédé de séparation de phase induite par l'intrusion de non-solvant « non-solvent induced phase separation » (NIPS) a été combiné à la technique de recuit sous vapeur de solvant « solvent vapor annealing » (SVA). La troisième partie de cette thèse consiste en l'étude des performances de filtration des membranes stimuli-répondantes fabriquées. Enfin, la dernière partie est consacrée à l'étude de l'auto-assemblage d'un mélange de terpolymère ABC linéaire avec d'autres copolymères à blocs amphiphiles afin d'améliorer l'hydrophilicité de la membrane et sa résistance à l'encrassement.

Dans la première partie de cette thèse, nous avons utilisé la polymérisation RAFT afin de synthétiser un terpolymère ABC linéaire composé de polystyrène-*block*-poly(2-vinylpyridine)-*block*-poly(*N*-isopropylacrylamide) (PS-*b*-P2VP-*b*-PNIPAM). Cette technique de polymérisation radicalaire contrôlée a été choisie car elle permet de synthétiser des polymères d'architectures bien définies, de haute fonctionnalité et de faible dispersité (~~Đ~~).[3]

Dans un premier temps, une série du premier bloc hydrophobe polystyrène (PS) a été synthétisée en présence d'un agent RAFT de type trithiocarbonate : le 4-cyano-4-[(dodecylsulfanylthiocarbonyl)sulfanyl] pentanoic acid (CDPA) et de l'amorceur azobisisobutyronitrile (AIBN) en solution (dioxane) ou en masse (voir **Schéma 1.a**).
Les homopolymères PS macro-CTA ainsi synthétisés ont été caractérisés par résonnance magnétique nucléaire (RMN) du proton en présence de dichlorométhane deutéré (CD_2Cl_2) et par chromatographie d'exclusion stérique (SEC) dans le tétrahydrofurane (THF).

Comme les bouts de chaînes de l'agent RAFT n'étaient pas visibles sur les spectres RMN, les masses moléculaires (M_n) du PS ont été déterminées, principalement par SEC dans le THF à 35°C, dans une gamme allant de 22 à 55 kg/mol, ~~Đ~~ < 1.20.

Les PS macro-CTA obtenus ont été utilisés pour la synthèse d'un copolymère dibloc de type PS-*b*-P2VP répondant à des changements de pH dans l'eau. Pour cela, le monomère 2-vinylpyridine (2VP) a été dissout dans le 1,4-dioxane (DOX) en présence d'AIBN et du PS macro-CTA. La réaction a été réalisée à 70°C comme présenté dans le **Schéma 1.b**. Tous les copolymères diblocs synthétisés sont composés majoritairement de PS avec un rapport moyen des fractions volumiques de l'ordre de 60% (PS:P2VP = 0.60:0.40), déterminé par RMN du proton. Les masses molaires déterminées par SEC dans le THF varient de 31 à 51 kg/mol, ~~Đ~~ < 1.40.

Les terpolymères ABC linéaires de type PS-*b*-P2VP-*b*-PNIPAM ont été synthétisés par extension des chaînes de PS-*b*-P2VP macro-CTA avec du monomère NIPAM en présence d'AIBN et de dioxane (voir **Schéma 1.c**). Ici la purification du terpolymère sensible au pH et à la température a dû être optimisée afin d'avoir un système suffisamment pur, et donc capable de s'auto-organiser sous forme de nanodomaines bien définies. Pour cela, nous avons utilisé l'extraction liquide-solide de type Soxhlet afin d'éliminer les chaînes de PNIPAM non-attachées au terpolymère.

Le terpolymère PS-*b*-P2VP-*b*-PNIPAM obtenu est alors caractérisé par RMN du proton dans le CD_2Cl_2. La présence des signaux du PS (δ = 6.40 – 7,05 ppm), du P2VP (δ = 6.40 - 7,05 ppm et δ = 8.23 ppm) et du PNIPAM (δ = 1.14 ppm et δ = 3.99 - 4.0ppm) sur le spectre RMN après purification confirme l'attachement du PNIPAM avec succès sur les chaînes de PS-*b*-P2VP. Le déplacement des courbes obtenues par SEC des plus petites masses molaires vers les plus hautes masses molaires est une preuve supplémentaire du bon déroulement de la réaction. Enfin, une analyse RMN à deux dimensions « diffusion ordered spectroscopy » (DOSY) a été effectuée. La présence d'un coefficient de diffusion unique sur le spectre RMN DOSY atteste de la pureté du terpolymère synthétisé.

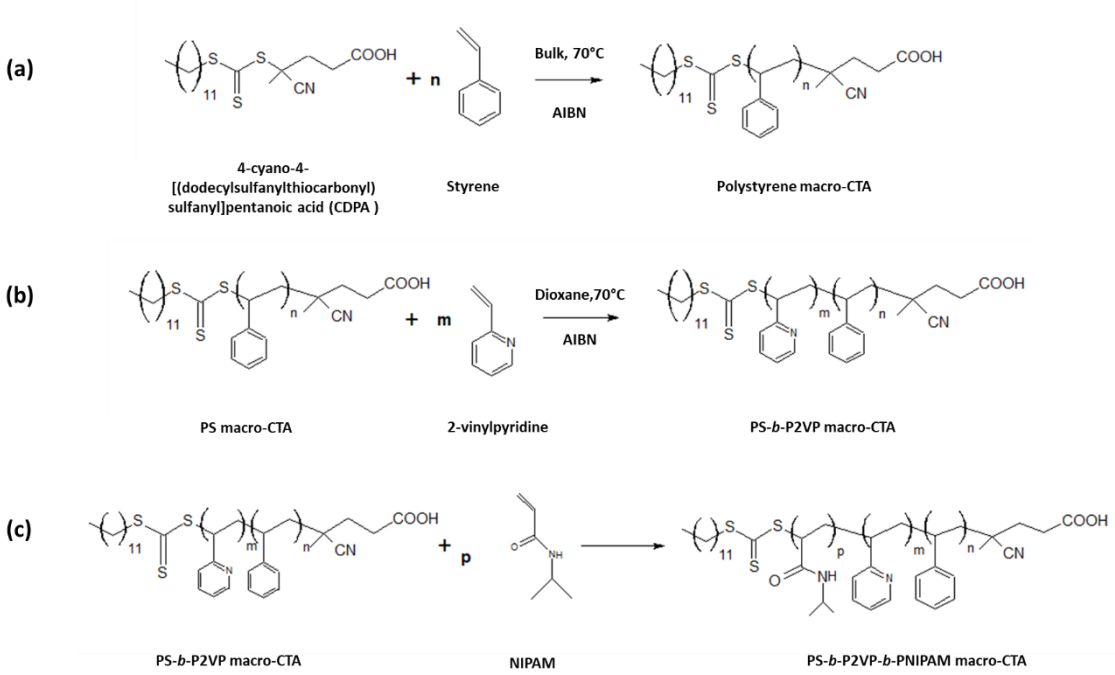

Schéma 1. Synthèse par polymérisation RAFT (a) de l'homopolymère PS macro-CTA, (b) du copolymère dibloc PS-*b*-P2VP macro-RAFT et (c) du terpolymère PS-*b*-P2VP-*b*-PNIPAM macro-CTA.

La deuxième partie de cette thèse consistait en l'étude des morphologies accessibles par l'auto-assemblage du terpolymère PS-*b*-P2VP-*b*-PNIPAM. Pour cela, nous avons utilisé le procédé séparation de phase induite par l'intrusion de non-solvant « non-solvent induced phase separation » (NIPS) afin de fabriquer des membranes asymétriques innovantes.[4]

Le terpolymère a été dissout dans un mélange de solvant constitué de DOX et de THF dans un rapport 1 pour 1. La solution de polymère à 18% en masse a ensuite été déposée sous forme de film épais sur un support en silicium à l'aide d'une racle disposée à une hauteur de 250 μm (« tape casting process »). Le film a ensuite été exposé à l'air pendant 30s, afin de densifier la surface libre du matériau par évaporation partielle le mélange de solvants, puis plongé dans un bain de coagulation (eau). Durant cette étape, le mélange DOX/THF diffuse dans le bain de coagulation alors que l'eau diffuse dans le film formant ainsi une membrane asymétrique constituée d'une couche supérieure dense et d'une sous-structure macroporeuse de type spongieuse.

Des images de microscopie à force atomique (AFM) et microscopie électronique à balayage (MEB) ont été réalisées afin de caractériser les surfaces des membranes préparées. L'image MEB présentée sur la **Figure 1.a** correspond à la vue en coupe d'une membrane de

PS-*b*-P2VP-*b*-PNIPAM générée par NIPS montrant bien une morphologie asymétrique constituée d'une couche supérieure dense et une sous-structure composée d'un réseau de pores ouverts. L'image AFM présentée sur la **Figure 1.b** montre la topographie de surface de la membrane préparée par NIPS qui se révèle être essentiellement constituée de pores désordonnés ayant une période de 12.1 nm. Afin de remplacer cette phase désordonnée, obtenue dans des conditions hors équilibre, il a alors été utilisé un procédé recuit par vapeur de solvant (SVA) permettant de promouvoir la mobilité des chaînes terpolymères vers un état d'équilibre thermodynamique. Cette étape de reconstruction de surface repose sur l'exposition d'un film polymère à une vapeur de solvant d'une manière constante et régulée.[5] Ici, la membrane préparée par NIPS a été traitée par une vapeur de chloroforme ($CHCl_3$) afin d'obtenir une nanostructuration de surface avec un ordre à longue portée. La **Figure 1.c** montre que la phase désordonnée générée NIPS sur surface libre de la membrane s'est entièrement transformée en une morphologie lamellaire perforée (PL) bien définie après exposition à une vapeur de $CHCl_3$ durant 6h. Cette phase PL, ayant une périodicité de 41 nm, consiste en une alternance de lamelles de PS et de lamelles de P2VP/PNIPAM perforées par des protrusions de PS.

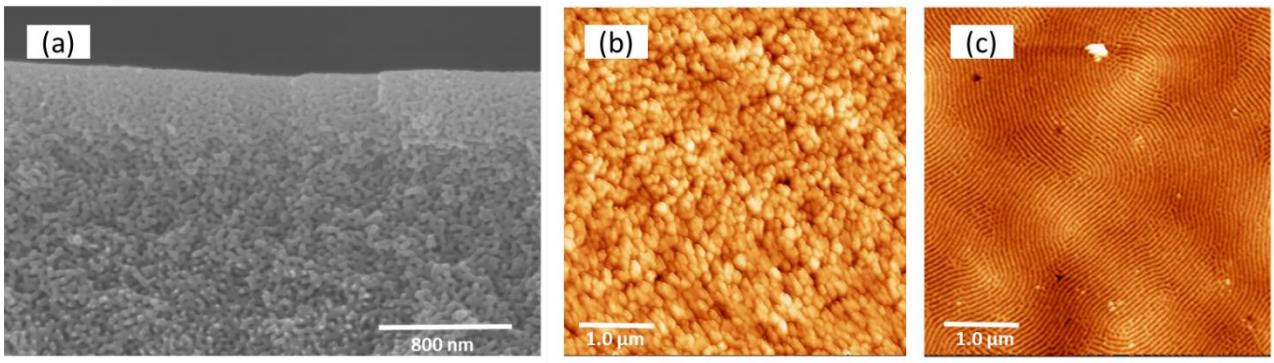

Figure 1. (a) Vue MEB en coupe de la membrane PS-*b*-P2VP-*b*-PNIPAM générée par NIPS, montrant une couche supérieure dense et une sous-structure sous forme de pores ouverts. (b) Image AFM topographique de la membrane obtenue par NIPS constituée de pores désordonnés. (c) Image AFM topographique de la même membrane obtenue par NIPS-SVA (6h, $CHCl_3$) montrant une reconstruction de surface libre constituée de lamelles perforées bien ordonnées.

La perméabilité à l'eau de la membrane terpolymère sensible au pH et à la température a été mesurée en utilisant un mode de filtration frontale (« dead-end filtration »). Il s'agit ici d'une filtration où la circulation de la solution à filtrer est perpendiculaire à la membrane. Dans notre cas, la perméabilité à l'eau des membranes a été mesurée à froid et à chaud, c'est-à-dire à des températures inférieures et supérieures à la température de transition critique inférieure (LCST) du PNIPAM qui est de l'ordre de 32°C dans l'eau. Le bloc thermosensible de PNIPAM a tendance à changer de conformation en fonction de la température de sorte qu'à des températures inférieures à 32°C, il est hydrophile et gonflé et au-delà, il devient hydrophobe et se recroqueville. Cette variation de configuration du bloc de PNIPAM, répondant à un changement de température de l'eau, permet de générer un mécanisme d'ouverture/fermeture des pores au sein de la membrane terpolymère, et ainsi de faire varier la perméabilité de cette dernière. Afin de contrôler plus finement, le mécanisme d'ouverture/fermeture des pores, le caractère pH-sensible du bloc de P2VP a aussi été exploité dans cette étude. Pour cela, nous avons fait varier simultanément la température et le pH de l'eau de sorte, notamment, à maximiser l'ouverture et la fermeture des pores puisque le bloc de P2VP deprotoné en milieu basique à tendance à se recroqueviller alors qu'il a tend à se gonfler sous sa forme protonée en milieu acide (voir **Figure 2**).

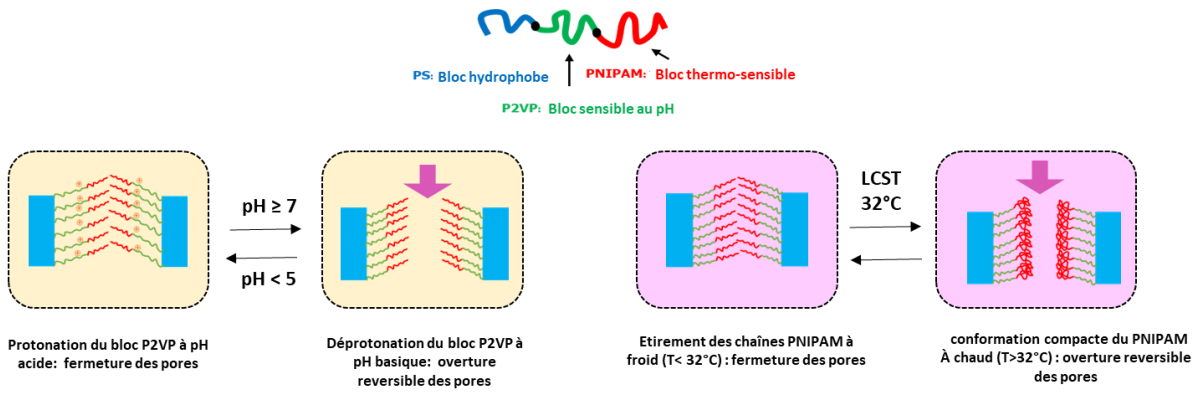

Figure 2. Dessin schématique du terpolymère PS-*b*-P2VP-*b*-PNIPAM et illustration du comportement des nanopores de P2VP/PNIPAM sensibles à différents stimuli. La porosité effective est régulée par le gonflement ou la rétraction des blocs P2VP et PNIPAM en fonction des changements de pH et de température.

La **Figure 3** représente les résultats de filtration de la membrane de PS-*b*-P2VP-*b*-PNIPAM en fonction de la température et du pH. A pH neutre, les courbes de flux présentées sur la **Figure 3.a** montrent que les nano-canaux cœur/couronne de P2VP/PNIPAM adoptent véritablement un état ouvert ou fermé en fonction de la température puisque les perméabilités, corrigées du

changement de viscosité de l'eau en fonction de la température, s'établissent respectivement à 2 et 18 $L.h^{-1}.m^{-2}.bar^{-1}$ pour une température inférieure (20°C) et supérieure (46°C) à la température du changement de conformation du bloc de PNIPAM (T_{LCST} = 32°C). De plus, pour une membrane donnée, il est observé que la porosité effective du matériau est aussi régit par le pH de l'eau puisque la valeur de flux est minimisée/maximisée en milieu acide/basique (0.8 $L.h^{-1}.m^{-2}$ à 1bar pour un pH= 3 et T= 20°C et 8.8 $L.h^{-1}.m^{-2}$ à 1bar pour un pH= 9.5 et T= 46°C) (voir **Figure 3.b**). Ces membranes terpolymères ont également démontré d'excellentes performances de réversibilité (c.à.d. cyclabilité) aux changements de température (**Figure 3.c**). En effet, une superposition des valeurs de perméabilité a été observée en faisant varier la température de l'eau en dessous et au-dessus de la T_{LCST} du PNIPAM sur plusieurs cycles, attestant ainsi une bonne stabilité du mécanisme d'ouverture/fermeture des pores mais aussi une bonne tenue mécanique de la membrane.

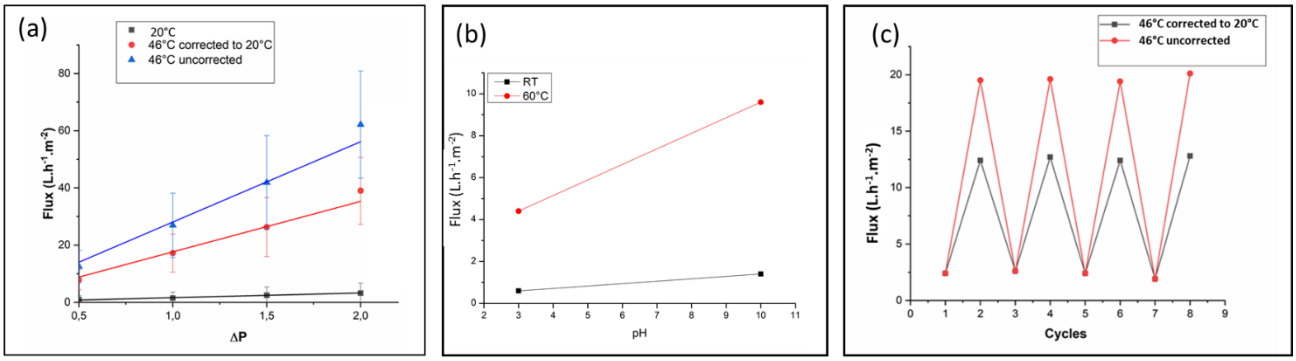

Figure 3. a) Flux d'eau obtenus pour des membranes PS-*b*-P2VP-*b*-PNIPAM à différentes températures : (carrés noirs) à 20°C et(points rouges) corrigés de la viscosité à 46°C. Les données non-corrigées (triangles bleus) mesurées à 46°C sont également données tandis que les barres d'erreur sont les écarts types des valeurs moyennes de perméabilité relative calculées pour deux échantillons différents. (b) Valeurs de perméabilité à l'eau mesurées dans un environnement acide et basique (pH = 3 et 9,5) à différentes températures : (carrés noirs) 20°C et corrigée de la viscosité (points rouges) 46°C. (c) Réversibilité de la perméabilité à l'eau en fonction des cycles de température (20°C et 46°C). Les données non-corrigées (triangles bleus) et corrigées en fonction de la viscosité (points rouges) sont données.

Enfin, dans la dernière partie de cette thèse, nous avons mélangé le terpolymère PS-*b*-P2VP-*b*-PNIPAM à d'autres copolymères amphiphiles afin d'accéder à de nouvelles morphologies par leur auto-assemblage et aussi d'augmenter l'hydrophilicité de la membrane ainsi que sa résistance à l'encrassement. Pour cela, par exemple, nous avons préparé des mélanges à base de PS-*b*-P2VP-*b*-PNIPAM et de PS-*b*-PNIPAM, à différents ratios, puis nous avons élaborés des membranes à l'aide du procédé NIPS-SVA. L'ajout de chaînes de PS-*b*-PNIPAM en faible pourcentage (25% en masse) au sein des membranes de PS-*b*-P2VP-*b*-PNIPAM a donné lieu à

la formation de nanopores bien définies (période = 46 nm) après l'étape de recuit sous une vapeur de $CHCl_3$ durant 6h (voir **Figure 6a**). De plus, l'incorporation de chaînes de PS-*b*-PNIPAM s'est révélée être bénéfique en matière de flux membranaire puisque, pour la première fois dans ce travail de thèse, la perméabilité à l'eau de la membrane terpolymère a augmenté après l'étape de SVA (6h, $CHCl_3$) pour atteindre une valeur maximale de ~80 $L.h^{-1}.m^{-2}.bar^{-1}$ à une température supérieure à la LCST du PNIPAM (46°C) (voir **Figure 6.b**).

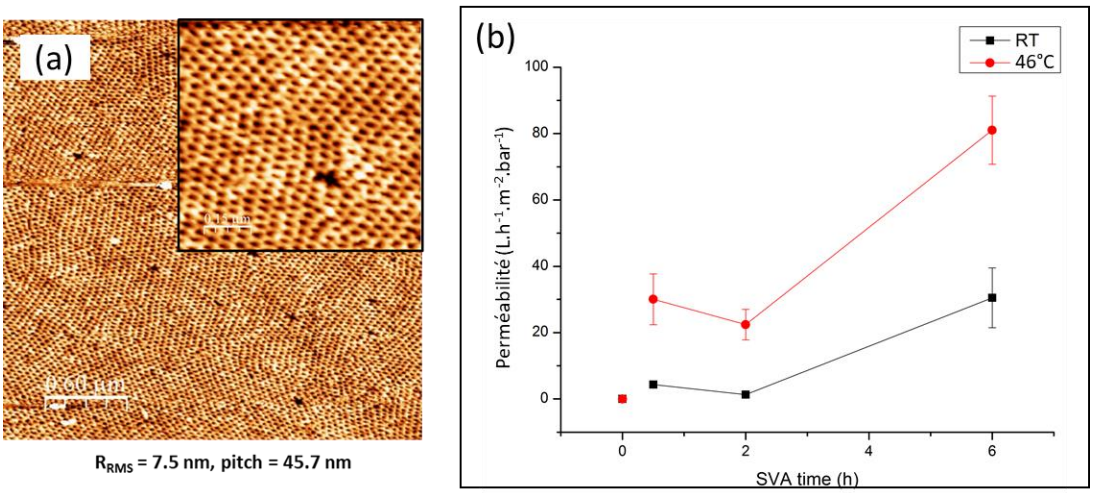

Figure 4. (a) Image AFM topographique d'une membrane PS-*b*-P2VP-*b*-PNIPAM/PS-*b*-PNIPAM préparée par NIPS-SVA (6h, CHCl3) présentant une reconstruction de la surface sous forme de nanodomaines bien ordonnées. (b) Valeurs de perméabilité pour le même type de membrane recueillies à différent temps de SVA pour deux températures : (carrés noirs) à 20°C et (points rouges) corrigées de la viscosité à 46°C. les barres d'erreur sont les écarts types des valeurs moyennes de perméabilité relative calculées pour deux échantillons différents.

Pour conclure, dans cette thèse, nous avons synthétisé pour la première fois une série de terpolymères ABC linéaires composés de PS, P2VP et PNIPAM par polymérisation RAFT. Cette voie de synthèse s'est révélée intéressante car les étapes de synthèses sont simples et quantitatives. En revanche, selon la taille de terpolymère souhaitée, l'étape de purification doit être optimisée. Dans notre cas, l'extraction de type Soxhlet était un bon moyen de purification permettant d'éliminer les chaînes de PNIPAM non-attachées et de garder un bon rendement final.

L'auto-assemblage des terpolymères ABC linéaires sous forme de nanodomaines bien définies a été démontré au sein de membranes asymétriques. Pour cela, le procédé NIPS a été combiné à un traitement SVA afin de promouvoir la mobilité des chaînes terpolymères, et donc de

reconstruire la surface de la membrane dotée d'une phase désordonnée après l'étape de fabrication par NIPS. Nous avons également montré que les membranes terpolymères préparées par NIPS-SVA sont sensibles au pH et à la température par l'étude de leur performance en mode filtration.

Enfin, nous avons mélangé le terpolymère PS-*b*-P2VP-*b*-PNIPAM à d'autres copolymères amphiphiles et nous avons montré qu'en respectant certaines règles de conception architecturale (telles que la taille des blocs et la nature chimique de ces derniers), il était possible d'augmenter la perméabilité de la membrane tout en gardant une nanostructuration de surface thermosensible avec un ordre à longue portée.

Références

1. Hampu, N., Werber, J. R., Chan, W. Y., Feinberg, E. C. & Hillmyer, M. A. Next-Generation Ultrafiltration Membranes Enabled by Block Polymers. *ACS Nano* **14**, 16446–16471 (2020).
2. John, R., Pal, K., Jayan, J. S., Appukuttan, S. & Joseph, K. New emerging review on advances in block copolymer based water purification membranes. *J. Mol. Struct.* **1231**, 129926 (2021).
3. Perrier, S. 50th Anniversary Perspective: RAFT Polymerization—A User Guide. 15 (2017).
4. Baig, M. I., Durmaz, E. N., Willott, J. D. & Vos, W. M. Sustainable Membrane Production through Polyelectrolyte Complexation Induced Aqueous Phase Separation. *Adv. Funct. Mater.* **30**, 1907344 (2020).
5. Sinturel, C., Vayer, M., Morris, M. & Hillmyer, M. A. Solvent Vapor Annealing of Block Polymer Thin Films. *Macromolecules* **46**, 5399–5415 (2013).

List of abbreviations

ACVA: 4,4'-azobis(4-cyanovaleric acid)

AFM: Atomic force microscopy

AIBN: Azobisisobutyronitrile

ATRP: Atom Transfer Radical Polymerization

Au-NPs : Gold nanoparticles

BCP: Block copolymer

C: Cylindrical

CA: Cellulose acetate

CD_2Cl_2: Deuerated dichloromethane

CDP: 4-cyano-4-[(dodecylsulfanylthiocarbonyl)sulfanyl]pentanol

CDPA: 4-cyano-4-[(dodecylsulfanylthiocarbonyl)sulfanyl]pentanoic acid

CF_4: Carbon tetrafluoride

$CHCl_3$: Chloroform

CMC: Critical micelle concentration

CPS: Closely packed spheres

CRP: Controlled radical polymerization

CTA: Chain transfer agent

~~Đ~~: Dispersity

DDMAT: 2-dodecylthiocarbonylthio-2-methyl proionic acid

DIS: Disordered phase

DLS: Dynamic light scattering

DMF: Dimethyformamide

DOX: 1,4-dioxane

DP: Degree of polymerization

f: Volume fraction

FE-SEM: Field emission scanning electron microscopy

GISAX: Grazing-Incidence Small-Angle X-ray Scattering

HEX: Hexagonally packed cylinders

hPNIPAM: poly(*N*-isopropyalcrylamide) homopolymer

hPS: Polystyrene homopolymer

ISL: Intermediate segregation limit

IUPAC: International Union of Pure and Applied Chemistry

L: Lamellae

LAMs: Less activated monomers

LCST: Lower critical solution temperature

MAMs: More activated monomers

Mn: Molecular weight by number

mTorr: Millitorr Pressur Unit

Mw: Molecular weight by weight

MWCO: Molecular weight cut-off

NIPS: Non-solvent induced phase separation

NMP: Nitroxide-Mediated Radical Polymerization

NMR: Nuclear magnetic resonance

ODT: Order-disorder transition

P2VP: Poly(2-vinylpyridine)

P4VP: Poly(4-vinylpyridine)

PA: Polyamide

PAA: Poly(acrylic acid)

PB: Polybutadiene

PDMAEMA: Poly(*N*,*N*-dimethylamino ethyl methacrylate)

PDMS: Polydimethylsiloxane

PDMSB: Poly(1,1-dimethylsilacyclobutane)

PEDOT: PSS: poly(poly(3,4-ethylenedioxythiophene) polystyrene sulfonate

PEG: Poly(ethylene glycol)

PEGMA: Poly(ethylene glycol) methyl ether methacrylate)

PEO: Poly(ethylene glycol)

PES: Polyethersulfone

PHFBM: Poly[2-(methacryloyxyl)ether trimethylammonium chloride)

PI: Poly(isoprene)

PL: Perforated Lamellae

PMMA: Poly(methyl methacrylate)

PNIPAM: Poly(*N*-isopropylacrylamide)

PS: Polystyrene

PS-*b*-P2VP-*b*-PNIPAM: Polystyrene-*block*-poly(2-vinylpyridine)-*block*-poly(*N*-isopropyalcrylamide)

PSD: Power spectral density

PSU: Polysulfone

PVDF: Polyvinylidene fluoride

RAFT: Reversible Addition-Fragmentation chain Transfer polymerization

Rrms: Roughness mean square

RT: Room temperature

S: Spherical

SAXS: Small Angle X-rays Scattering

sccm: Standard Cubic Centimeters per Minute

SCFT: Self-consistent field theory

SEC: Size exclusion chromatography

SEM: Scanning electron miscroscopy

SNIPS: Self-assembly and non-solvent induced phase separation

SSL: Strong segregation limit

SVA: Solvent vapor annealing

SVN: Polystyrene-*block*-poly(2-vinylpyridine)-*block*-poly(N-isopropyalcrylamide)

SVO: Polystyrene-*block*-poly(2-vinylpyridine)-*block*-poly(ethylene oxide)

T: Temperature

THF: Tetrahydrofuran

TIPS: Thermally induced phase separation

UCST: Upper critical solution temperature

UNESCO: United Nations Educational, Scientific and Cultural Organization

VIPS: Vapor induced phase separation

WSL: Weak segregation limit

ΔG_m: Gibbs free energy

ΔH_m: Enthalpy

ΔS_m: Entropy

Φ: Volume fraction

General introduction

The global freshwater deficit is becoming one of the most economic and social challenges. Access to safe drinking water is one of the first priorities following a disaster. Today, millions of people in Europe are drinking contaminated water, often without knowing it. The World Health Organization (WHO) estimates that over 14 people die every day from diarrheal diseases due to lack of water and hygiene. The population growth, the industrialization demand and the climate change are the principal reasons of the drinking water deficit.

The increase of drinking water supplies can be accomplished by two different strategies: wastewater treatment and seawater desalination. To this end, one of the current promising strategy is membrane filtration. The use of a porous film designed to control the passage or retention of components under the action of a driving force is intensely used in water treatment and often involved in the development of innovative systems. However, this technique remains limited by one of the major problem in membrane technology, which is fouling. The accumulation of colloids, particles or organic matters on the surface or inside the pores of the membrane has a direct consequence in a decrease of membrane flux over time and a crucial need of the use of chemical and/or mechanical cleaning with a significant impact on the environment. It is therefore necessary to design new innovative materials able to respond to the current problems of society not only in water field treatment, but also in other domains such as environmental protection, food, health, etc.

The development of fouling resistant membranes composed with a high density of smart isopores able to adjust their size in response to an external stimulus such as temperature, pH, magnetic field, etc., are interesting materials to effectively prevent the common problem of fouling considered as one of the biggest challenges in membrane technology.

The aim of this PhD thesis is based on the development of new nanostructured block copolymer smart membranes manufactured by phase inversion process. For that, we will first focus on the synthesis and the characterization of double stimuli-responsive linear ABC terpolymers. Then, we will study the self-assembly of the synthesized terpolymers into well-defined nanostructures formed on asymmetric membranes as well as the filtration performances of the resulted materials. Finally, the last part of this work will be devoted to the study of the self-assembly of blends comprising the double stimuli-responsive linear ABC terpolymers and other amphiphilic

block copolymers in order to improve the hydrophilicity of the blended membrane, and consequently its resistance to fouling.

Chapter 1 will introduce the different concepts addressed in this work for a better understanding of the general context of this thesis. After a brief description of membrane classifications and the fundamental notions regarding the bulk self-assembly of block copolymers, we will introduce the different membrane manufacture processes related to this work. Finally, we will discuss about smart and stimuli-responsive membranes as well as their potential applications.

Chapter 2 of this manuscript will describe the Reversible addition−fragmentation chain-transfer (RAFT) polymerization used to prepare well-defined linear ABC terpolymers consisted of polystyrene (PS), a pH-responsive poly(2-vinylpyridine) (P2VP) and a thermo-responsive poly(*N*-isopropylacrylamide) (PNIPAM). Analytical methods, such as nuclear magnetic resonance (NMR) and size-exclusion chromatography (SEC) were used to characterize the synthesized terpolymers.

In **Chapter 3,** we will first detail the fabrication of asymmetric PS-*b*-P2VP-*b*-PNIPAM thick films by non-solvent induced phase separation (NIPS) followed by the transformation of their top surfaces from a poorly-defined phase into a well-ordered perforated lamellar structure when treated by solvent vapor annealing (SVA). We will then evaluate the thermo/pH dual responsive behavior of the prepared membranes by water permeability measurements.

Chapter 4 will be devoted to the study of the self-assembly of blends comprising the PS-*b*-P2VP-*b*-PNIPAM chains and different amphiphilic block copolymers. The combination of the NIPS technique and the SVA process was used to produce blended PS-*b*-P2VP-*b*-PNIPAM thick films with improved hydrophilicity.

Chapter 5 constitutes the experimental part of this manuscript and gathers all the methods, techniques and syntheses carried out in this work.

CHAPTER 1

Bibliographic study

Table of contents

1. Introduction

Membrane filtration is considered as the main technology in water treatment. According to United Nations Educational, Scientific and Cultural Organization (UNESCO), global demand for good quality water will increase by 55% in 2050 due to population growth, industrialization demand and due to climate change that highly affect the supply of clean water.[1] Therefore, selective membrane technologies are good candidates for the development of sustainable water economy and prevent disruption in supply of clean water as well as the use of all the available water sources. Nowadays, membrane separation techniques contribute 53% of world's clean water.[2] They present an ease of handling, energy efficiency, manufacturing scalability and cost effectiveness.

In 1963, Loeb and Sourirajan[3] introduced the first example of high-effective processing of synthetic polymer into functional membranes *via* the non-solvent induced phase separation (NIPS) technique. The obtained integral asymmetric membranes exhibit continuous pores, thin selective layers and high water permeability.[1] This technique opened access to significant progress in membrane manufacturing on large-scales and great advances in porous membrane performances.

Current commercially available membranes present a permeability-selectivity trade-off limiting their use over time.[4] In addition, they face another crucial problem in membrane technology, which is fouling. It corresponds to the deposition of unwanted materials (called foulants) on membrane surface, resulting in a strong flux decline and reduction of the pore size. Nowadays, the biggest challenge in membrane technology is the development of new class of advanced fouling-resistant membranes able to surpass the existing trade-off.

The aim of this thesis work is to address conception of novel nanostructured block copolymer smart membranes fabricated by phase inversion technique. The innovative membranes will be composed of a high areal density of pores with well-controlled sizes in order to eventually reach high selectivity and high permeability. Furthermore, thanks to the phase inversion process and to the different block copolymers properties, the envisioned smart membranes will surpass the current permeability-selectivity trade-off and will be fouling-resistant.

This first chapter will introduce the different concepts addressed in this work for a better understanding of the rest of the study. After a brief description of membrane classifications, the

bibliographic study will describe the fundamental concepts concerning bulk self-assembly of block copolymers and polymerization techniques. Different membrane manufacture processes will then be described. Finally, this chapter will report on smart and stimuli-responsive membranes as well as their potential applications.

2. Membrane technology

2.1. Definition

Membranes are selective barriers that can separate substances with different physical/chemical properties.[5] Components that pass through the pores of the membrane are called permeate and must be smaller than the pore size of the membrane whereas the ones remaining at the surface of the membrane are called retentates (see **Figure 1**).Membrane separation efficiency depends on different parameters: permeability, selectivity, pore size and molecular weight cut-off (MWCO). Permeability is defined by the trans-membrane flux that evaluates the productivity of membrane processes while the selectivity is characterized by the ability of membrane for the rejection/permeation of specific substances. Both permeability and selectivity depend on the pore size and surface properties of the membrane. Finally, molecular weight cut-off is the lowest molecular weight (in Dalton) at which greater than 90% of a polymer with given molar mass is retained by the membrane. MWCO determines size distribution of the membrane and its retention capabilities.

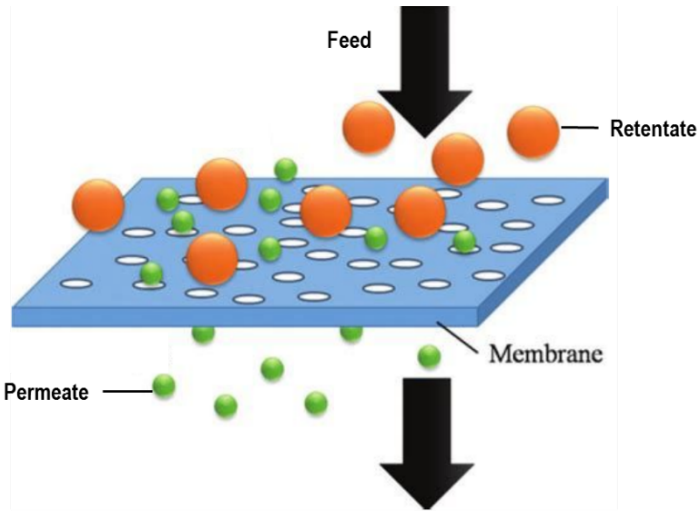

Figure 1. Schematic illustration of a membrane separation.[6]

2.2. Classification of membranes

Membranes can be classified according to different parameters: origin, structure, geometry or pore size (see **Figure 2Erreur ! Source du renvoi introuvable.**). Firstly, depending on their nature, membranes are categorized into biological or synthetic. In fact, this is the simple classification since these two types of membranes are completely different from each other both in their structure and in their functionality.[6] Biological membranes are of great importance as a model and source of inspiration for separation processes, however, they will not be discussed in this study.

❖ Classification by natures

Synthetic membranes are classified according to the used material into organic (liquid/polymer) or inorganic (metal/ceramic). Ceramic membranes are generally prepared from alumina, zirconium oxide, titanium oxide or silicon carbide. Moreover, they have good chemical resistance (use of organic solvent) and good mechanical properties (application of high pressure).

In this study, we were interested in polymeric membranes. They are mostly prepared from cellulose acetate (CA), polysulfone (PSU), polyethersulfone (PES), polyamide (PA) or polyvinylidene fluoride (PVDF). Comparing to ceramic membranes, they have a flexible structure facilitating their implementation, but they have a low chemical and mechanical resistance.

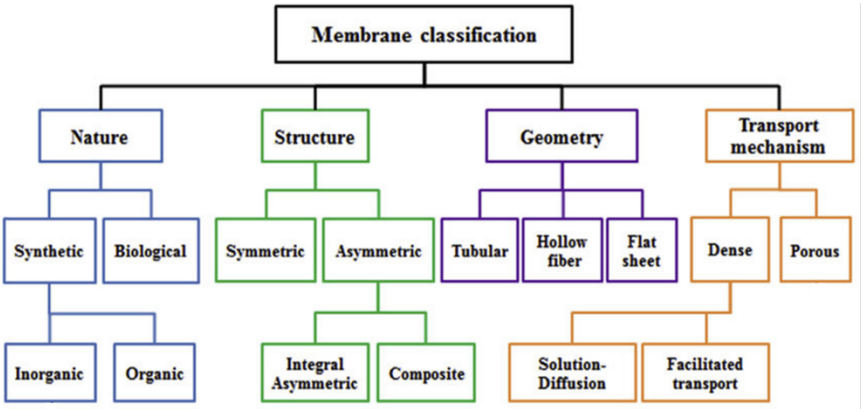

Figure 2. Membrane classification.[8]

❖ **Classification by geometries**

Membranes are also classified according to their geometries into two categories: planar or cylindrical. Planar membranes are either arranged in stacks or wound in a spiral. Cylindrical membranes have tubular wound or hollow fiber. Depending on their wound type, membranes can be used in different separation applications. For example, hollow fiber membranes are used in reverse osmosis, gas separation and nanofiltration. Spiral wound membranes are used in reverse osmosis for water desalination. Planar wound membrane types are used in tangential flow filtration for bio-pharmaceutical application or frontal filtration that is used for clarification or debacterization.

Frontal filtration, also referred as dead-end filtration, is based on perpendicular circulation of the fluid to be filtered in relation to the membrane. This filtration mode is limited by formation of accumulation of retentates at the surface resulting in fouling and in decrease in filtration flow.

Tangential flow filtration (crow-flow filtration) is based on parallel circulation preventing the accumulation of solutes at the surface and limiting fouling issue. This separation technique is the most widely used industrially because it can operate more easily continuously.

❖ **Classification by structures**

Based on their morphologies and structures, membranes can be categorized such as dense, porous and composite. Porous membranes are essentially used for ultrafiltration and microfiltration. Non-porous membranes are generally used for reverse osmosis, nanofiltration and molecular separation in the gas phase.

Porous membranes can be symmetric or asymmetric: symmetric are of uniform structure and their thickness ranges from 10 to 200 μm, they may be homogeneous dense or porous. The constant pores diameter throughout the symmetric membrane cross section limit the mass transfer during filtration.

Asymmetric membranes are composed of either a porous or dense skin layer with a thickness from 50 to 150 μm and a sponge-like substructure.

They are divided into integrally porous, non-porous and composite skin layer. The pores generated by porous membranes are classified into Chemistry (IUPAC) : micropores (pores smaller than 2 nm), mesopores (2-50 nm) and three categories by their size according to the International Union of Pure and Applied macropores (larger than 50 nm). Comparing to symmetric membranes, asymmetric ones are less prone to fouling issues thanks to the difference in pore size from the surface to the substructure. Furthermore, asymmetric membranes are used in several sectors of industry like water purification/treatment [7], biopharmaceutical separation [8] and electronic processing.[9]

The existing membranes are usually facing an important decrease in their productivity. In one hand, this productivity limitation can be caused by a significant decrease in permeability during filtration through concentration polarization that corresponds to a change in the concentration of a specific component at the boundary layer near to the membrane surface. In the other hand, fouling is another phenomenon limiting the filtration and membrane lifetime. In fact, it corresponds to the accumulation of retentates at the membrane surface and it can be reversible or irreversible. Reversible fouling corresponds to the attachment of retentates to the membrane surface and thus can be easily removed by rinsing with water or organic solvent. Irreversible fouling is more difficult to eliminate and it corresponds to an interne fouling due to adsorption of particles *via* intermolecular interactions (hydrophobic, hydrogen bonds or van der Waals) between the substances and the membrane.

Current commercial NIPS-made homopolymer membranes for ultrafiltration are limited by an inadequate separation and poor fouling resistance (see **Figure 3**Erreur ! Source du renvoi introuvable.**.a**).[1] However, block copolymer (BCP) membranes are able to tailor the membranes surface chemistries (see **Figure 3**Erreur ! Source du renvoi introuvable.**.b**). Indeed, the block copolymer self-assembly into periodic nanostructures with controllable morphologies offers the potential to build uniform pore size in a highly-areal density within the membrane skin layer and the development of smart fouling resistant (self-cleaning) membranes.

The next section is devoted to an introduction on the BCP self-assembly and their use in the development of membranes with controlled morphologies.

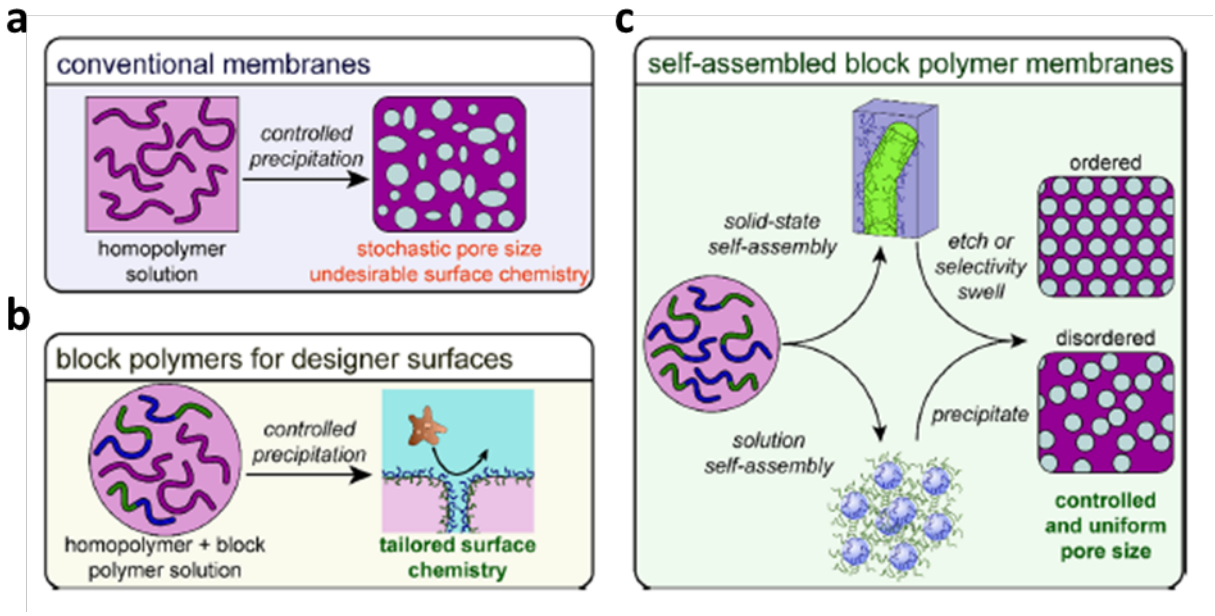

Figure 3. a) Illustration of homopolymer membrane obtained by NIPS limited by stochastic pore sizes and undesirable surface chemistries. b) Illustration of block copolymer membrane with improved surface chemistry and c) illustration of block copolymer self-assembly in bulk or in solution into an ordered or disordered state generating uniform pore size in both cases.[1]

3. Porous polymeric membranes

Block copolymers are composed of at least two different monomer units (A and B) linked together with a covalent bond. BCPs are categorized based on the arrangements and number of the connected blocks, depending on this block number, they are called di-, tri- or multi-block copolymers. For example, a diblock copolymer composed of two monomer units A and B is called poly(A)-*block*-poly(B) while a triblock copolymer with the same monomer units is called poly(A)-*block*-poly(B)-*block*-poly(A) or poly(B)-*block*-poly(A)-*block*-poly(B) depending on the central block. Another triblock copolymer type exists composed with three monomer units A, B and C, termed triblock terpolymer poly(A)-*block*-poly(B)-*block*-poly(C). BCPs are also classified based on their arrangement into linear, grafted and star miktoarm (see **Figure 4 Erreur ! Source du renvoi introuvable.**).

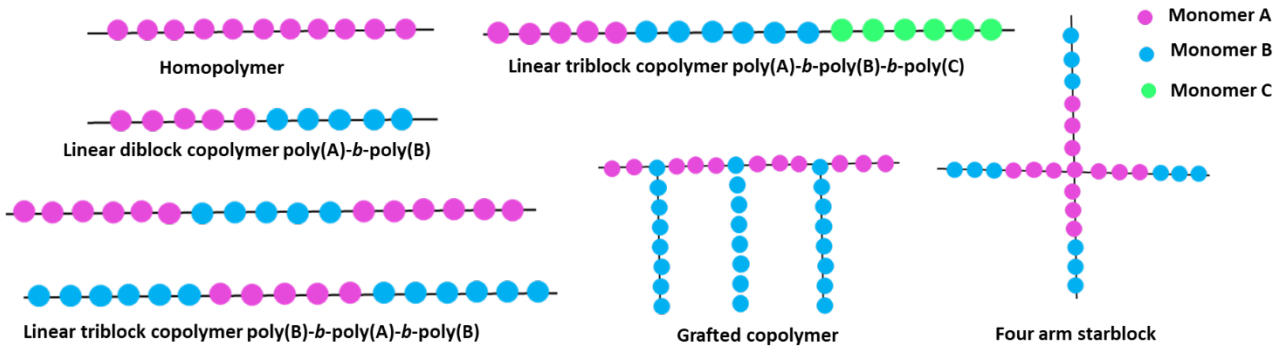

Figure 4. Block copolymers arrangement.

Porous polymeric membranes are of great interest in the development of new membranes with controlled morphologies. Indeed, thanks to the well-known self-assembly of BCPs, membrane structures can be well tuned. Block copolymer self-assembly can be as well in solution as in bulk and different nanostructures can be obtained.

In this study, we are interested in the use of block copolymers for membrane preparations with controlled morphologies. Therefore, it seemed essential to us to deepen their self-assembly in bulk, the following part is then devoted to this aspect.

3.1. Self-assembly of block copolymer in bulk

In a mixture of immiscible polymers, one of the polymers would tend to minimize the contact interface by forming a dispersion in the second one, this phenomenon comparable to water in oil emulsion is called macrophase separation.

Otherwise, in the case where immiscible polymers are connected by a junction point like block copolymers, this macrophase separation is not possible anymore due to the covalent bond. Thermodynamically, the phase separation of block copolymer can be explained by the Gibbs free energy: $\Delta G_m = \Delta H_m - T\Delta S_m$ and it occurs when $\Delta G_m > 0$.

ΔH_m represents the enthalpy and is determined by the Flory-Huggins parameter χ which is related to the interactions between the blocks. ΔS_m is the entropy and it depends on the polymerization degree N of the chains. When the temperature T increases, the magnitude of

$T\Delta S_m$ approaches the one of ΔH_m and the self-assembly of the AB-type BCP becomes progressively less effective. However, their self-assembly occurs spontaneously if ΔG_m is positive and accompanied by a loss of enthalpy and entropy. The loss of enthalpy is due to the repulsion of polymer chains while the entropy opposes the macrophase separation due to the junction between the blocks (see **Figure 5**).[10]

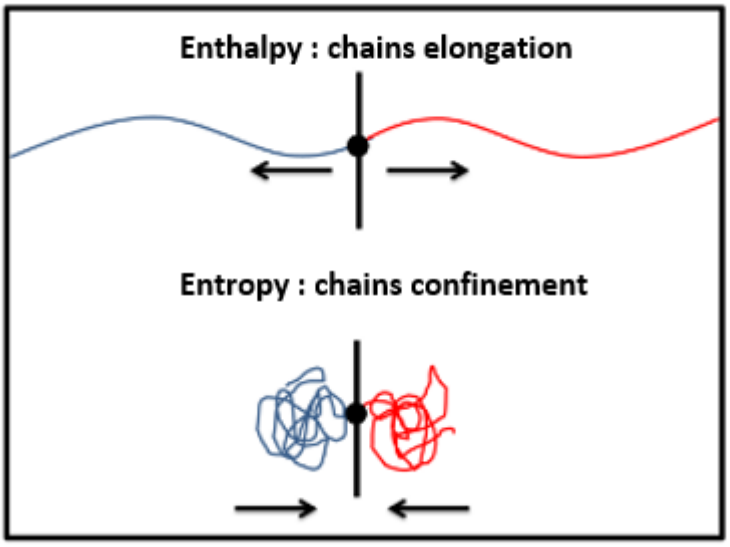

Figure 5. Enthalpy and entropy balance during phase separation. [10]

3.1.1. AB diblock copolymers

Over 30 years, the microphase separation of linear AB-type BCPs have been studied and numerous structures have been identified depending on the volume fractions *f* of each block ($f_A + f_B = 1$) and the segregation strength between the blocks, represented by the product χN.

AB diblock copolymer self-assembly is the simplest and can be predicted by Matsen and Bates phase diagram (see **Figure 6**) which is represented as a function of volume fraction and the segregation strength between two blocks.

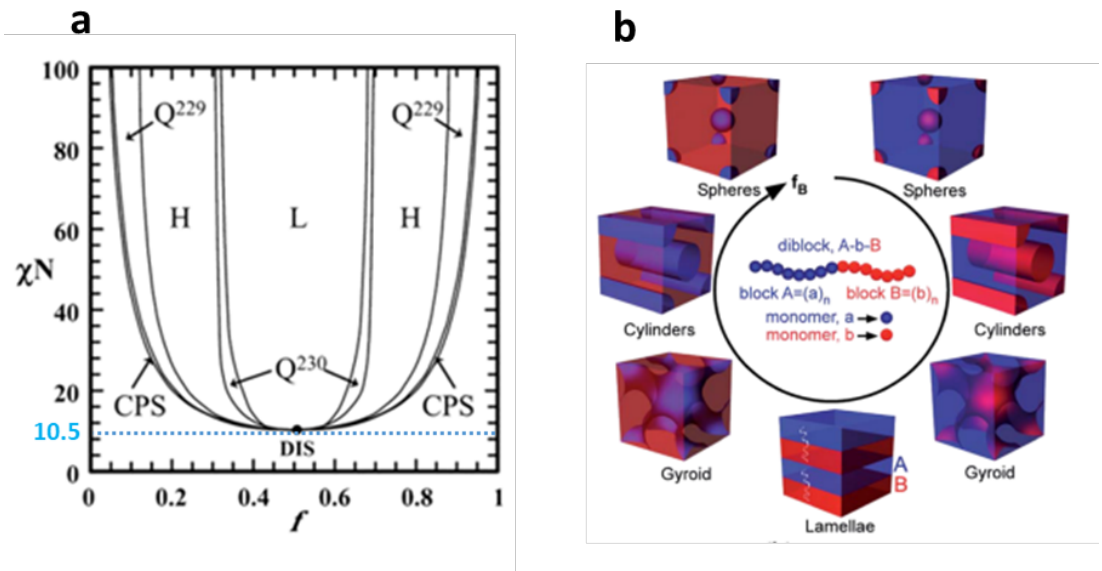

Figure 6. a) Phase diagram of diblock copolymer predicted by self-consistent field theory (SCFT). *f* : volume fraction of one block, χ : Flory-Huggins interaction parameter, N : degree of polymerization, L: lamellae, H : hexagonally packed cylinders, Q^{230} : double-gyroid phase, Q^{229} : body centered spheres, CPS : closed-packed spheres and DIS : disordered phase. b) Schematic representation of some accessible morphologies depending on volume fraction.[14]

According to the self-consistent field theory (SCFT) [11] different morphologies can be predicted such as the "classical" lamellar (L), cylindrical (C), spherical (S) phases and the more complex double gyroid (G)[12] structure (see **Figure 6.b**).

By increasing the volume fraction of the block A or B, the microdomain arrangement changes from closely packed spheres (CPS), to body centered cubic spheres (Q^{229}), to hexagonally packed cylinders (H), to bicontinuous gyroid (Q^{230}), and finally to Lamellae.[13]

The segregation of A and B blocks is dictated by the product χN. The critical lower limit is defined at $\chi N = 10.5$ below this value the entropy dominates and a disordered phase (DIS) is observed. Conversely, when $\chi N > 10.5$, A and B blocks become immiscible causing an order-disorder transition (ODT).[13]

The lamellar phase is formed at nearly symmetric compositions of the A and B blocks ($f_A = f_B$). The other phases depend on the arrangement of the minor block. In the case where

the minority component forms hexagonal cylinders, the cylindrical phase is obtained. On the other hand, when this block forms spheres arranged on a centered cubic lattice, the spherical phase is formed. The gyroid structure is observed when the minority domain forms two interweaving threefold coordinated lattices. Another reported metastable complex phase is a perforated lamellar phase (PL). Here the minority component layers of the lamellar structure exhibit a hexagonal or tetragonal array of passages through which the majority component layers are connected *via* protrusions.

Three different segregation regimes can be defined in AB diblock copolymer self-assembly based on χN value. When $\chi N < 15$, a weak segregation limit (WSL) is noted. The intermediate segregation limit (ISL) and strong segregation limit (SSL) regions are reached for $15 < \chi N < 100$ and $\chi N > 100$, repectively.

For instance, Matsen *et al.*[14] described the phase behavior occurring in the intermediate segregation limit, for values of $\chi N = 20$. In this regime, a sequence of different morphologies can be predicted based on theoretical calculations, including the lamellar, gyroid, cylindrical and spherical phases.

3.1.2. ABA triblock copolymers

The self-assembly of ABA triblock copolymers is similar to the one of AB-type BCP. Here, however, the critical lower limit χN is found to be 18.0.[15]

In the case of AB-type BCP, the polymers have a “tail” conformation binding the A and B domains. On the other hand, in the case of ABA triblock copolymers, the central block can form a "loop" in which the latter folds back on itself to anchor the terminal blocks in adjacent areas. A "bridge" configuration is observed when the central block connects two distant zones, making that the mechanical strength in the solid state of the material and the compatibility in solution are greatly improved.

The incorporation of a third different block constitutes another class of BCP self-assembly in bulk that is different from the one of AB- and ABA-type BCPs. In this case, the presence of a

third C-block will change the parameters controlling the self-assembly, resulting in the formation of new ordered structures. The self-assembly of ABC-type BCP is detailed hereafter.

3.1.3. ABC triblock copolymers

The addition of a third (or more) block(s) in BCPs increases the level of self-assembly complexity in bulk and can provide more tuning of the morphology. [16] It can also generate unusual geometries and introduce structural hierarchies. [17] In addition, ABC-type BCPs offer a great opportunity to manufacture membranes with a panoply of network structures.[4,18] Several studies have been focused on ABC linear triblock terpolymer self-assembly in bulk, suggesting the existence of at least 30 different morphologies.[19]

In the case of linear ABC-type triblock terpolymers, the number of observable morphologies is increased and depends on the position of each block and on the parameters listed below:

- Three independent volume fractions with $f_A + f_B + f_C = 1$
- Three interaction parameters χ_{AB}, χ_{BC} and χ_{AC} between linked A / B and B / C blocks and unbound A / C blocks
- The order of the blocks (ABC / ACB / BAC)

Depending on the topology of the terpolymer chains and on the interactions between the blocks, different frustration types are described. At molecular scale, frustration corresponds to the phase separation of different blocks while the chain connectivity prevents a macroscopic phase separation. At mesoscopic scale, frustration occurs as long as the polymeric domains tend to maintain a uniform shape and fill the space. These frustrations constitutes the main driving force to form complex ordered phases.

Bates *et.al* [20] have summarized different structures obtained according to these parameters. For equal volume fractions ($f_A = f_C$) and same interaction parameters ($\chi_{AB} = \chi_{BC} = \chi_{AC}$), the triblock terpolymer adopt a lamellar morphology.

In the case where χ_{AC} is larger than the other interaction pairs, there is absence of any frustration (called a type 0 frustration). The contact between A and C blocks is not favorized, allowing the formation of core-shell morphologies. (see **Figure 7.f,g and i**)

A type I frustration is observed when the Flory-Huggins interaction parameters are organized as follows $\chi_{AB} = \chi_{AC} < \chi_{BC}$. Hückstädt *et al.*[21] reported in their work on self-assembly of polystyrene-*block*-polybutadiene-*block*-poly(2-vinylpyridine) (PS-*b*-PB-*b*-P2VP) into a core-shell double gyroid morphology. The small P2VP block formed the core, surrounded by a shell of the highest incompatible PB block.

A type II frustration is noted when χ_{AC} is smaller than the other interactions. Here, the central B block becomes strongly incompatible with the A and C blocks, the domains B become discontinuous. New morphologies were observed such as hexagonal array where A and C form cylindrical microdomains in B matrix.[22]

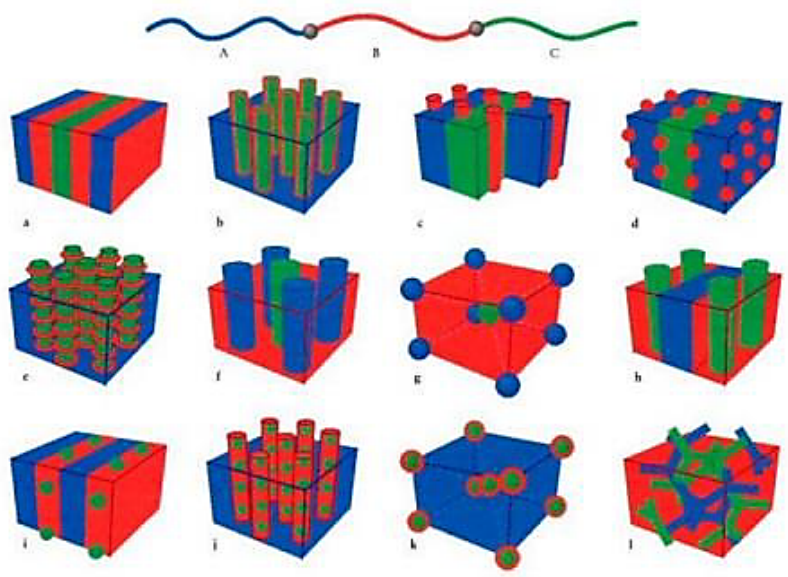

Figure 7. Types of nanostructures formed by linear triblock terpolymers in different block order sequence (ABC, ACB or BAC).[16]

In 2020, Miskaki *et al* [23] summarized in their work the different morphologies observed in the literature depending on block sequence, molecular weight range and annealing conditions used in the case of linear ABC-type triblock terpolymers,

For example, the self-assembly of polystyrene-*block*-poly(isoprene)-*block*-poly(2-vinylpyridine) (PS-*b*-PI-*b*-P2VP) triblock terpolymers has been studied in different works. For a PS-*b*-PI-*b*-P2VP molecular weight of 43 kg.mol^{-1} and equal volume fractions f_{PS}:f_{PI}:f_{P2VP}

(0.33:0.33 0.33) Gido *et al.*[24] observed a lamellar structure. At a higher molecular weight value (196 $kg.mol^{-1}$) and higher PI volume fraction (0.18:0.66:0.16), Matsushita *et al.*[25] observed an ordered tricontinuous double diamond (OTDD) structure.

For a similar ABC triblock terpolymer system having, however, a different block order sequence (*i.e.*, PI-*b*-PS-*b*-P2VP), Mogi *et al.*[26,27] identified different types of morphologies by changing the volume fraction of the midblock from 0.48 to 0.66. The observed morphologies were: the core-shell lamellar, OTDD, cylindrical and spherical phases.

Bailey *et al.*[28] studied another system composed of polystyrene-*block*-poly(isoprene)-*block*-poly(ethylene glycol) (PS-*b*-PI-*b*-PEO) with different volume fraction of PEO, ranging from 2.9% to 33.2%. They observed the formation of two- and three-domain lamellar structures, hexagonally packed core-shell cylinders and pentacontinuous core-shell gyroid morphology. In the same strategy but by changing the block sequence order to PI-*b*-PS-*b*-PEO, the same research group [18] observed three different morphologies (*i.e.*, the orthorhombic O^{70} (Fddd) network morphology, and 3-phase 4-layer lamellae (LAM)) that were obtained by increasing volume fraction of PEO from 0.12 to 0.33.

These examples show how the effect of the molecular weight of the ABC-type BCP, the block sequence order as well as the interactions between the multiple blocks strongly affect the final morphology.

As described in this part, the addition of a third block in BCP increased the level of self-assembly complexity, giving rise to new complex well-defined morphologies. In order to push the complexity even further, distinctly different block copolymers can be combined together, also known as blend of BCPs. This strategy has a huge potential for the design of new well-defined and controlled superstructures. The following section is devoted to this aspect.

3.1.4. Blend of block copolymers

More advanced and complex morphology also called “nonclassical” morphologies can be observed by blending block copolymers with multimodal dispersity of the targeted blocks.

The morphologies observed in the case of blend copolymers can be the same as for classical polymers (*i.e.* lamellae, perforated lamellae, gyroid, cylinder or spheres) accompanied with a shift in the phase diagram boundaries.[29]

Blending block copolymers can also open more possibilities for more complex architecture and new morphologies different from the classical ones.

Block copolymer morphologies by blending can be influenced by different parameters. Some of the examples of blending linear block copolymers are presented in the following part.

In 1998, Koneripalli *et al.*[30] studied the blending of two asymmetric diblocks composed of PS-*b*-P2VP with same molar mass but a different volume fraction of PS, they observed that this blending mixture leaded to a lamellar structure even the individual diblocks exhibit a nonlamellar morphology.

The use of small molecules for blending block copolymer may be the simplest way to achieve new morphologies. For example Ruokolainen *et al.*[31] added pentadecyl phenol (PDP) to their PS-*b*-P4VP system and observed formation of asymmetric lamellar structure due to the H-bonding between PDP and P4VP, inducing restriction of block copolymer junctions on the microdomain interface.

❖ Blending with homopolymers

In the same strategy of H-bonding, Dobroseielska *et al.*[32] blended PS-*b*-P2VP diblock copolymer for average molecular weight , Mw, of 130 kg.mol^{-1} with poly(4-hydroxystyrene) (Mw ~ 14 kg.mol^{-1}). They observed a morphological transition from cylindrical to spherical structures upon addition of large amount of poly(4-hydroxystyrene). Here the morphology was more tunable due to H-bonding interactions between the added homopolymer and P2VP moiety. These results were compared with those obtained from blends of PS-*b*-P2VP with P2VP homopolymer (Mw = 6.6 kg.mol^{-1}). The initial PS-*b*-P2VP diblock copolymer was arranged in a hexagonally packed cylindrical structure while the addition of the homopolymer resulted in a lamellar structure.

Whitmore *et al.*[33] and Matsen *et al.*[34] explained the effect of blending an AB diblock copolymer with an A-type homopolymer with high- and low-molecular weight. In the case where the

diblock exhibit lamellae morphology is blended with high-molecular weight homopolymer, there is an attractive interaction between diblock bilayers causing a macrophase separation between the diblock-rich lamellar phase and homopolymer-rich disordered phase. In the case where a low-molecular-weight homopolymer is added, a repulsive interaction between bilayers occurs and the homopolymer is added to the lamellar phase indefinitely without macrophase separation.

❖ **Blending with diblock copolymers**

The use of block copolymer as blend is more complicated, since several parameters can influence the morphology transition. For example, Chen *et al.*[35] reported the morphology and phase behaviors of polystyrene-*block*-poly(methyl methacrylate) (PS-*b*-PMMA) diblock copolymers in their blend films. The AB-type BCPs were composed with similar molecular weights but different PS volume fractions (f_{PS} = 0.3 and 0.7), the observed morphologies depend on the interaction between the solvent and the block and on the differences in chain lengths. Multilayered microphase morphologies composed of spheres and triple coaxial circular microdomain structure with PS as core and PMMA as shell were reported.

In another study, Guo *et al.*[36] observed the same behavior in thin film of blends of two asymmetric PS-*b*-PB with molecular weight of 137 and 96.5 kg.mol^{-1} and PS volume fractions of 0.24 and 0.62, respectively. They observed a new morphology that they named "sphere between cylinders" where the PS form cylinders in PB in the first BCP and PB cylinders in PS matrix in the second one.

❖ **Blending with triblock terpolymers**

In the case of blends containing ABC-type terpolymers, a larger variety of specific behavior can be observed due to the presence of central block forming a bridge conformation. Matsushita *et al.*[37] studied the blend of three PI-*b*-PS-*b*-P2VP with different molecular weights (26, 96 and 150 kg.mol^{-1},respectively). They observed lamellar structures at low dispersity values (Đ = 1.03 to 1.04) and undulated lamellar structure when Đ value increased from 1.1 to 1.5.

Asai *et al.*[38] studied the blend of different PI-*b*-PS-*b*-P2VP chains composed with the same molar mass of 130 kg.mol^{-1} and same middle-block volume fraction but different end-block

volume fractions (0.39:0.56:0.05 and 0.06 : 0.62: 0.32). Here tricontinuous gyroid structures were transformed into cylindrical ones, by forming a new tetragonal arrangement.

In this series of examples on PI-*b*-PS-*b*-P2VP, Ahn *et al*.[39] reported the blend of the terpolymer system with a diblock composed of PI-*b*-PS, in this case, a coexistence of spheres and cylinders with tetragonal packing was observed. Depending on the volume fraction used, for binary mixture of PI-*b*-PS-*b*-P2VP and PI-*b*-PS with overall volume fraction $f_{PI} = 0.12, f_{PS} = 0.79$ and $f_{P2VP} = 0.09$ a core-shell double gyroid was observed where P2VP was the matrix, PS formed thick shell and PI thin core.

Low dispersity values and high purity of block copolymers are of great importance in self-assembly, several polymerization techniques have been developed in order to achieve new polymer structures suitable for different applications. The next section details the synthesis procedure for block copolymers used in this thesis.

4. Linear ABC terpolymer synthesis

Several methods have been developed to synthesize myriad of structures of block copolymers with precise control of the chain-growth polymerization having a relatively narrow molecular weight distribution, or dispersity ($Đ \leq 1.5$).[40] The methods generally employed are living polymerization (anionic/cationic) or controlled radical polymerization (CRP): Nitroxide-Mediated Radical Polymerization (NMP), Atom Transfer Radical Polymerization (ATRP) or Reversible Addition-Fragmentation chain Transfer polymerization (RAFT).

The choice of polymerization mechanism to employ is adapted to the need of the polymer scientist depending on the final chemical functionality of the membrane.

For example, living anionic polymerizations offer excellent control of the block copolymer molecular weights and molecular weight distribution,[41] however this synthesis route is limited to a select number of monomers and the synthesis of multiblock polymers but also by the reaction medium which must be completely inert in order to avoid termination reactions.[42]

Conversely, controlled radical polymerization mechanisms are more compatible with different monomer types and less sensitive to ambient conditions than other controlled polymerization

mechanisms and can be easily scaled up. NMP, ATRP and RAFT polymerizations [43,44,45] all three have been used to generate nanostructured membranes from block polymer templates with a high degree of success each of these CRP polymerizations has its own unique set of positive aspects and potential drawbacks.

In this study, we used RAFT polymerization for the synthesis and design of linear ABC tribock terpolymers, the principals of the polymerization mechanism are detailed hereafter.

4.1. RAFT polymerization

RAFT polymerization was established for the first time at CSIRO laboratory in 1998[46–48] and since that time more than 8000 publications have been reported in the topic. RAFT polymerization is a versatile synthetic method to prepare highly functional polymers. This polymerization is mediated by a thiocarbonylthio compound called RAFT chain transfer agent (CTA) such as: dithioesters, trithiocarbonates, xanthates or thiocarbamates (**Figure 8**). Generally, CTA possesses a leaving group R and stabilizing Z group.[49] It ensures a reversible equilibrium in the reaction, minimizes irreversible termination and prevents termination giving polymers with high molecular weight and low polydispersity values. Finally, CTA can be easily removed at the end of the synthesis, if necessary for further applications.

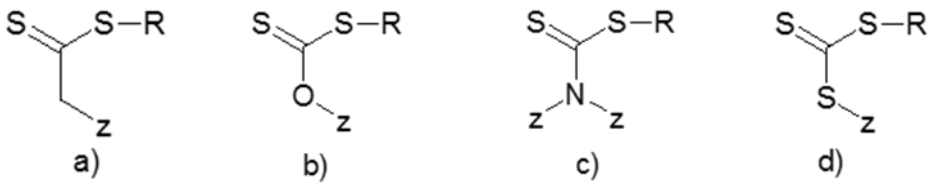

Figure 8. Chemical structures of several thiocarbonylthio transfer agents a) dithioester, b) xanthate, c) dithiocarbamate and d) trithiocarbonate.

Polymer chains synthesized by RAFT polymerization have the same degree of polymerization (DP) at a given time and the kinetic of the reaction depends on the insertion of the monomer between the **Z** and **R** groups on the CTA.[50]

RAFT mechanism is based on five steps as describe shown in **Figure 9**:

1. The two first steps are activation (or initiation) and propagation. Activation corresponds to radical initiation from free-radical source (*i.e.,* azobisisobutyronitrile AIBN), radical fragments generated will afterward react with a monomer to initiate chain growth. During propagation, longer chains are formed by the reaction of the growing chain with more monomer molecules.
2. The pre-equilibrium step corresponds to the addition of radicals on RAFT agent in order to enter in equilibrium between active and dormant species. The formed RAFT radical can fragment in both directions and the resulting leaving group R will act as new radical.
3. In the re-initiation step, another active polymer chain is started by the reaction of leaving group radical's and monomer.
4. The next step corresponds to the main equilibrium of RAFT polymerization, termed degenerate, since it involves a reversible transfer to the functional chain end-group. For an effective process, the addition/fragmentation equilibrium should be faster than the propagation, resulting in addition of less than one monomer unit added per activation cycle, finally all chains will have narrow dispersity and similar degree of polymerization at a given time.
5. The final step is termination, it represents the formation of a dead polymer formed for instance by coupling of two radicals.

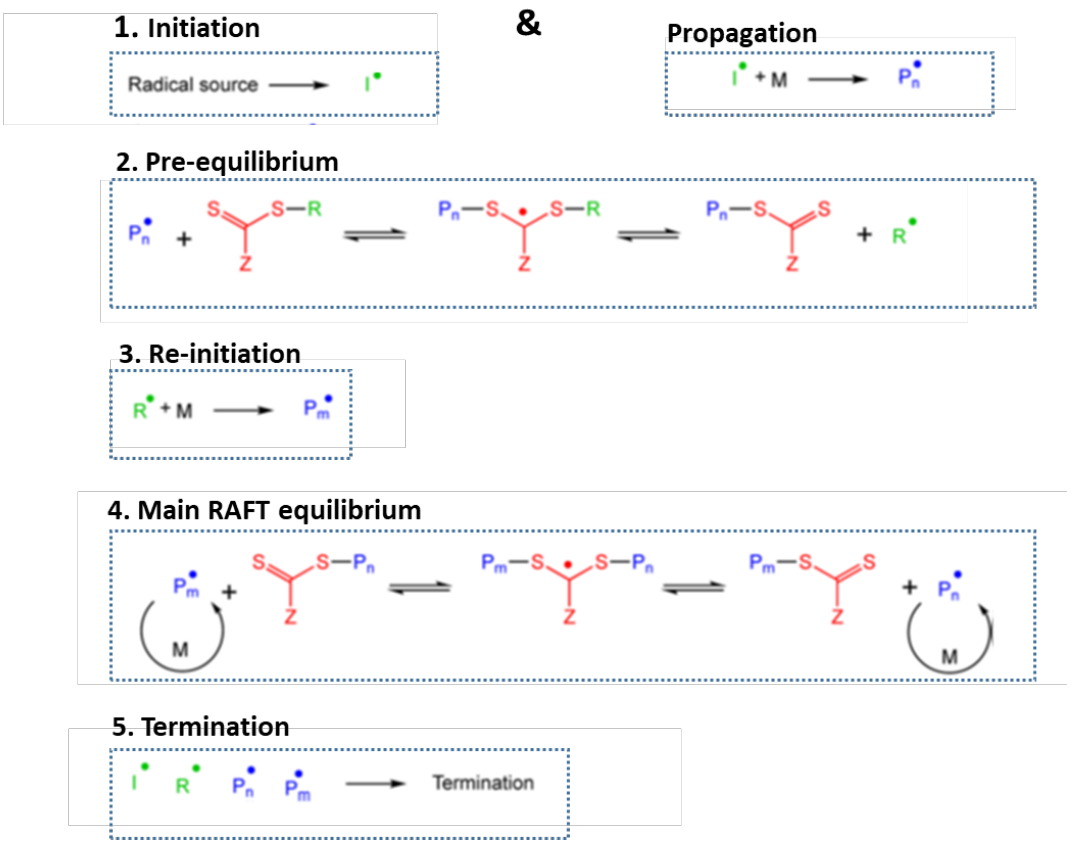

Figure 9. Mechanism of Reversible Addition-Fragmentation Chain Transfer (RAFT) polymerization.[54]

4.2. Parameters influencing RAFT polymerization

An optimal RAFT polymerization requires the tuning of different parameters that are detailed below.

4.2.1. Choice of RAFT agent

The choice of the RAFT agent is crucial for the synthesis of well-controlled architectures. It is chosen according to the target molecular weight and to insure good purity and low polydispersity. The effectiveness of CTA is determined by the substituents Z (the activating group) and R (the homolytic leaving group). The Z group determines the stability of the intermediate radicals and modifies both the rate of addition of propagating radicals to the

thiocarbonyl group and the rate of fragmentation of the intermediate radicals. For an optimal control of the reaction, the R group must be a good homolytic leaving group, in order to avoid any retardation effect, the generated radical (R•) must be able to reinitiate efficiently the polymerization.

RAFT agent should have an appropriate solubility in the reaction medium and possess the terminal group functionality required for the intended application, it must have a higher transfer constant, it should not undergo side reactions or retardation effect during the polymerization. In this work, the RAFT agent used for the synthesis of the ABC triblock terpolymers were purchased, nevertheless, different methods are available for the synthesis of RAFT agents.

Keddie *et al.*[51] have listed in their work, the different procedures for the design of RAFT agents, among them: carbodithioate salt with an alkylating agent, various thiocylation procedures, ketoform reaction, thiol exchange, radical substitution of a bis(thioacyl) disulfide and radical-induced R-group exchange.

4.2.2. Choice of monomer

Monomers used in RAFT polymerization are divided into two families according to their reactivity: “more activated” monomers MAMs and “less activated” monomers LAMs.

MAMs have a vinyl group conjugated either to a double bond, to a carbonyl compound or to a nitrile function, such as: butadienes, isoprenes, styrenes, vinylpyridines, (meth)acrylates or acrylonitriles. LAMs have an adjacent double bond to an oxygen, a nitrogen or a halogen, such as vinyl acetate, *N*-vinylpyrrolidones or vinyl chloride.

MAMs monomers generally produce more stable radicals and therefore require Z groups capable of ensuring the stability of the intermediate radical formed, but also in order to promote its addition to C = S bond of the CTA. Trithiocarbonates (Z = S-alkyl) or dithiobenzoates (Z = Ph) are generally designated to control the polymerization of monomers of MAMs type.

LAMs monomers are very reactive and poor homolytic groups, so they require a less stable intermediate radical than MAMs monomers. Therefore, xanthates (Z = O-alkyl) or dithiocarbamates (Z = N-alkyl) are generally designed in order to promote the fragmentation and the propagation step of the radical.

Beside, R group should be a good initiating group, to quickly reinitiate the propagation and thus to ensure low molecular weight dispersity and form radical with sufficient reactivity allowing it to be added to the monomer.

4.2.3. Reaction medium

RAFT polymerization process can be performed in homogenous as well as in heterogeneous medium. Similarly to conventional radical polymerization, RAFT polymerization can be performed in solution (organic solvent or water) or in bulk. At the exception of strong nucleophilic solvents that may degrade the thiocarbonylthio group of RAFT agent, most of organic solvents used in conventional radical polymerization can be used in RAFT polymerization.

Heterogeneous RAFT polymerization is often based on a self-assembly approach for instance *via* dispersion in aqueous system. Briefly, during this process, an amphiphilic macro-RAFT agent is formed which undergoes self-assembly into micelles then forming polymer particles.

Polymerization medium is a critical parameter during the reaction, since it can highly affect the kinetic.

4.2.4. RAFT kinetic

The rate of RAFT polymerization is highly dependent on the number of radicals initially present in the reaction. Indeed, in degenerative transfer system, the use of radical source allows tuning of the polymerization rate and the number of living and dead chains *via* the appropriate choice of polymerization conditions. Typically, in the case of initiation by thermal initiator *i.e.,* diazo or peroxide compounds, based on the amount of the decomposed with initiator in the time, the number of dead chains can be predicted. Furthermore, radical source in RAFT polymerization is key to the process, since it assures:

- good control of the reaction as the amount of dead chains in the system is determined by the number of radicals generated
- the polymerization rate which is directly related to radical concentration

The control of initiator concentration allows the control of the reaction by balancing rate speed of the reaction and livingness of the resulting polymeric chains. Typically, for a good control of the reaction, CTA: initiator ratio should be between 5 and 10. In this case, the number of radicals from the initiator are lower than the number of CTA, so the majority of chains come from the R-group during the re-initiation step.

The number of dead chains is governed by the number of radicals generated during the polymerization. Nevertheless, the rate at which the radicals are generated has no influence on the control of the reaction. Therefore, the polymerization rate is highly influenced by the rate of radical generation. For example the initiator 4,4'-azobis(4-cyanovaleric acid) (ACVA, half-life time of 10 h at 69 °C) result in 85% decomposition in 24h at 70°C in water, while the initiator 2,2′-azobis[2-(2-imidazolin-2-yl)propane] dihydrochloride (VA-044, half-life time of 10 h at 44 °C) undergoes 95% decomposition in 2h under the same conditions.

In this study, we used thermal initiation for the synthesis of the triblock but there exist other ways to initiate the reaction in RAFT polymerization such as redox initiation or light-induce initiation.

Finally, once the target polymer length has been reached, the reaction is generally stopped by cooling down the temperature and exposing the reaction medium to oxygen. The oxygen will react with the negligible amount of living radical in a termination way. The obtained polymer is in between the R group and thiocarbonate moiety of CTA. The polymerization can restart at any time by the addition of an initiator and another monomer in order to synthesize block copolymers, this is the reason why RAFT polymerization is called reversible.

In this work, RAFT polymerization was used for the synthesis of linear ABC triblock terpolymers in order to fabricate innovative isoporous membranes.
Different fabrication techniques have been developed for the conception of porous membranes. In the following section, we introduced the different process related to this study.

5. Fabrication techniques for polymeric membranes

An ideal membrane present high permeability and good selectivity with high density of pores that all possess a single and well-defined size. Currently, a trade-off between permeability and selectivity exists.[52] Membrane performances are highly dependent on the fabrication technique used. In this section, we will describe the most common techniques used to manufacture

membranes including details of the basic theory. A discussion of their advantages and limitations will be also conducted.

5.1. Track etching and others

Track etching technique is based on irradiating polymers with either energetic heavy ions, electrons, X-ray irradiation or UV light, resulting in the formation of linear damaged tracks through the exposed polymeric film (see **Figure 10.a**). The damaged tracks are transferred into pores using either properly selected wet chemical etching conditions or an applied electric field.[53]

Track-etched membranes have nearly uniform pore size distribution, resulting in highly selective membranes, but since the pores are sparsely distributed, this decreases the permeability (see **Figure 10.b).**

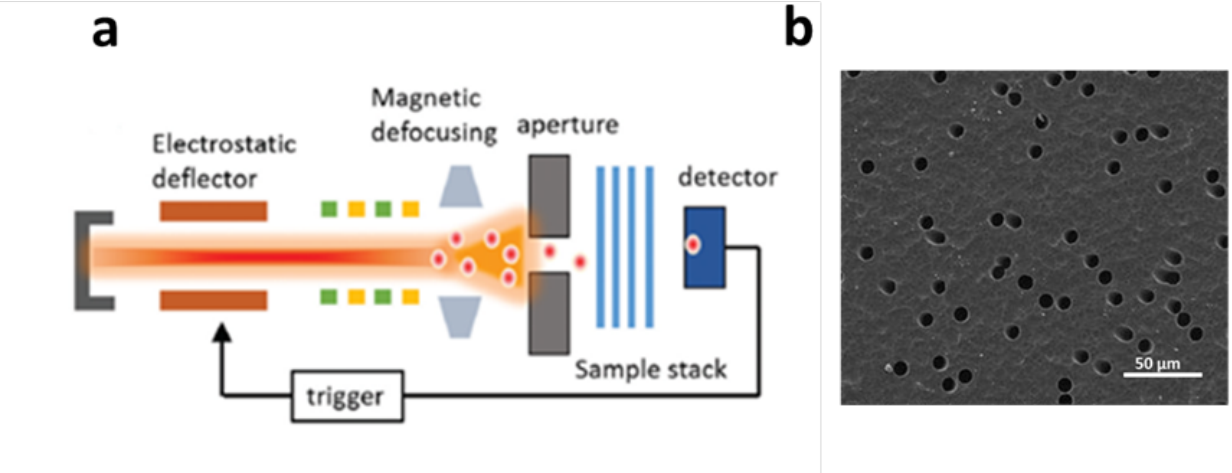

Figure 10. a) Sketch of track etching single irradiation setup [9] , b) SEM image of track-etched membrane.[58]

Lithography-based process is another type of manufacturing of porous polymeric membranes. It is based on a pressing of a template against (*i.e.,* mold) a deformable resist layer deposited on a substrate.[54] It can be easily scaled up and overcomes the issues of scaling up and fabrication

time. In addition, it can overcome the range of pore size, shape and density (obtained with track-etching). However, it remains limited by the high-cost fabrication of the master mold.

In order to improve the permeability of membranes, another technique based on the phase separation of polymers is currently used in the fabrication of porous polymeric membranes. During this process, the polymer passes in a controlled manner from a solution to a solid state. The membrane preparation is driven by a transition from a state in a homogeneous solution to a state with two liquids, this separation is also called liquid-liquid demixing. During the demixing process, the phase with the highest polymer concentration solidifies to form a solid matrix, leading to a control of the membrane morphology. By controlling the initiation of the phase transition, porous as well as non-porous membranes can be prepared. The well-known phase inversion processes for the fabrication of asymmetric membranes include: non-solvent induced phase separation (NIPS), self-assembly and non-solvent induced phase separation (SNIPS), thermally induced phase separation (TIPS), and vapor induced phase separation (VIPS).

In this work, we were interested on the use of the NIPS and SNIPS processes for the preparation of polymer structures with small nanopores. The next section will present the details regarding the fabrication of porous polymeric membranes derived from the block copolymer self-assembly.

5.2. Non-solvent Induced Phase Separation (NIPS)

This technique was introduced for the first time in 1962 by Loeb *et al.*[3] for the conception of asymmetric membranes for reverse osmosis. The asymmetric membranes are composed of a porous support layer providing mechanical strength and stability, covered by a thin selective layer providing separation capabilities. The membrane structure obtained is a result of a combination of a matter transfer and phase separation. During the NIPS process, the polymer solution (solvent + polymer) is casted on a suitable support using a doctor blade in order to achieve an homogenous thickness.[55] The polymer film is then plunged in a coagulation bath containing the non-solvent (the solvent used and the non-solvent must be miscible).At this stage, the solvent will diffuse into the coagulation bath while the non-solvent diffuses into the

film (see **Figure 11**). After a certain time, the exchange between the solvent and the non-solvent gives rise to a demixing in the solution. The resulting membrane, with a dense surface layer and a sponge-like sublayer, shows in many cases high flux, good selectivity and good mechanical stability.[55]

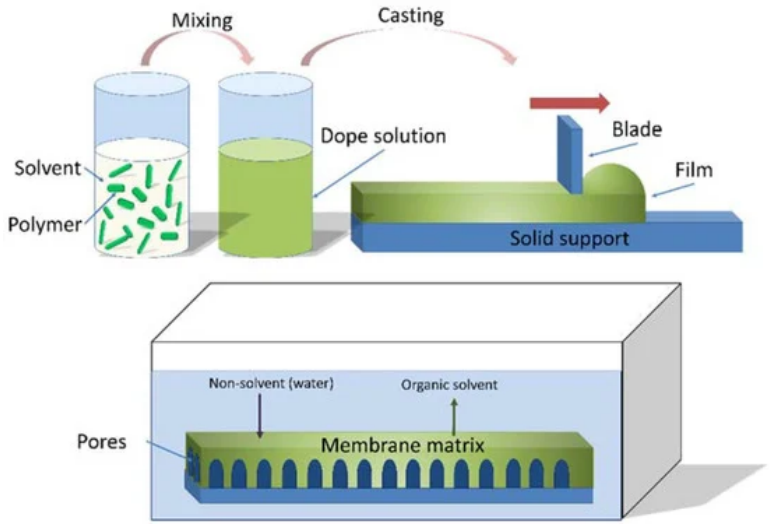

Figure 11. Schematic of the Non-solvent Induced Phase Separation (NIPS) technique.[61]

The final morphology of the membrane depends on several parameters:

- Choice of the polymer
- Choice of the solvent
- Polymer concentration in solution
- Molecular weight of the polymer
- Coagulation bath
- Temperature of the solution and of the coagulation bath
- Evaporation time
- Relative humidity
- The use of additives in the film

The membrane morphology can be modified from an open porous structure to a dense non-porous membrane by varying one or more of these parameters.

Comparing to track-etched membranes, the ones fabricated using a phase separation technique present high permeability thanks to their high porosities but are limited by a non-uniform pore size distribution that lower their selectivity.

In order to face this permeability-selectivity trade-off, it is essential to improve the fabrication of innovative materials having high density of pores with well-controlled size to produce membrane combining good selectivity and high permeability.[4]

5.3. Self-assembly and Non-solvent Induced Phase Separation (SNIPS)

SNIPS was developed for the first time by Peinemann and Abetz [56] for preparing isoporous block copolymer membranes having pores in a high-areal density. The SNIPS technique is a combination of the self-assembly of block copolymers with NIPS.

Similarly, to the NIPS process, the final membrane structure is determined by several parameters that should be carefully tuned such as choice of the block copolymer, concentration of polymer solution, choice of solvent or solvent mixture, evaporation time before precipitation and rate of solvent evaporation. In addition, the environmental conditions (temperature and humidity), nature of the non-solvent bath, initial thickness of membrane precursor and precipitation bath conditions are important parameter that governs the membrane structure.

In general, a successful SNIPS process implies the formation of monodisperse pores on the membrane top surface that strongly depends on the state of micellization of block copolymers in solution as well as on the morphology of the formed micelles and their stability (see **Figure 12**).

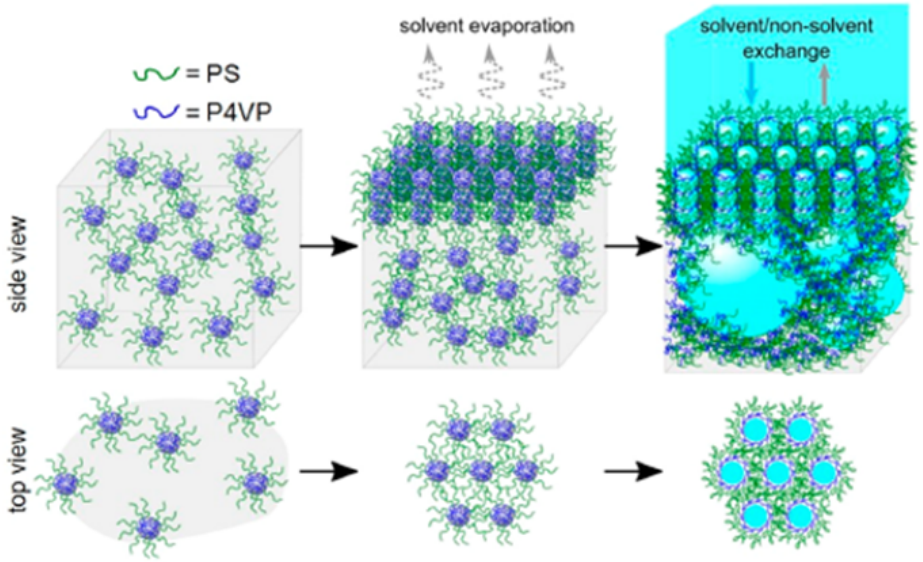

Figure 12. Schematic showing the different steps required to prepare of a PS-*b*-P4VP membrane by SNIPS where P4VP and PS form the core (blue) and corona (green) of micelles: (left) the film casting, (middle) the evaporation step, and (right) the precipitation in the non-solvent. The initially disordered micelles transform into packed and ordered hexagonal arrangement of cylinders.[1]

In SNIPS, the BCP self-assembly occurs in different steps: in the first one, a micellization takes place because of the unfavorable interactions between the solvent and one of the blocks above the critical micelle concentration (CMC). [57] In the second step, the micellization happens due to the interactions between the two polymer blocks at the surface-air interface.[58] The change in solution concentration and solvent selectivity caused by the variation of polymer-solvent interactions during the partial solvent evaporation, tune the initial stage of the emerging structural features and control the structure of the micelles. Additionally, the packing of block copolymer micelles in solution has an important impact on the final membrane structure.s

Finally, the obtained morphology depends on different parameters, firstly the nature of solvents used. The simplest case is the use of a solvent mixture showing equal affinities with the two blocks. In such conditions, the BCP chains can form an isoporous membrane with pores having a cylindrical morphology.[59] Conversely, a preferential segregation and unequal distribution in domains take place in the case of a solvent mixture where one solvent shows preferential affinities with one block.

In **Figure 13**, cross sectional views of PS-*b*-P4VP membranes obtained by SNIPS are presented. They show the effect of the evaporation time and the molar mass on the self-assembly. From the **Figure 13**, we can see that the thickness of the (effective) skin layer increases as a function of the evaporation time while the pore size increases as a function of the BCP molecular weight.

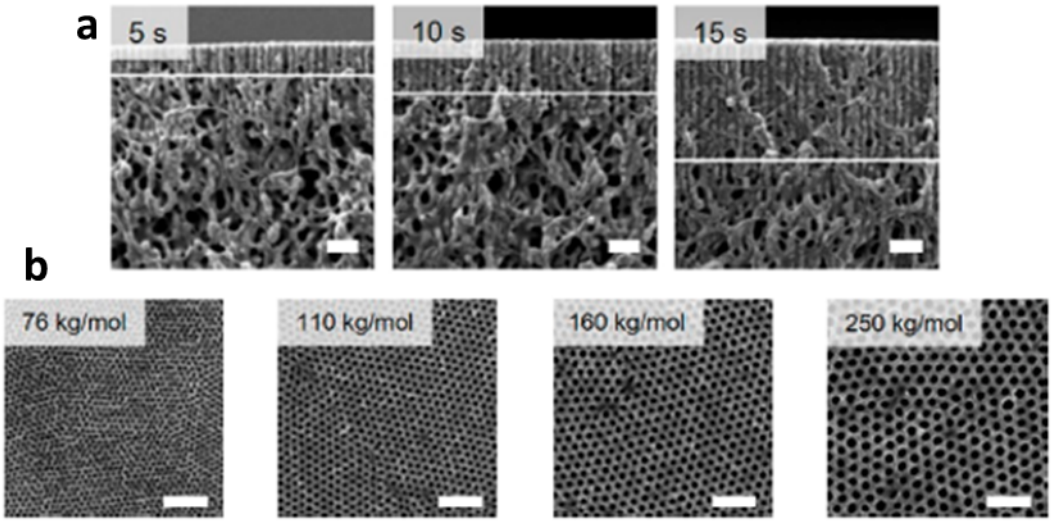

Figure 13. a) cross-sectional morphology of the formed PS-*b*-P4VP membrane showing an increase of the active layer with increase of evaporation time (scale bars of 200 nm) [67] and b) A larger average pore size is obtained by increasing the molar mass of the block copolymer (scale bars of 0.5 µm).[68]

5.4. Parameters influencing the SNIPS process

5.4.1. Concentration effect

Another critical parameter is the solution concentration. Timothy *et al.*[60] showed that the polystyrene-*block*-poly(ethylene)-*block*-poly(propylene) system presents different morphologies depending on the solution concentrations, including disordered spherical micelles, body-centered cubic spheres (BCC), hexagonally packed cylinders (HEX) and lamellae (LAM).

Foroutani *et al.*[61] showed that the formation of an ordered pore network is a highly concentration-dependent process, determined by the solvent evaporation time. They observed the formation of a highly permeable asymmetric isoporous polystyrene-*block*-poly(acrylic acid) (PS-*b*-PAA) membrane at relatively low casting solution concentration (15wt%) and over a wide range of evaporation time (40-120s) (see **Figure 14**). For such conditions, a hexagonal close-packed structure of micelles assembly was observed on the membrane selective layer.

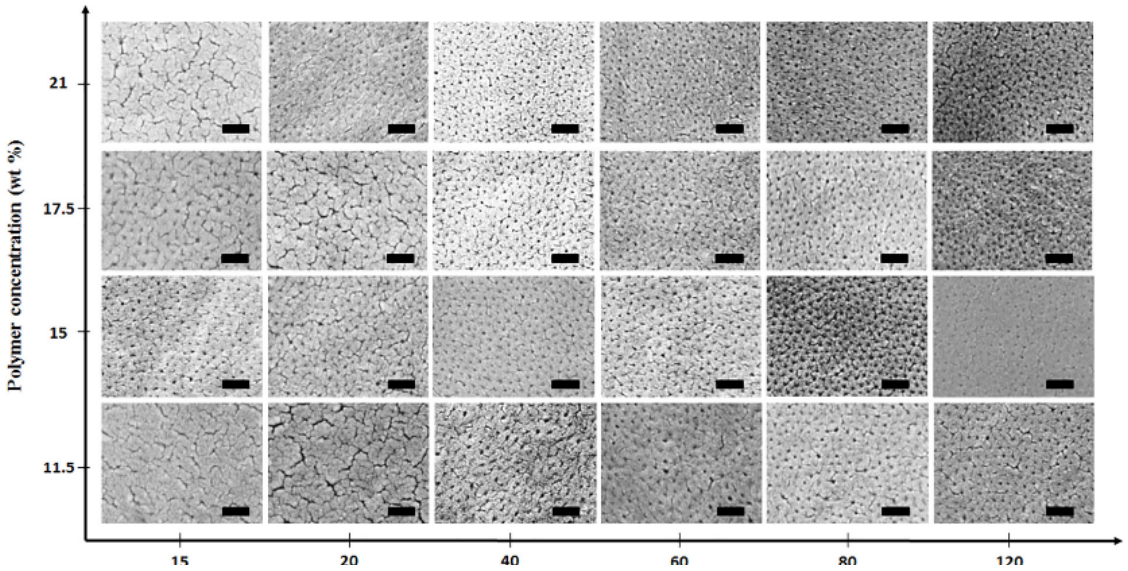

Figure 14. Field emission scanning electron microscopy (FE-SEM) micrographs of the top surface of PS-*b*-PAA membranes prepared from different casting solution and evaporation times (scale bars of 200nm).[70]

Finally, the polymer concentration and solvent selectivity are important parameters to insure the reproducibility of the SNIPS process, whatever the composition of block copolymers.

5.4.2. Phase inversion effect

In SNIPS, the solvent evaporation time is a critical parameter for the development of the nanophase. The time required to induce the desired nanostructure should match with the casting rate. Once the nanostructure is formed on the membrane top surface, it is trapped by plunging the film into a non-solvent bath.

Different studies focused on the analysis of what really happen when the casted film is immersed into coagulation bath. It can be realized by comparing the pore ordering on final membrane with structure obtained from the casting solution.[62] For instance, Stegelmeier *et al.*[63] showed that a large amount of a non-solvent can fully trap the transient pore structure by spraying a predefined volume of water onto the film that has be analyzed by in-situ SAXS analysis.

Other parameters can also affect the final morphology of the nanostructured membrane. Nunes *et al.*[64] studied the effect of pH of water bath on the formation of P4VP pores. They observed a decrease in the pore size concurrent with an increase of their density in acidic pH (from 6 to 2). Conversely, the pore formation was ineffective when the pH was increased to 10.

Jung *et al.*[65] studied the effect of temperature of the precipitation bath on the pore formation within isoporous PS-*b*-P2VP membranes. They observed the formation of uniform and regulated pores in water having a temperature under 3°C.They stated that the solvent exchange rate decreased in cold bath and the solution viscosity increased which is important to maintain the polymer assemblies during the phase inversion.

The final morphology of the isoporous SNIPS-made membranes are highly dependent on different parameters such as the molecular weight, polymer composition, temperature, solvent properties, polymer concentration, phase inversion and evaporation.[66] Therefore, the pore formation reproducibility as well as the surface functionalization are challenging to achieve by a SNIPS strategy. Besides the advantages of this technique, isoporous membranes obtained by SNIPS have permeability values lower than the theoretical predictions, this is due to the thick sublayer which shows a large flow resistance.[67]

To tackle this issue, additives can be added in order to increase the process reproducibility and tailor the polymer assembly during the pore formation. The performance of additives on regulating the polymer assembly highly depends on the polymer/additive properties and solution conditions.[68,69] These additives can be metal salts reacting with the block copolymer *via* coordination, like: $CuCl_2$, $Cu(Ac)_2$,$Cu(NO_3)_2$, $CuSO_4$, $AgNO_3$, $HAuCl_3$, $Zn(Ac)_2$, $Mg(Ac)_2$, LiCl, $Fe(Ac)_2$, $Co(Ac)_2$, Ni(Ac) or some sugars : glucose, saccharose.[70]

Polymers can also be used as additives reacting *via* H-bonding, van der Waals force or chain entanglement. The polymeric additive can be a homopolymer (*e*.g., P4VP, PAA, poly(ethylene

glycol) PEG, PS) or even a block copolymer such as: PS-*b*-PAA, PS-*b*-P4VP, PI-*b*-PS-*b*-P4VP or poly(isoprene)-*b*-polystyrene-*b*-poly(2(dimethylamino)ethylmethacrylate) (PI-*b*-PS-*b*-PDMAEMA). [71]

Nanomaterials like carbon nanotubes (CNTs), TiO_2 nanoparticles or graphene oxides (GOs) can as well be used as additives interacting *via* π-π interaction or H-bonding.[70]

The most popular additives used for the SNIPS process are metal salts and polymers. Metal salts form excellent coordination sites with the hydrophilic block of amphiphilic block copolymers. For example, the addition of copper acetate $Cu(Ac)_2$ to the casting solution of PS-*b*-P4VP promoted the formation of isoporous structure. Here, the Cu^{2+} ions were located within the P4VP corona lead to a stabilization of the phase-separated structures *via* a coordination interaction and protection of the polymer assemblies from deformation during phase inversion, thereby generating the formation of isoporous structure by SNIPS.

Cu-based heavy metal ions are generally used for the formation of isoporous membranes. However, their use in biological applications remains limited because of their toxicity. These toxic metal ions can be replaced by other heavy metal ions such as Mg^{2+} and Zn^{2+}, Ag^{+} or Au^{3+} having a much weaker coordination with BCP, so that the reduction of ions into nanoparticles is a facile way to eliminate their bad effect and endow membranes with desirable functions.[72] In this work, we were interested on the use of polymer additives rather than metal additives.

On one hand, polymer additives are often used in NIPS process to face the trade-off effect since they enable to tailor the surface wettability, improve fouling-resistance and manufacture membranes with novel functionalities[73,74]. On the other hand, polymer additives play a much more complicated role in the SNIPS process since their effect depend on the property, molecular weight and composition of polymers. In the next section, polymer additives are presented for both the NIPS and SNIPS processes according to their hydrophilicity and nature, (*i.e.*, homopolymer *vs*. block copolymer).

5.4.3. Hydrophilic homopolymer additives effect

Generally, isoporous membranes are prepared from block copolymers, so the use of polymer additives and especially hydrophilic homopolymers helps to tailor the block copolymer self-assembly as well as the membrane conception. Indeed, the hydrophilic homopolymer added will preferentially interact with the hydrophilic segments of the block copolymer *via* H-bonding interaction, which help to effectively avoid the undesirable macrophase separation during the mixing. Moreover, this selective interaction favors a pore size tailoring during the pore-formation due to the segregation of hydrophilic polymer additives.

For example, Phillip *et al.*[75] observed an increase of the pore size from 16 to 30 nm and a decrease in the uniformity of the isoporous structure by adding P4VP homopolymer to the casting solution of a PI-*b*-PS-*b*-P4VP system. In another study, Yang *et al.*[67] used PEGs with different molecular weight, and showed that the one with molecular weight close to that of the hydrophilic block in BCP presented the best pore-forming performance. Moreover, these authors demonstrated that the maximum loading amount preserving the isoporous structure was independent of the PEG molecular weight. They added two PEGs with a molecular weight of 20 kg/mol and 10 kg/mol and, they observed, in both cases, an increase in the pore size within the isoporous layer and a suppression of fingerlike pores leading to a decrease of the permeability of isoporous membranes.

Hydrophilic homopolymers are also used as promoters to drive the microphase separation of BCPs with low interaction parameters (χ). For example, Zhu *et al.*[76] used a hydrophilic PAA homopolymer as additive to blend a PS-*b*-PNIPAM membrane. The authors showed that the thermoresponsive PS-*b*-PNIPAM system has a low interaction parameter ($\chi \sim 0.05$) and was unable to form isoporous structure during the SNIPS process. In contrast, by using a blending strategy, a microphase separation happened due to H-bonding of the two hydrophilic PAA and PNIPAM polymers. This interaction resulted in a decrease in chain conformation of PAA and increase of interaction parameter (see **Figure 15**).

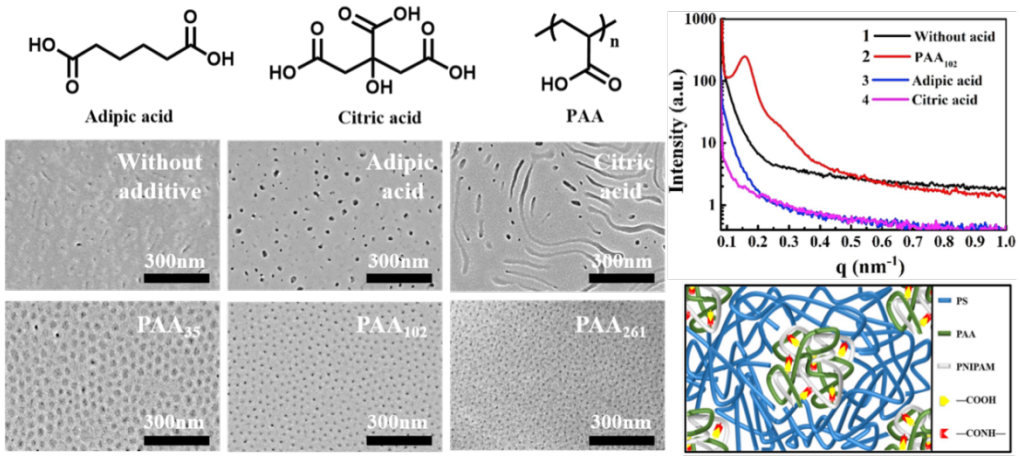

Figure 15. (Right) SEM images of isoporous membranes prepared from the blending of the PS-*b*-PNIPA film with PAA chains. (Left) SAXS results and scheme for PAA induced microphase separation in the casting solution.[78]

The use of polymer as additives can also affect the membrane flow resistance *via* an increasing the porosity at the cross-section. Yang *et al.*[67] observed that PEG homopolymers increased the finger-like pores at the cross-section, and reduced flow resistance of the support layer resulting in increase of membrane permeability. Ulbricht *et al.*[77] compared the effects of different additives on polyethersulfone (PES) ultrafiltration membranes. The additives were composed of polyvinylpyrrolidone (PVP), PEG and poly(ethylene oxide)-*b*-poly(propylene oxide)-*b*-polyethylene oxide), also called Pluronic®, Plu. The results showed that Pluronic was the best additive since the membranes characteristics and performances, including surface hydrophilicity, surface charge and water flux and rejection tests.

5.4.4. Hydrophobic homopolymer additives effect

Hydrophobic polymers had been more used to regulate the BCP self-assembly within thin films than as additives in SNIPS. This is due to the weak molecular interaction and the risk to induce a macrophase-separation.

Kenneth *et al.*[78] and Mayes *et al.*[79] observed that the homopolymer distribution and their role in the polymer self-assembly is highly dependent on their molecular weight. Yang *et al.*[70] used

a PS homopolymer with a low molecular weight as additive within PS-*b*-PAA membranes and observed a change in the pore orientation. Indeed, the cylindrical pores, oriented parallel to the free surface of unblended membranes, adopt a perpendicular orientation within PS-*b*-PAA/PS membranes (see **Figure 16**).

The use of hydrophobic homopolymers as additives remains limited since they tend to decrease the hydrophilic segment effectiveness and potentially lead to fouling issues.

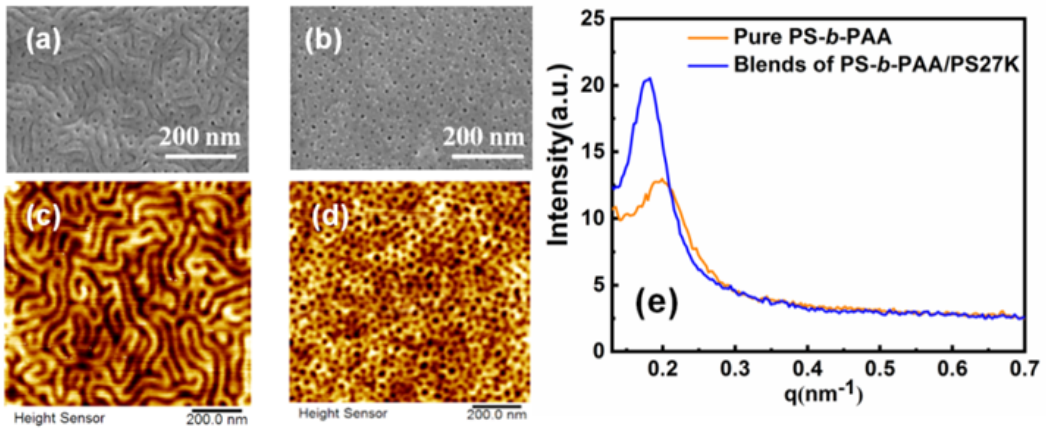

Figure 16. SEM images of membranes prepared (a) from pure PS-*b*-PAA chains and (b) from a blend of PS-*b*-PAA and PS. (c) AFM topographic images of solvent-annealed (dioxane, 9h) thin films casted (c) from pure PS-*b*-PAA chains and (d) from a blend of of PS-*b*-PAA and PS. (e) SAXS results for casting solution with pure PS-b-PAA and a blend of PS-*b*-PAA and PS

5.4.5. Block copolymers as additives effect

The use of block copolymer as additives is more complicated than homopolymers since the co-assembly of block copolymer pairs is difficult to predict. In the case of AB diblock copolymers, blending of block copolymers can be through different ways: 1) A-B/A'-B' (A' and B' are of the same nature as A and B blocks with varied compositions and molecular weights), 2) A-B/A'-C, and 3) A-B/C-D.[80,60,81,36] Depending on compositions and selective interaction between blocks, the blending classification can be subdivided into subgroups.

Commonly, in SNIPS process, produced isoporous membranes are from cylindrical self-assembly of block copolymers in equilibrium. The blending is limited to A-B/A'-B' and A-B/A'-C where A and A' are major blocks while B and C are minor blocks.

Maryam *et al.*[82] compared isoporous membrane formation from the blending of PS-*b*-P4VP diblock copolymers with different compositions and molecular weights. They firstly reached the concentrations allowing the preparation of isoporous membrane at any blending ratio, then they adjusted the mixing ratio in order to regulate the pore size.

Yu *et al.*[59] studied the blending of two PS-*b*-PAA block copolymers with different molecular weights. They found that the load of a BCP with a low molecular weight was favorable to reach the exact thermodynamic conditions for self-assembly, resulting in the formation of hexagonal pores.

The fabrication of isoporous membranes by SNIPS from the blending of different block copolymers at any ratio, remains a big challenge. However, the strategy of blending opens the accessibility to diverse pore functionalities, improve membranes hydrophilicity, fouling-resistance, stimuli-responsiveness and separation performances from a simple fabrication process.

5.5. Comparison between SNIPS and NIPS

The procedures of SNIPS and NIPS are almost identical but the self-assembly in SNIPS makes the major difference. The porosity within the thick sublayer of isoporous membranes fabricated by SNIPS is induced by NIPS mechanism. Since both processes share a close relationship, it seemed important to us to compare the additive performances in both processes.

In NIPS process, there is no microphase-separation occurring during the preparation of the porous membranes. In this case, the use of additives leads to a regulation of the macrophase separation that is determined by the competition between thermodynamic and kinetic effects. Commonly, membranes prepared by NIPS present a disordered porous structure with a broad pore size distribution, poor defects control and no structural reproducibility compared to isoporous membranes prepared by SNIPS. As seen in the previous section, additives are able to

increase the porosity and pore connectivity in the sublayer resulting in an improvement of the trade-off effect. Yang et al.[70] resumed the additive effects on pore-forming functions in NIPS and SNIPS.

To improve the tradeoff effect, in NIPS process, it is preferable to use homopolymers with high molecular weights and broad distributions, while in SNIPS, block copolymers can be used. The difference between the two process is also illustrated during different steps. For example, in NIPS process it is not required to drive microphase separation since neither to control pore orientation, the evaporation induced self-assembly is also absent. Moreover, comparing to SNIPS, there is no increase in structure reproducibility, but it is necessary to tailor the surface roughness.

In conclusion, NIPS technique is a revolutionary technology in membrane preparation, although the uncontrolled phase demixing lead to broad pore size distributions that limit the membrane selectivity. SNIPS process is an innovative strategy to face this problem by combining block copolymer self-assembly with NIPS. Additives such as metal salts, small organics, polymers or nanomaterials play an important role in the reproductive generation of isoporous structures. Additives used as porogens drive the microphase separation and regulate the formation of isopores. The ones used as functional modifiers allow for the preparation of isoporous membranes with new functionalities such as stimuli-responsiveness, fouling-resistance, etc.

Finally, SNIPS process is an improvement of NIPS process, but without the use of additives, it remains limited by the formation of kinetically trapped low-dimensional nanostructure, making inaccurate the fabrication of highly selective, well-controlled and reproducible membranes.[4]

In this work, we were also interested in another technique capable to drive the BCP self-assembly into long-range ordered nanostructures, namely, the solvent vapor annealing (SVA). This process allows the formation of well-ordered three-dimensional morphologies with control of the growing network structure. The following section is devoted on the principals of this technique and its application in the formation of isoporous membranes.

5.6. Solvent Vapor Annealing (SVA)

The solvent vapor annealing technique was firstly used as an alternative to thermal annealing for BCPs with thermal degradation problematic. SVA is a powerful technique to achieve long-range ordered nanostructures, due to the increase of the chain mobility of the polymers. During this process, BCP film is exposed to vapors of one or several organic solvents, depending on the affinity between blocks and solvent(s) and Hildebrand solubility parameter, polymer will preferentially absorb the "good" solvent and swell, resulting in the formation of thicker film. Within the swollen film, the polymer chain mobility increases due to decrease of glass transition below room temperature.[83]

Comparing to other techniques such as thermal annealing, nonequilibrium metastable phases can be obtained.[84,85] Indeed, thermal annealing technique is based on heating of a thin BCP film above the glass temperature (T_g) and below the order-to-disorder transition temperature (ODT). Thermal annealing is limited to block copolymers with low χ values or low molecular weights, otherwise, high annealing temperature and longer time are required to reach lower configuration.

The SVA apparatus is composed of a sealed chamber containing polymer film casted on appropriate substrate connected to a solvent reservoir held at room temperature with no additional controls over temperature. The SVA is also equipped with mass flow controler in order to get greater control over the degree of swelling and improved reproducibility (see **Figure 17**). The final morphology obtained by SVA is highly dependent on several parameters such as the annealing chamber volume, surface area and the absence of any solvent vapor leak.

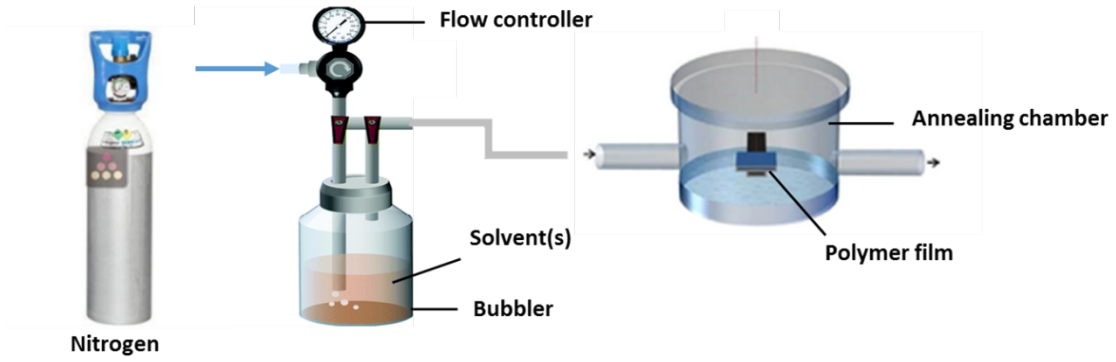

Figure 17. Solvent Vapor Annealing (SVA) setup. Adapted from [93,94**].**

Despite the formation of long-range-ordered morphologies, the mechanism involved in SVA process is not understood yet.[86] In situ analysis is critical to understand the intermediate degree of swelling and to control the reproducibility.

The efficacy of the vapor annealing can be affected by several parameters that have to be considered when preparing block copolymer thin film *via* SVA. Firstly, the choice of the BCP composition, the χ-parameter between the blocks and the solubility of the BCP in the solvent used. Secondly, the nature of substrate surface, depending on its hydrophilicity, the wettability of the film can be influenced, resulting in a change during the film deposition (change in thickness and uniformity) which is a critical parameter in thin film formation. Furthermore, the thickness of the film is also highly dependent on the polymer deposition process. Finally, solvent vapor annealing conditions within the chamber such as: temperature, relative humidity, time of annealing, purity of solvent and size of annealing chamber play major roles in final morphology of thin film. The choice of solvent is a critical parameter, it must be neutral or selective for one of the blocks. Once exposed to solvent vapor, polymer film swells until thermodynamic equilibrium represented by equal chemical potential of the solvent in the film and solvent in the vapor phase.

In 1998, Albalak *et al*. [87] suggested in their work that during the SVA process, the polymers swell and reach a thermodynamically preferred arrangement. In the same year, Kim *et al*.[88] studied the effect of the evaporation rate on the final morphology obtained from a polystyrene-*block*-poly(butadiene)-*block*-polystyrene terpolymer casted from toluene. Fukunaga *et al.*[89] and Knoll *et al.*[90]showed in their work how vapor solvent exposure allows rearrangements from disordered to well-ordered state. In 2004, Kim *et al*.[91] explained in their work that drying have an important influence on the final structure in the dried film. They suggested that domains have a preferential orientation in a direction perpendicular to the solvent front, resulting from the evaporation of the solvent at the free surface that generating a front propagating from the interface through the thickness of the film.[86]

Inversely to thermal annealing, heat-sensitive polymer can be used in SVA since the process can be performed below the BCP glass temperature. SVA is a very versatile technique since a wide range of solvents with different characteristics (solubility parameters, vapor pressure, etc.) can be used.

In the following part, some examples of solvent-annealed linear triblock terpolymers are presented.

In 2018, Lee *et al.*[92] studied the morphology evolution as a function of the as-cast film thickness and solvent affinity of a PS-*b*-PDMS-*b*-PS triblock terpolymer. By using a solvent mixture of toluene and heptane, they observed a morphology transition from a bilayer of cylinders to a bilayer of lamellae, passing through a bilayer of perforated lamellae.

Lee *et al.*[93] studied the morphology evolution of the PDMSB-*b*-PS-*b*-PMMA (DSM) and PDMSB-*b*-PS-*b*-PLA (DSL) systems during the SVA process (in chloroform) using an in-situ grazing-incidence small-angle X-ray scattering (GISAXS) technique. They observed the formation of in-plane core-shell PMMA-PS cylinders within a 90 nm thick DSM film and out-of-plane core-shell PLA-PS cylinders within perforated lamellae oriented parallel to the substrate for a 150 nm thick DLS film. In another study, Lee *et al.*[94] studied the self-assembly of three triblock PS-*b*-PI-*b*-PMMA with different compositions in THF and in chloroform. In this study, they explained that the phase behavior during SVA is not simply predictable by solubility parameters and separate swelling measurements. THF and $CHCl_3$ have similar solubility parameters and both are neutral for all blocks. Interestingly, under a chloroform vapor, the ABC triblock terpolymers showed different morphologies from the one obtained from thermal annealing, and the cylinder-in-cylinder (cic), cylinder-on-cylinder (coc) and cylinder-on-lamellar (col) phases were observed. Otherwise, under THF vapor, no change in self-assembly was noticed. This is due to a preferential swelling of the blocks in the solvents. Indeed, in this case, PMMA swells preferentially in chloroform than PI and PS, resulting in change of PMMA volume fraction. Meanwhile, THF swells all the blocks equally.

More recently in 2020, Vayer *et al.*[95] studied bulk sample of binary PI-*b*-PS-*b*-P2VP, they observed new morphological composition illustrated by hexagonal morphology composed of centered hexagons of PI surrounded by P2VP. Here the chain length difference of PI favored the formation of bigger domain with stable conformation entropy.

As part of conception of new porous membrane from block copolymer self-assembly, SVA technique can be associated to SNIPS or NIPS in order to generate a new membrane generation.

Aissou *et al.*[96] combined NIPS and SVA to produce long-range ordered network. In this work, the triblock terpolymer composed of PDMSB-*b*-PS-*b*-PMMA generated a disordered phase by

NIPS on the film top surface. The disordered phase was then transformed into a highly ordered bicontinuous network without disrupting the substructure morphology.

In the same strategy, a sponge-like substructure topped by a nanostructured dense top layer was obtained from a PDMSB-*b*-PS-*b*-P2VP system by combining the SNIPS and SVA techniques.[4]

In this work, the square array morphology formed on the membrane top surface by SNIPS was transformed into a thick core-shell perforated lamellae after 3h of annealing in $CHCl_3$, and by increasing the duration of SVA (18h), monolith entirely composed of bicontinuous perforated lamellae were obtained.

Nowadays, membranes play a major role in sustainable development of several fields (energy, environment, human health, etc.), however, efficient membrane applications are generally restricted due to the pore fouling generated by the accumulation of retentates on the membrane top surface. Inspired by biological membranes with stimuli-responsive channels, synthetic membranes with artificial stimuli-responsive smart gating are developed by chemically/physically incorporation of stimuli-responsive materials into porous membrane in order to provide smart membranes with advanced functions and improved performances for breaking trade-off of traditional membrane technologies. In this study, we work on the development of smart stimuli-responsive membranes with anti-fouling properties. The following section is devoted to the principles of smart membrane preparations.

6. Antifouling membranes

The development of smart membranes with self-regulated permeability and selectivity can expand and create new opportunities for membrane applications. External stimuli-responsive functions can be incorporated chemically or physically into porous membrane substrates as functional gates. These environmental stimuli can be temperature, pH, specific ions/molecules, light, magnetic fields and redox. They will provide a conformational switch for adjusting the pore size and/or the surface properties of the membrane.

Self-regulated membranes with enhanced performances are used in myriad of applications. In the next section, we will focus on the introduction of these stimuli-responsive gates on porous membranes, specifically the fabrication strategies and advanced applications.

It can be passive fouling-resistant, fouling-release mechanism or active antibacterial mechanism.

6.1. Passive fouling release membranes

Fouling-release membranes are generally fabricated from low surface energy materials that firstly weaken the interaction between membrane surfaces and foulants and secondly, release the foulants under low shear forces.[97]

Passive mechanism aims to prevent the initial adsorption of foulants on the membrane surface without affecting the intrinsic feature of the membrane, while active antifouling strategy is based on the presence of antimicrobial agents able to kill bacteria by interfering with biochemical. [98]

As an example in the fabrication of fouling release membrane, Zhao *et al*.[99] manufactured amphiphilic membranes from PEO-*b*-polydimethylsiloxane (PEO-*b*-PDMS) by NIPS where the hydrophilic PEO block was used to prevent the adsorption of biofoulants while the hydrophobic PDMS block having a low surface energy was used to drive away the adsorbed foulants. In the same strategy, a variety of amphiphilic copolymers composed of hydrophilic block (*e.g.* PEG) and non-polar, low surface energy segments (*e.g.* fluoroalkyl and semifluorinated side chains and perfluoropolyether segments) were also used to generate membranes.[98] Gao *et al*.[97] fabricated antifouling and antibacterial membranes from poly(hexafluorobutyl methacylate)-*block*-poly(ethylene glycol) methyl ether methacrylate)-*block*-poly[2-(methacryloyxyl)ether trimethylammonium chloride) (PHFBM-*b*-PEGMA-*b*-PMTAC) since PHFBM has a low surface energy, PGEMA is hydrophilic and PMTAC is antibacterial. In this case, a combination of passive fouling-release mechanism (via PHFBM and PEGMA segments) and active antibacterial mechanism (via PMTAC segment) was obtained.

Several antifouling mechanisms can be combined and form multi-defense mechanism membranes that can be more efficient for oil fouling for example. In this study, we worked on the development of fouling-resistant membranes from stimuli-responsive block copolymers.

6.2. Stimuli-responsive membranes

Biological cell membranes with stimuli-responsive channels (also called "smart gates") able to selectively open or close for specific substances to transfer across and to maintain the desired intracellular and extra cellular concentrations to insure life activities are of great inspiration for the development of artificial smart membranes for achieving advanced performances. [100]

By definition, smart gating membrane are synthetic membranes with responsive gates (in the membrane pores) able to regulate the trans-membrane transport of substances in response to external stimuli.[101]

Generally, the open/close state of the pores is achieved through the shrinking/swelling transitions of stimuli-responsive gates, which leads to an increase/decrease of permeability. Furthermore, the hydrophobic/hydrophilic transition associated with the shrinking/swelling behavior of the gates can adjust the surface properties of the pores.[5]

The stimuli-responsive gates can be introduced in two different ways: during the membrane preparation or after the membrane preparation. In the next section, we will present the different strategies for introduction of stimuli-responsive gates.

6.2.1. Introduction of stimuli-responsive gates after the membrane formation

This strategy is more popular, consisting on the introduction of responsive domains into or onto the pre-formed pores[101] by different methods including chemical grafting, physical coating or pore-filling.[102] The chemical grafting can be divided into the "grafting-from" and "grafting-to" methods.

For the "grafting-from" technique, membranes are fabricated by polymerizing functional monomers from the active site to form cross-linked networks in the pores or linear polymers. This grafting can be chemical, UV-induced or plasma-induced. A wide range of functional gates can be incorporated into various membrane substrates to create smart gating membranes.

The "grafting to" strategy is based on the incorporation of the pre-formed functional gates in the form of polymer chains or microspheres onto the pores surfaces. The incorporated polymer chains or microspheres can be pre-synthesized by well-established methods, resulting in well-

controlled macrostructures. This grafting strategy offers improved controllability and flexibility for the microstructure.

Otherwise, such methods provide good control of the mechanical properties of the membrane but could cause an inherent conflict between the flux and the responsive property: the more responsive domains introduced, the more significant the responsive property and the lower is the flux.

Beside the effect of the responsive property on the membrane flux, the introduction of stimuli-responsive gates after membrane preparation techniques requiring two-step processes are still difficult to be scaled up and it is difficult to have an efficient grafting rate.

6.2.2. Introduction of stimuli-responsive gates during the membrane formation

Conversely, this strategy is one-step process, during which stimuli-responsive gates are introduced during membrane formation. The gates are generally stimuli responsive block copolymers, they are usually blended with membrane-forming polymers during the membrane formation.

The main advantage of this one-step method for membrane modification is the easy scale-up to industrial membrane fabrication.

There are different external stimuli-responsive gates in the smart membrane fabrication. Typically temperature and pH are the most common parameters varying in biological/chemical reactions and organ tissues[103], moreover ions (such as potassium ions) are essential for biological metabolism.[104] The biological system can also be influenced by other parameters such as concentration of glucose molecules in the blood which is a critical indicator for diabetes and hypoglycemia, light and magnetic fields are also important parameters.[105,106] 5

In the following section, few examples of smart stimuli-responsive membranes are presented.

6.3. pH-responsive membranes

Polymers with weak alkaline groups able to be protonated or deprotonated are also used as pH-responsive gates. For example, poly(*N,N*-dimethylamino ethyl methacrylate) (PDMAEMA) is a pH-responsive polymer where in acidic conditions, it can swell due to the electrostatic repulsion between protonated amine groups and *vice versa* in basic conditions, it is deprotonated and PDMAEMA is shrunk.

Inversely, pH-responsive gates having weak acidic groups and can gain or lose protons in response to pH changes. In this case, in acidic environments, polymer chains can shrink due to the formation of intermolecular hydrogen bonding and in basic conditions, they can swell due to the electrostatic repulsion between the protonated carboxylic groups.

In this strategy, Fan *et al.*[107] fabricated a dual pH-responsive smart gating membrane by blending PDMAEMA microgels into poly(ether sulfone). The protonation and deprotonation of the pH responsive PDMAEMA in acidic and basic environment, respectively, resulted in opening and closing of the membrane pores. The resulting dual pH-responsive membrane can be used in myriad applications such as sewage treatment or drug delivery.

Xiang *et al.*[108] modified PVDF membrane by incorporation of pH-responsive PDMAEMA hydrogels. The membrane has been used for the separation of surfactant-stabilized water-in-oil and oil-in-water emulsions. The protonation and deprotonation of tertiary amine side-groups in PDMAEMA affect the wettability of the membrane. High flux separation and anti-fouling properties have been obtained.

6.4. Thermo-sensitive membranes

Thermo-responsive polymers such as *N*-substituted polyamides, polyethers, poly (2-oxazoline), poly(vinyl caprolactone) and poly(methyl vinyl ether) are widely used for fabrication of positively responsive gating membranes.

For example, poly(*N*-isopropylacrylamide) PNIPAM with its low critical solution temperature (T_{LCST}~ 32°C) is widely used in membrane fabrication. At temperature below LCST, the PNIPAM chains are hydrophilic and swollen due to the hydrogen bonding between the amide function and water molecules, hence the membrane pores are "closed". On the other hand, by increasing temperature above LCST, the hydrogen bonds are cleaved since the polymer is shrunken and hydrophobic, making that membrane pores are "opened".

Thermo-sensitive polymers with an upper critical solution temperature (UCST) can also be used to tune the membrane pores, such as polymers with interpenetrating networks (IPNs) composed of poly(acrylamide) (PAAm) and (PAAc).[5] Inversely to polymers with LCST, in this case, at temperature below the IPN UCST, PAAm and PAAc form complex *via* hydrogen bonds resulting in pore "opening". At temperature above UCST, the hydrogen bonds break allowing a pore "closing" state.

Finally, LCST and UCST of polymers can be tuned by incorporating hydrophilic or hydrophobic groups into the polymer chains, thus, the membrane pores can switch from an "open" to a "closed" state once the temperature increases or decreases.

Huang *et al*.[109] grafted poly(*N*-isopropylacrylamide)-*b*-poly(ethylene glycol) methacrylate) PNIPAM-*b*-PGEMA chains on the surface of porous polypropylene (PP) by plasma-initiated method. The hydrophilic BCP was able to improve both anti-fouling and self-cleaning membrane's performances. Bovine serum albumin (BSA) was used as foulant and the membrane presented high water flux recovery with 98.2% less BSA on the surface.

Cetintas *et al*.[110] prepared a fully reversible thermo-responsive membrane of PS-*b*-PNIPAM by SNIPS. The resulting membrane with worm like cylinders morphology with interconnected nanopores presented a higher permeability value (up to 400%) going from room temperature to 50°C. Zhao *et al.* [111] prepared smart anti-fouling and self-cleaning membrane from PNIPAM-SiO_2 (silicon dioxide) nanoparticles grafted on PVDF ultrafiltration membrane *via* a blending method. The resulting membrane showed increased permeability values between 25°C and

37°C, and decreased values in irreversible fouling ratio. The self-cleaning properties were represented by a continuous increase in BSA adsorption-desorption ratio with temperature switching around LCST.

Different stimuli-responsive gates can be combined to form novel smart membrane. In this strategy, Clodt *et al*.[112] prepared pH and thermo-sensitive membrane by modification of asymmetric PS-*b*-P4VP membrane with PNIPAM by surface linking reaction. The resulting membrane showed an increase in permeability with increase of temperature from 22 to 40°C.

7. Conclusion

In this bibliographic study, a general context of this thesis work was described. The existing ultrafiltration membranes face a selectivity-permeability trade-off and practical challenges such as fouling, degradation and material failure that limit their use.

Currently, the main challenge in membrane technology is the development of next-generation membranes with uniform nanopores to surpass the existing selectivity-permeability trade-off. In this context, block copolymers are excellent candidates due to their capability of self-assembly into periodic nanostructures with a range of controllable morphologies. Block copolymers membranes produced by phase inversion are limited by the uncontrolled formation of regular pores on the skin layer, which limit the use of this technique on large scale. The combination of solvent vapor annealing process with phase inversion technique open access to broad structural diversity and manufacture of asymmetric membrane having an equilibrium morphology within the skin layer.

Fouling-resistant membranes composed with smart isopores are highly desired in order to reach next-generation ultrafiltration membranes. In this strategy, stimuli-responsive polymers can be used due to their “open-close” behavior in response to an external stimulus (temperature, pH, UV-light …etc.) leading to an increase/decrease of membrane permeability and to an adjustment of the pores surface properties.

8. References

1. Hampu, N., Werber, J. R., Chan, W. Y., Feinberg, E. C. & Hillmyer, M. A. Next-Generation Ultrafiltration Membranes Enabled by Block Polymers. *ACS Nano* **14**, 16446–16471 (2020).
2. John, R., Pal, K., Jayan, J. S., Appukuttan, S. & Joseph, K. New emerging review on advances in block copolymer based water purification membranes. *J. Mol. Struct.* **1231**, 129926 (2021).
3. 1963 loeb and sourirajan.
4. Aissou, K. *et al.* Bicontinuous Network Nanostructure with Tunable Thickness Formed on Asymmetric Triblock Terpolymer Thick Films. *Macromolecules* **52**, 4413–4420 (2019).
5. Liu, Z., Wang, W., Xie, R., Ju, X.-J. & Chu, L.-Y. Stimuli-responsive smart gating membranes. *Chem. Soc. Rev.* **45**, 460–475 (2016).
6. Querelle, S. Synthèse et utilisation de copolymères triblocs ABA pour l'élaboration de membranes poreuses à morphologies et performances contrôlées. 311.
7. Shannon, M. A. *et al.* Science and technology for water purification in the coming decades. in *Nanoscience and Technology* 337–346 (Co-Published with Macmillan Publishers Ltd, UK, 2009). doi:10.1142/9789814287005_0035.
8. van Reis, R. & Zydney, A. Membrane separations in biotechnology. *Curr. Opin. Biotechnol.* **12**, 208–211 (2001).
9. Olson, D. A., Chen, L. & Hillmyer, M. A. Templating Nanoporous Polymers with Ordered Block Copolymers. *Chem. Mater.* **20**, 869–890 (2008).
10. Chrystilla Reboul. Auto-assemblage de copolymères à blocs à haute force de ségrégation dans une configuration de film mince. Autre. Université Sciences et Technologies - Bordeaux I, 2013. Français. ffNNT : 2013BOR15235ff. fftel-01017175f.

11. Kassam, A.-K. & Trefethen, L. N. Fourth-Order Time-Stepping for Stiff PDEs. *SIAM J. Sci. Comput.* **26**, 1214–1233 (2005).
12. Lodge, T. P., Bang, J., Li, Z., Hillmyer, M. A. & Talmon, Y. Introductory Lecture : Strategies for controlling intra- and intermicellar packing in block copolymer solutions: Illustrating the flexibility of the self-assembly toolbox. *Faraday Discuss.* **128**, 1 (2005).
13. Nisticò, R. Block copolymers for designing nanostructured porous coatings. *Beilstein J. Nanotechnol.* **9**, 2332–2344 (2018).
14. Matsen, M. W. & Bates, F. S. Origins of Complex Self-Assembly in Block Copolymers. *Macromolecules* **29**, 7641–7644 (1996).
15. Morphologies and tensile properties of block copolymers with different molecular architectures. 133.
16. Musteata, V. *et al.* Self-assembly of polystyrene- b -poly(2-vinylpyridine)- b -poly(ethylene oxide) triblock terpolymers. *Eur. Polym. J.* **100**, 121–131 (2018).
17. Hiekkataipale, P. *et al.* Controlling the shape of Janus nanostructures through supramolecular modification of ABC terpolymer bulk morphologies. *Polymer* **107**, 456–465 (2016).
18. Bailey, T. S., Hardy, C. M., Epps, T. H. & Bates, F. S. A Noncubic Triply Periodic Network Morphology in Poly(isoprene- *b* -styrene- *b* -ethylene oxide) Triblock Copolymers. *Macromolecules* **35**, 7007–7017 (2002).
19. Abetz, V. & Simon, P. F. W. Phase Behaviour and Morphologies of Block Copolymers. in *Block Copolymers I* (ed. Abetz, V.) vol. 189 125–212 (Springer-Verlag, 2005).
20. Bates, F. S. & Fredrickson, G. H. Block Copolymers—Designer Soft Materials. *Phys. Today* **52**, 32–38 (1999).
21. Hückstädt, H., Göpfert, A. & Abetz, V. Influence of the block sequence on the morphological behavior of ABC triblock copolymers. *Polymer* **41**, 9089–9094 (2000).

22. Brinkmann, S., Stadler, R. & Thomas, E. L. New Structural Motif in Hexagonally Ordered Cylindrical Ternary (ABC) Block Copolymer Microdomains. *Macromolecules* **31**, 6566–6572 (1998).
23. Miskaki, C. *et al.* Self-Assembly of Low-Molecular-Weight Asymmetric Linear Triblock Terpolymers: How Low Can We Go? *Molecules* **25**, 5527 (2020).
24. Gido, S. P., Schwark, D. W., Thomas, E. L. & do Carmo Goncalves, M. Observation of a non-constant mean curvature interface in an ABC triblock copolymer. *Macromolecules* **26**, 2636–2640 (1993).
25. Matsushita, Y., Tamura, M. & Noda, I. Tricontinuous Double-Diamond Structure Formed by a Styrene-Isoprene-2-Vinylpyridine Triblock Copolymer. *Macromolecules* **27**, 3680–3682 (1994).
26. Mogi, Y., Mori, K., Matsushita, Y. & Noda, I. Tricontinuous morphology of triblock copolymers of the ABC type. *Macromolecules* **25**, 5412–5415 (1992).
27. Mogi, Y. *et al.* Superlattice Structures in Morphologies of the ABC Triblock Copolymers. *Macromolecules* **27**, 6755–6760 (1994).
28. Bailey, T. S., Pham, H. D. & Bates, F. S. Morphological Behavior Bridging the Symmetric AB and ABC States in the Poly(styrene- *b* -isoprene- *b* -ethylene oxide) Triblock Copolymer System. *Macromolecules* **34**, 6994–7008 (2001).
29. Matsushita, Y., Takano, A., Vayer, M. & Sinturel, C. Nonclassical Block Copolymer Self-Assembly Resulting from a Constrained Location of Chains and Junctions. *Adv. Mater. Interfaces* **7**, 1902007 (2020).
30. Koneripalli, N. *et al.* Ordering in Blends of Diblock Copolymers. *Macromolecules* **31**, 3498–3508 (1998).

31. Ruokolainen, J. *et al.* Supramolecular Routes to Hierarchical Structures: Comb-Coil Diblock Copolymers Organized with Two Length Scales. *Macromolecules* **32**, 1152–1158 (1999).
32. Dobrosielska, K., Wakao, S., Takano, A. & Matsushita, Y. Nanophase-Separated Structures of AB Block Copolymer/C Homopolymer Blends with Complementary Hydrogen-Bonding Interactions. *Macromolecules* **41**, 7695–7698 (2008).
33. Whitmore, M. D. & Noolandi, J. Theory of phase equilibria in block copolymer-homopolymer blends. *Macromolecules* **18**, 2486–2497 (1985).
34. Matsen, M. W. Phase Behavior of Block Copolymer/Homopolymer Blends. *Macromolecules* **28**, 5765–5773 (1995).
35. Chen, Y., Wang, Z., Gong, Y., Huang, H. & He, T. Solvent-Induced Novel Morphologies in Diblock Copolymer Blend Thin Films. *J. Phys. Chem. B* **110**, 1647–1655 (2006).
36. Guo, R. *et al.* Effect of the Nature of Annealing Solvent on the Morphology of Diblock Copolymer Blend Thin Films. *Macromolecules* **41**, 890–900 (2008).
37. Matsushita, Y. *et al.* Formation of undulated lamellar structure from ABC block terpolymer blends with different chain lengths. *J. Chem. Phys.* **133**, 194901 (2010).
38. Asai, Y., Yamada, K., Yamada, M., Takano, A. & Matsushita, Y. Formation of Tetragonally-Packed Rectangular Cylinders from ABC Block Terpolymer Blends. *ACS Macro Lett.* **3**, 166–169 (2014).
39. Ahn, S. *et al.* Gyroid Structures at Highly Asymmetric Volume Fractions by Blending of ABC Triblock Terpolymer and AB Diblock Copolymer. *Macromolecules* **50**, 9008–9014 (2017).
40. Zhang, Y., Sargent, J. L., Boudouris, B. W. & Phillip, W. A. Nanoporous membranes generated from self-assembled block polymer precursors: *Quo Vadis* ? *J. Appl. Polym. Sci.* **132**, n/a-n/a (2015).

41. Hirao, A. & Hayashi, M. Recent advance in syntheses and applications of well-defined end-functionalized polymers by means of anionic living polymerization. *Acta Polym* 13 (1999).
42. Cramail, H. Chimie macromoléculaire et matériaux polymères. 9.
43. Grubbs, R. B. Nitroxide-Mediated Radical Polymerization: Limitations and Versatility. *Polym. Rev.* **51**, 104–137 (2011).
44. Matyjaszewski, K. Atom Transfer Radical Polymerization: From Mechanisms to Applications. *Isr. J. Chem.* **52**, 206–220 (2012).
45. Hawker, C. J., Bosman, A. W. & Harth, E. New Polymer Synthesis by Nitroxide Mediated Living Radical Polymerizations. 28.
46. Chiefari, J. *et al.* Living Free-Radical Polymerization by Reversible Addition−Fragmentation Chain Transfer: The RAFT Process. *Macromolecules* **31**, 5559–5562 (1998).
47. Bouhadir, G. Xavier Franck, Chevilly Larue (FR); 19.
48. Moad, G. & Rizzardo, E. A 20th anniversary perspective on the life of RAFT (RAFT coming of age). *Polym. Int.* **69**, 658–661 (2020).
49. Houillot, L. Polymérisation par voie RAFT en dispersion organique: synthèse de copolymères à blocs et autoassemblage simultanés. 235.
50. Perrier, S. 50th Anniversary Perspective: RAFT Polymerization—A User Guide. 15 (2017).
51. Keddie, D. J., Moad, G., Rizzardo, E. & Thang, S. H. RAFT Agent Design and Synthesis. *Macromolecules* **45**, 5321–5342 (2012).
52. Moon, J. D., Freeman, B. D., Hawker, C. J. & Segalman, R. A. Can Self-Assembly Address the Permeability/Selectivity Trade-Offs in Polymer Membranes? *Macromolecules* **53**, 5649–5654 (2020).

53. Tan, X. & Rodrigue, D. A Review on Porous Polymeric Membrane Preparation. Part I: Production Techniques with Polysulfone and Poly (Vinylidene Fluoride). *Polymers* **11**, 1160 (2019).

54. Shiohara, A., Prieto-Simon, B. & Voelcker, N. H. Porous polymeric membranes: fabrication techniques and biomedical applications. *J. Mater. Chem. B* **9**, 2129–2154 (2021).

55. Abetz, V. Isoporous Block Copolymer Membranes. *Macromol. Rapid Commun.* **36**, 10–22 (2015).

56. Peinemann, K.-V., Abetz, V. & Simon, P. F. W. Asymmetric superstructure formed in a block copolymer via phase separation. *Nat. Mater.* **6**, 992–996 (2007).

57. Oss-Ronen, L. *et al.* Characterization of Block Copolymer Self-Assembly: From Solution to Nanoporous Membranes. *Macromolecules* **45**, 9631–9642 (2012).

58. Phillip, W. A., O'Neill, B., Rodwogin, M., Hillmyer, M. A. & Cussler, E. L. Self-Assembled Block Copolymer Thin Films as Water Filtration Membranes. *ACS Appl. Mater. Interfaces* **2**, 847–853 (2010).

59. Yu, H. *et al.* Asymmetric block copolymer membranes with ultrahigh porosity and hierarchical pore structure by plain solvent evaporation. *Chem. Commun.* **52**, 12064–12067 (2016).

60. Shibayama, M., Hashimoto, T., Hasegawa, H. & Kawai, H. Ordered structure in block polymer solutions. 3. Concentration dependence of microdomains in nonselective solvents. *Macromolecules* **16**, 1427–1433 (1983).

61. Foroutani, K., Ghasemi, S. M. & Pourabbas, B. Ordered isoporous membranes from ionic diblock copolymers via SNIPS: Optimizing effective factors with a structural survey. *Prog. Org. Coat.* **161**, 106554 (2021).

62. Dorin, R. M. *et al.* Solution Small-Angle X-ray Scattering as a Screening and Predictive Tool in the Fabrication of Asymmetric Block Copolymer Membranes. *ACS Macro Lett.* **1**, 614–617 (2012).
63. Stegelmeier, C. *et al.* Evaporation-Induced Block Copolymer Self-Assembly into Membranes Studied by *in Situ* Synchrotron SAXS. *Macromolecules* **48**, 1524–1530 (2015).
64. Nunes, S. P. *et al.* From Micelle Supramolecular Assemblies in Selective Solvents to Isoporous Membranes. *Langmuir* **27**, 10184–10190 (2011).
65. Jung, A., Rangou, S., Abetz, C., Filiz, V. & Abetz, V. Structure Formation of Integral Asymmetric Composite Membranes of Polystyrene -*block*- Poly(2-vinylpyridine) on a Nonwoven: Structure Formation of Integral Asymmetric Composite Membranes …. *Macromol. Mater. Eng.* **297**, 790–798 (2012).
66. Marques, D. S. *et al.* Self-assembly in casting solutions of block copolymer membranes. *Soft Matter* **9**, 5557 (2013).
67. Yang, C. *et al.* Tailoring the pore size and permeability of isoporous membranes through blending with poly(ethylene glycol): Toward the balance of macro- and microphase separation. *J. Membr. Sci.* **598**, 117755 (2020).
68. Tung, S.-H., Kalarickal, N. C., Mays, J. W. & Xu, T. Hierarchical Assemblies of Block-Copolymer-Based Supramolecules in Thin Films. *Macromolecules* **41**, 6453–6462 (2008).
69. Ikkala, O. & ten Brinke, G. Hierarchical self-assembly in polymeric complexes: Towards functional materials. *Chem. Commun.* 2131 (2004) doi:10.1039/b403983a.
70. Yang, C., Zhu, G., Yi, Z., Zhou, Y. & Gao, C. Critical contributions of additives on the fabrication of asymmetric isoporous membranes from block copolymers: A review. *Chem. Eng. J.* **424**, 128912 (2021).

71. Loh, C. H., Wang, R., Shi, L. & Fane, A. G. Fabrication of high performance polyethersulfone UF hollow fiber membranes using amphiphilic Pluronic block copolymers as pore-forming additives. *J. Membr. Sci.* **380**, 114–123 (2011).
72. Cheng, J. *et al.* Metal ions 'sewing' isoporous membranes with polystyrene-block-poly (acrylic acid) block copolymer. *J. Membr. Sci.* **587**, 117086 (2019).
73. Kang, G. & Cao, Y. Application and modification of poly(vinylidene fluoride) (PVDF) membranes – A review. *J. Membr. Sci.* **463**, 145–165 (2014).
74. Hester, J. F. *et al.* ATRP of Amphiphilic Graft Copolymers Based on PVDF and Their Use as Membrane Additives. *Macromolecules* **35**, 7652–7661 (2002).
75. Phillip, W. A. *et al.* Tuning Structure and Properties of Graded Triblock Terpolymer-Based Mesoporous and Hybrid Films. *Nano Lett.* **11**, 2892–2900 (2011).
76. Tirumala, V. R., Romang, A., Agarwal, S., Lin, E. K. & Watkins, J. J. Well Ordered Polymer Melts from Blends of Disordered Triblock Copolymer Surfactants and Functional Homopolymers. *Adv. Mater.* **20**, 1603–1608 (2008).
77. Susanto, H. & Ulbricht, M. Characteristics, performance and stability of polyethersulfone ultrafiltration membranes prepared by phase separation method using different macromolecular additives. *J. Membr. Sci.* **327**, 125–135 (2009).
78. Shull, K. R. & Winey, K. I. Homopolymer distributions in lamellar copolymer/homopolymer blends. *Macromolecules* **25**, 2637–2644 (1992).
79. Mayes, A. M., Russell, T. P., Satija, S. K. & Majkrzak, C. F. Homopolymer distributions in ordered block copolymers. *Macromolecules* **25**, 6523–6531 (1992).
80. Jiang, S., Göpfert, A. & Abetz, V. Novel Morphologies of Block Copolymer Blends via Hydrogen Bonding. *Macromolecules* **36**, 6171–6177 (2003).

81. Asari, T., Matsuo, S., Takano, A. & Matsushita, Y. Three-Phase Hierarchical Structures from AB/CD Diblock Copolymer Blends with Complemental Hydrogen Bonding Interaction. *Macromolecules* **38**, 8811–8815 (2005).

82. Radjabian, M. & Abetz, V. Tailored Pore Sizes in Integral Asymmetric Membranes Formed by Blends of Block Copolymers. *Adv. Mater.* **27**, 352–355 (2015).

83. Jin, C., Olsen, B. C., Luber, E. J. & Buriak, J. M. Nanopatterning via Solvent Vapor Annealing of Block Copolymer Thin Films. *Chem. Mater.* **29**, 176–188 (2017).

84. Luo, M. & Epps, T. H. Directed Block Copolymer Thin Film Self-Assembly: Emerging Trends in Nanopattern Fabrication. *Macromolecules* **46**, 7567–7579 (2013).

85. Chao, H., Koski, J. & Riggleman, R. A. Solvent vapor annealing in block copolymer nanocomposite films: a dynamic mean field approach. *Soft Matter* **13**, 239–249 (2017).

86. Sinturel, C., Vayer, M., Morris, M. & Hillmyer, M. A. Solvent Vapor Annealing of Block Polymer Thin Films. *Macromolecules* **46**, 5399–5415 (2013).

87. Albalak, R. J., Capel, M. S. & Thomas, E. L. Solvent swelling of roll-cast triblock copolymer films. *Polymer* **39**, 1647–1656 (1998).

88. Kim, G. & Libera, M. Morphological Development in Solvent-Cast Polystyrene−Polybutadiene−Polystyrene (SBS) Triblock Copolymer Thin Films. *Macromolecules* **31**, 2569–2577 (1998).

89. Fukunaga, K., Elbs, H., Magerle, R. & Krausch, G. Large-Scale Alignment of ABC Block Copolymer Microdomains via Solvent Vapor Treatment. *Macromolecules* **33**, 947–953 (2000).

90. Knoll, A. *et al.* Phase Behavior in Thin Films of Cylinder-Forming Block Copolymers. *Phys. Rev. Lett.* **89**, 035501 (2002).

91. Kim, S. H., Misner, M. J., Xu, T., Kimura, M. & Russell, T. P. Highly Oriented and Ordered Arrays from Block Copolymers via Solvent Evaporation. *Adv. Mater.* **16**, 226–231 (2004).

92. Lee, S. *et al.* Double-Layer Morphologies from a Silicon-Containing ABA Triblock Copolymer. *ACS Nano* **12**, 6193–6202 (2018).

93. Lee, S. *et al. In Situ* Study of ABC Triblock Terpolymer Self-Assembly under Solvent Vapor Annealing. *Macromolecules* **52**, 1853–1863 (2019).

94. Lee, J., Park, J., Jung, J., Lee, D. & Chang, T. Phase Behavior of Polystyrene- *b* -polyisoprene- *b* -poly(methyl methacrylate) Triblock Terpolymer upon Solvent Vapor Annealing. *Macromolecules* **52**, 5122–5130 (2019).

95. Vayer, M. *et al.* Transition between tetragonal and hexagonal pattern in binary blends of ABC block copolymers with different chain lengths. *Eur. Polym. J.* **138**, 109986 (2020).

96. Aissou, K. *et al.* Periodic Bicontinuous Structures Formed on the Top Surface of Asymmetric Triblock Terpolymer Thick Films. *ACS Macro Lett.* **8**, 923–930 (2019).

97. Gao, K. *et al.* Creation of active-passive integrated mechanisms on membrane surfaces for superior antifouling and antibacterial properties. *J. Membr. Sci.* **548**, 621–631 (2018).

98. Zhang, R. *et al.* Antifouling membranes for sustainable water purification: strategies and mechanisms. *Chem. Soc. Rev.* **45**, 5888–5924 (2016).

99. Zhao, X. *et al.* Engineering amphiphilic membrane surfaces based on PEO and PDMS segments for improved antifouling performances. *J. Membr. Sci.* **450**, 111–123 (2014).

100. Jiang, Y. *et al.* The open pore conformation of potassium channels. *Nature* **417**, 523–526 (2002).

101. Luo, F. *et al.* Smart gating membranes with in situ self-assembled responsive nanogels as functional gates. *Sci. Rep.* **5**, 14708 (2015).

102. Wandera, D., Wickramasinghe, S. R. & Husson, S. M. Stimuli-responsive membranes. *J. Membr. Sci.* **357**, 6–35 (2010).

103. Schmaljohann, D. Thermo- and pH-responsive polymers in drug delivery☆. *Adv. Drug Deliv. Rev.* **58**, 1655–1670 (2006).

104. Cui, M.-R., Chen, L.-X., Li, X.-L., Xu, J.-J. & Chen, H.-Y. NIR Remote-Controlled "Lock–Unlock" Nanosystem for Imaging Potassium Ions in Living Cells. *Anal. Chem.* **92**, 4558–4565 (2020).

105. Mondal, S. & Wickramasinghe, S. R. Photo-induced graft polymerization of N-isopropyl acrylamide on thin film composite membrane: Produced water treatment and antifouling properties. *Sep. Purif. Technol.* **90**, 231–238 (2012).

106. Thévenot, J., Oliveira, H., Sandre, O. & Lecommandoux, S. Magnetic responsive polymer composite materials. *Chem. Soc. Rev.* **42**, 7099 (2013).

107. Fan, X.-X. *et al.* Dual pH-responsive smart gating membranes. *J. Membr. Sci.* **555**, 20–29 (2018).

108. Xiang, Y., Shen, J., Wang, Y., Liu, F. & Xue, L. A pH-responsive PVDF membrane with superwetting properties for the separation of oil and water. *RSC Adv.* **5**, 23530–23539 (2015).

109. Ye, Y., Huang, J. & Wang, X. Fabrication of a Self-Cleaning Surface via the Thermosensitive Copolymer Brush of P(NIPAAm-PEGMA). *ACS Appl. Mater. Interfaces* **7**, 22128–22136 (2015).

110. Cetintas, M. *et al.* Free-standing thermo-responsive nanoporous membranes from high molecular weight PS-PNIPAM block copolymers synthesized via RAFT polymerization. *Polym. Chem.* **8**, 2235–2243 (2017).

111. Zhao, Y. *et al.* Thermo-responsive separation membrane with smart anti-fouling and self-cleaning properties. *Chem. Eng. Res. Des.* **156**, 333–342 (2020).

112. Clodt, J. I. *et al.* Double Stimuli-Responsive Isoporous Membranes via Post-Modification of pH-Sensitive Self-Assembled Diblock Copolymer Membranes. *Adv. Funct. Mater.* **23**, 731–738 (2013).

CHAPTER 2

Synthesis and characterization of linear ABC triblock terpolymers by RAFT polymerization

Table of contents

1. Introduction

The aim of this thesis work was the conception of fouling-resistant and high performance separation membranes derived from the self-assembly of block copolymers (BCPs).

As discussed in the bibliographic part, BCPs are excellent candidates for the manufacture of next-generation ultrafiltration membranes. This is mainly due to their capability to self-assemble into periodic nanostructures with controllable morphologies that can be used as innovative platform to build uniform pore size within the membrane skin. The addition of a third block within the BCP chains opens access to a broader structural diversity and allows for the fabrication of membranes with nanopores having more functionalities (*e.g.*, a dual pH- and thermo-sensitive behavior of pores). However, the use of ABC-type BCP chains having a well-defined composition as well as a narrow size distribution is mandatory for an efficient design of asymmetric and nanostructured membranes. To this end, a series of well-defined linear polystyrene-*block*-poly(2-vinylpyridine)-*block*-poly(*N*-isopropyalcrylamide) (PS-*b*-P2VP-*b*-PNIPAM) terpolymers was prepared for the first time by RAFT polymerization in order to produce smart dual responsive membranes (see **Figure 1.a**).

The linear ABC triblock terpolymer chains envisioned in this work contain a hydrophobic and rigid PS block, known as an amorphous and glassy polymer having a glass-transition temperature around 100°C. For such reasons, only ABC-type BCP chains having a large PS composition have been synthetized in order to generate mechanically robust PS-rich membranes by phase inversion. Our ABC-type BCP system also includes a pH-responsive poly(2-vinylpyridine) mid-block to produce smart nanopores. Indeed, the protonation/deprotonation transition state of the nitrogen atom (in the pyridine ring) occurring at pH~4.8 allows for the regulation of the pore size (see **Figure 1.b**). To produce bifunctional ABC-type BCP chains, the gold standard thermo-sensitive poly(*N*-isopropylacrylamide) has been selected as third-block. Due to a lower critical solution temperature (LCST) behavior, PNIPAM undergoes a coil-globule transition at ~32°C in water that can be exploited to simultaneously control both the size and hydrophilic/hydrophobic character of the pores, thereby leading to the conception of improved fouling-resistant membranes (see **Figure 1.c**). Note that depending on the water mild conditions, the configuration of P2VP-*b*-PNIPAM chains inside the membrane nanopores can vary as follows: fully stretched (pH > 4.8 and T < 32°C), partially stretched (pH > 4.8 and T < 32°C or pH < 4.8 and T > 32°C) or even fully

compressed (pH < 4.8 and T > 32°C). Such different configurations of the P2VP-*b*-PNIPAM chains can be used to fine-tune the effective size of the nanochannels formed on the membrane substructure (see **Figure 1.d**)

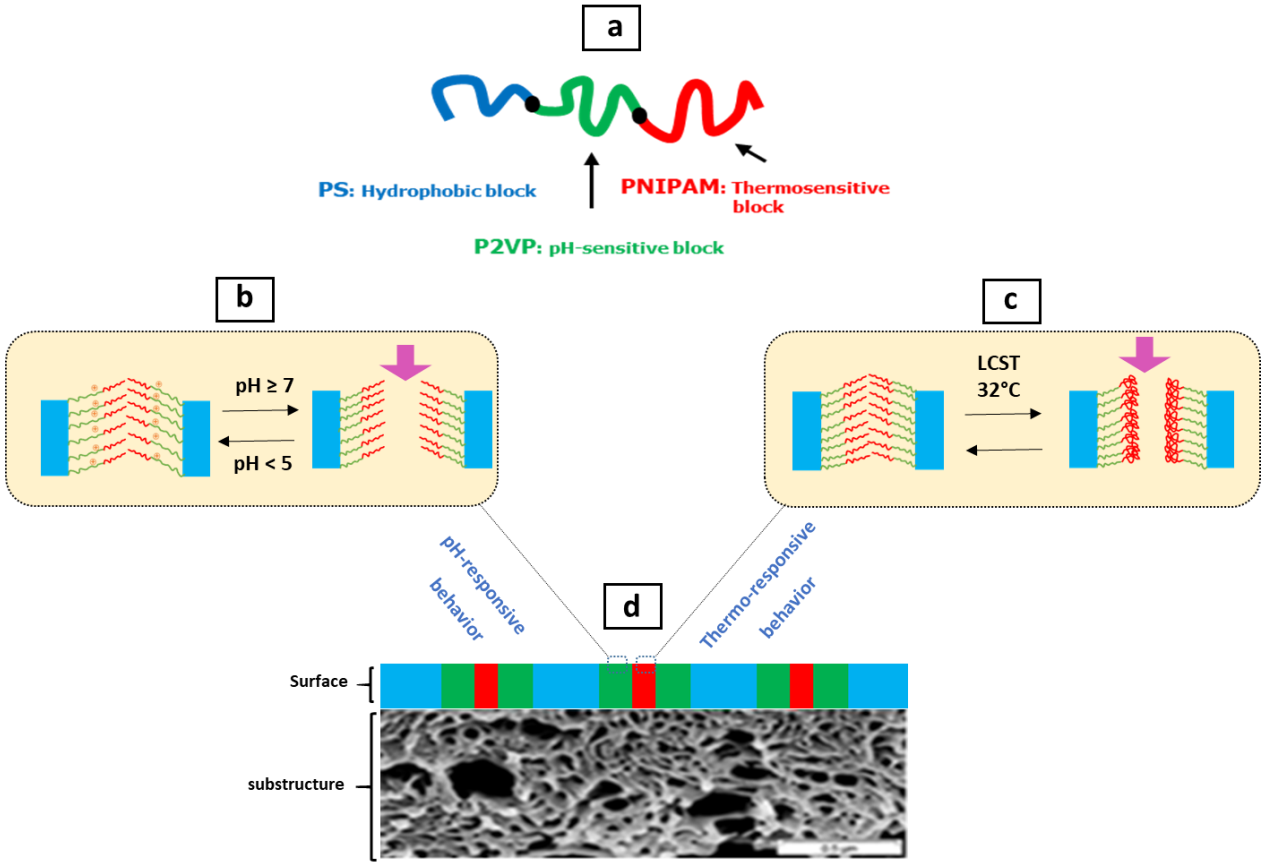

Figure 1. (a) Schematic representation of the linear PS-*b*-P2VP-*b*-PNIPAM triblock terpolymer studied in this work. (b) Protonation (close) and deprotonation (open) state of the P2VP block in response to the pH variation. (c) Swelling (close) and shrinking (open) state of the PNIPAM block in response to the water temperature variation. (d) Cross-section view of the envisioned membrane consisting of a core-shell cylindrical structure within the top surface layer and a macroporous

In this chapter, we will describe the synthesis RAFT polymerization route used to prepare well-defined dual stimuli-responsive PS-*b*-P2VP-*b*-PNIPAM triblock terpolymers. The livingness of the polymerization was confirmed by the chain extension of 2VP using PS as macro RAFT agent first, and then by the chain extension of NIPAM using the PS-*b*-P2VP diblock as macro-CTA.

2. Polystyrene homopolymer (hPS)

2.1. Synthesis of PS macro-RAFT agents

The aim of this section was the synthesis of a series of polystyrene homopolymers by RAFT polymerization with different molecular weights. To this end, three different trithiocarbonate RAFT agents were used with same stabilizing Z-group and different leaving R-groups: 4-cyano-4-[(dodecylsulfanylthiocarbonyl)sulfanyl]pentanoic acid (CDPA), 4-cyano-4-[(dodecylsulfanylthiocarbonyl)sulfanyl]pentanol (CDP) and 2-dodecylthiocarbonylthio-2-methyl proionic acid (DDMAT) (see **Scheme 1.a,b and c**). Azobisisobutyronitrile (AIBN) was used as initiator (see **Scheme 1**.**d**).

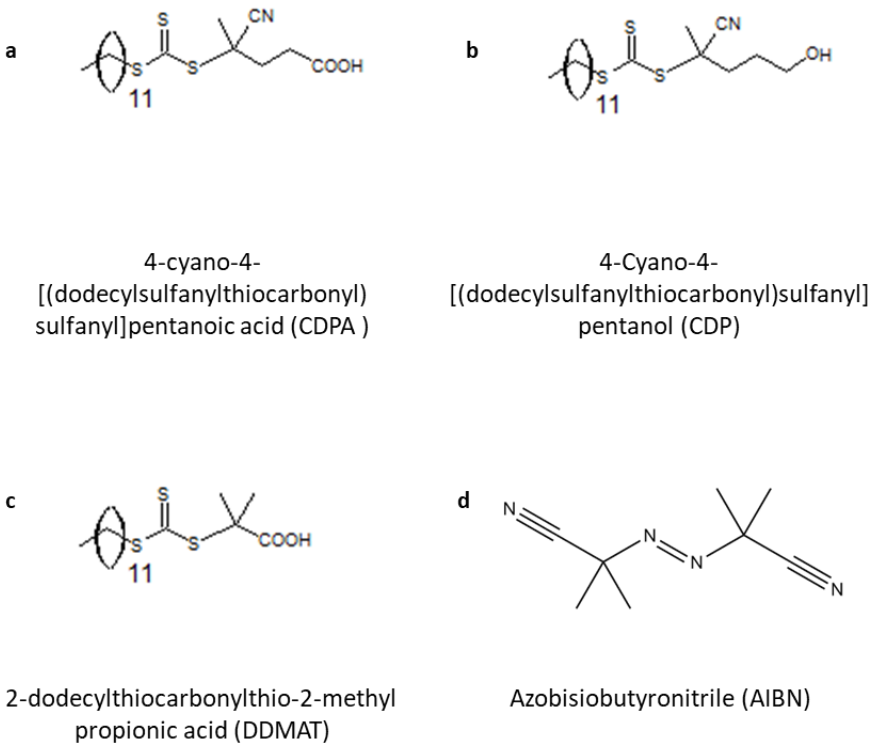

Scheme 1. The RAFT agents (a,b and c) and initiator (d) chemical structures used in this work.

The control of the RAFT polymerization is strongly dependent on the reaction medium since the choice of the solvent and reagent concentrations (monomer, CTA and initiator) as well as a good degassing can affect both the molecular weight and size distribution of the targeted terpolymers. The good control of the RAFT polymerization and the absence of any potential retardation effect[1] are also highly dependent on the choice of the initiator and the Z and R groups of the RAFT agent as well as the order of the monomer sequence for the BCP synthesis.

Therefore, the choice of the monomer sequence order in this study was not arbitrary. Here, the hPS macro-CTA was chosen as starting block for the synthesis of linear PS-*b*-P2VP-*b*-PNIPAM triblock terpolymers. It was reported that it is preferable to start the block copolymerization with the monomer having the lowest chain transfer constant (CTC)[2] which is the case of styrene.

Additionally, styrene belongs to the family of more activated monomers "MAMs"[3] and trithiocarbonate RAFT agents are suitable for polymerization of MAMs since they can balance activity and stability. Such RAFT agents are also less sensitive to degradation and no discernable polymerization has been noticed with these reagents. The choice of AIBN as initiator to prepare the linear PS-*b*-P2VP-*b*-PNIPAM triblock terpolymers was motivated by the fact that the 2-cyano-2-propyl radical is a good leaving group.[4]

The two series of PS macro-CTAs synthesized in this study are summarized in **Table 1**. The first series (S1 to S8) was synthesized in bulk with a targeted theoretical molecular weight ($M_{n,theo,targeted}$) of about 30 kg/mol. The second series (S9 to S12) was synthesized in solution (1,4-dioxane) to target higher theoretical molecular weight ($M_{n,theo,targeted}$ ~ 50 kg/mol).

Polymer	M/CTA/AIBN	CTA	solvant	Reaction time (h)	Temperature (°C)	$M_{n,theo}$ [a] (kg/mol)	Conversion [b] (%)	M_n (SEC) kg mol^{-1}	M_w/M_n [c]
S1	864 / 1 / 0.2	CDPA	No	15h	70	26	29	22.6	1.12
S2	864 / 1 / 0.2	CDPA	No	19h	70	32	36	25.4	1.12
S3	864 / 1 / 0.2	CDPA	No	20h	70	26	29	27.3	1.09
S4	864 / 1 / 0.2	CDPA	No	20h	70	29	32	26.4	1.13
S5	863 / 1 / 0.2	CDP	No	20h20	70	30	33	31.5	1.09
S6	861 / 1 / 0.2	CDP	No	20h	70	32	36	28.8	1.09
S7	484 / 1 / 0.2	CDPA	No	24h	70	35	39	28.2	1.09
S8	863 / 1 / 0.2	DDMAT	No	45h	70	41	46	22.3	1.06
S9	863 / 1 / 0.2	DDMAT	DOX	24h	70	27	30	25.3	1.11
S10	864 / 1 / 0.2	DDMAT	DOX	24h	110	33	37	19.1	1.74
S11	864 / 1 / 0.2	DDMAT	DOX	48h	110	21	23	12.9	1.03
S12	960 / 1 / 0.2	DDMAT	DOX	62h	110	81	90	34.5	1.41
S13	960 / 1 / 0.2	CDPA	DOX	34h	70	41	46	40.5	1.12
S14	960 / 1 / 0.2	CDPA	DOX	34h	70	33	37	49.9	1.19
S15	950 /1 / 0.2	CDPA	DOX	34h	70	46	51	54.7	1.19

CDPA : 4-cyano-4-[(dodecylsulfanylthiocarbonyl) sulfanyl]pentanoic acid. **CDP** : 4-Cyano-4-[(dodecylsulfanylthiocarbonyl)sulfanyl]pentanol. **DDMAT** : 2-dodecylthiocarbonylthio-2-methyl propionic acid. **DOX** : 1,4-dioxane. [a] Theoretical average molar mass : $M_{n,theo}$ = ([styrene]/|CTA] x conversion) x $M_{styrene}$ + M_{CTA} , where $M_{styrene}$ and M_{CTA} are the molar masses of styrene and CTA respectively. [b] conversion determined by ^1H NMR spectroscopy. [c] determined by SEC in THF.

Table 1. Two series of PS macro-CTAs prepared by RAFT with bulk and solution polymerization.

As an example of a PS macro-CTA synthesized in bulk, hereafter is presented the experimental procedure for the S7 synthesis. For that purpose, a round-bottom flask was charged with styrene, CDPA as RAFT agent and AIBN. The reaction vessel was sealed and stirred until the full dissolution of CDPA and AIBN in styrene. The sealed reaction vessel was purged with nitrogen to remove any oxygen traces and then was placed in a preheated oil bath at 70°C for 24h (see **Scheme 2**). The reaction was stopped abruptly by lowering the temperature of the reaction into an ice bath.

An aliquot was withdrawn from the solution to determine the monomer conversion before precipitation of the resulting PS macro-CTA three times in cold methanol. The obtained polymer was dried overnight in a vacuum oven at room temperature (RT) to give a white-yellowish powder (the color is indicating the incorporation of the RAFT CDPA group within the polymer chains).

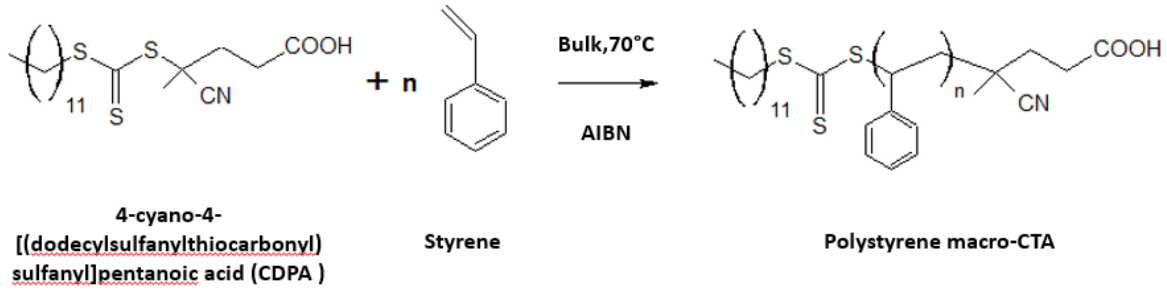

Scheme 2. Polystyrene macro-CTA synthesis by RAFT polymerization in bulk.

It was reported that hPS with high molecular weight (> 10^5 g/mol) and low dispersity (~~Đ~~ = M_w/M_n < 2) values have improved mechanical properties than PS homopolymers with a low molecular weight. Such polymer materials have improved impact strength, high heat-resistance and high environmental stress crack resistance.[5]

In this study, the first series of syntheized hPS in bulk have a molecular weight of ~30 kg/mol. For the synthesis of the second series of PS macro-CTAs in solution using 1,4-dioxane (DOX) as solvent, several conditions were tested to achieve a M_n of ~50 kg.mol^{-1}. First, we tried the same reaction conditions as in bulk, *i.e.*, same monomer/CTA/AIBN concentrations, at 70°C and for 24h (S9 in **Table 1**). The molecular weight and ~~Đ~~ of the obtained polymer were about 25.3 kg.mol^{-1} and 1.11, respectively. Here, the presence of dioxane decreased the reaction rate and 24h were not sufficient to reach the targeted M_n with a narrow ~~Đ~~.

As another example, the synthesis of S10 (see **Table 1**) was performed at 110°C for 24h. By increasing the temperature, the control of polymerization was affected, and thus hPS chains with a high dispersity value (~~Đ~~ =1.74) were prepared. This result indicate that high temperatures are not suitable for the synthesis of well-defined PS macro CTAs in solution. This is due to a high decomposition rate of AIBN with a half-life time ($t_{1/2}$) of few minutes for a temperature higher than 100°C [6] (*vs*. 5h at 70°C) which results in the production of more initiated radical species that react with styrene to form propagating PS chains. In addition, the uncontrolled synthesis of PS chains at high temperature is due to the appearance of a high termination rate and more side reactions resulting in the formation of new chains generated both by AIBN and thermal self-initiation.

Comparing to synthesis in bulk, several parameters should be carefully chosen to prepare well-defined PS macro-CTAs in solution with a high molecular weight. The best way to synthesize the targeted hPS chains in DOX was to use a temperature of 70°C to prevent reaction disruptions by inappropriate decomposition of AIBN and avoid the quick consumption of radicals conducing to a loss of polymerization control. In addition, half of initial AIBN amount must be added each 24h followed by a good degassing of the reaction in order to ensure presence of the required number of radicals in the solution. By using this protocol, well-defined PS macro-CTAs with a molecular of ~50 kg/mol and low $Đ$ values (<1.2) were prepared (see S14 and S15 in **Table 1**).

In summary, the synthesis of PS homopolymers in bulk was quite simple since macro-CTAs having the targeted molecular weight (~30 kg.mol^{-1}) and low dispersity values (<1.2) were prepared. Conversely, the synthesis in solution of PS homopolymers with a higher M_n revealed to be more complicated. The optimum conditions for the synthesis of hPS in solution with M_n > 30 kg.mol^{-1} were reached by (*i*) working at 70°C as reaction temperature, (*ii*) periodically adding the good quantity of AIBN and (*iii*) choosing the required amount of solvent.

2.2. Characterization of hPS by ^{1}H NMR and SEC

The PS homopolymers synthesized were characterized by ^{1}H nuclear magnetic resonance (NMR) spectroscopy (400MHz) in deuterated dichloromethane (CD_2Cl_2) at room temperature. After cooling down the reaction vessel into an ice bath, an aliquot was collected from the solution to determine the conversion by ^{1}H NMR. This was done by comparing the integrated aliphatic protons signals of the PS group at 1.92 ppm to those of the monomer at 5.83-5.88 ppm (see **Figure 2.a**), and a conversion of 39% was found for the polymer S7 synthesized in bulk. The resulting PS macro-RAFT was then purified by two successive precipitations into an excess of cold methanol and dried under vacuum overnight. **Figure 2.b** represents the ^{1}H NMR spectrum of the purified PS macro-CTA where the peaks were indexed as follows: δ = 6.60-

7.05 (5H, m, Ph), 1.1- 1.47 (3H,m,CH-CH2-). No traces of remaining monomer are visible in the spectrum, hence confirming the presence of pure PS chains.

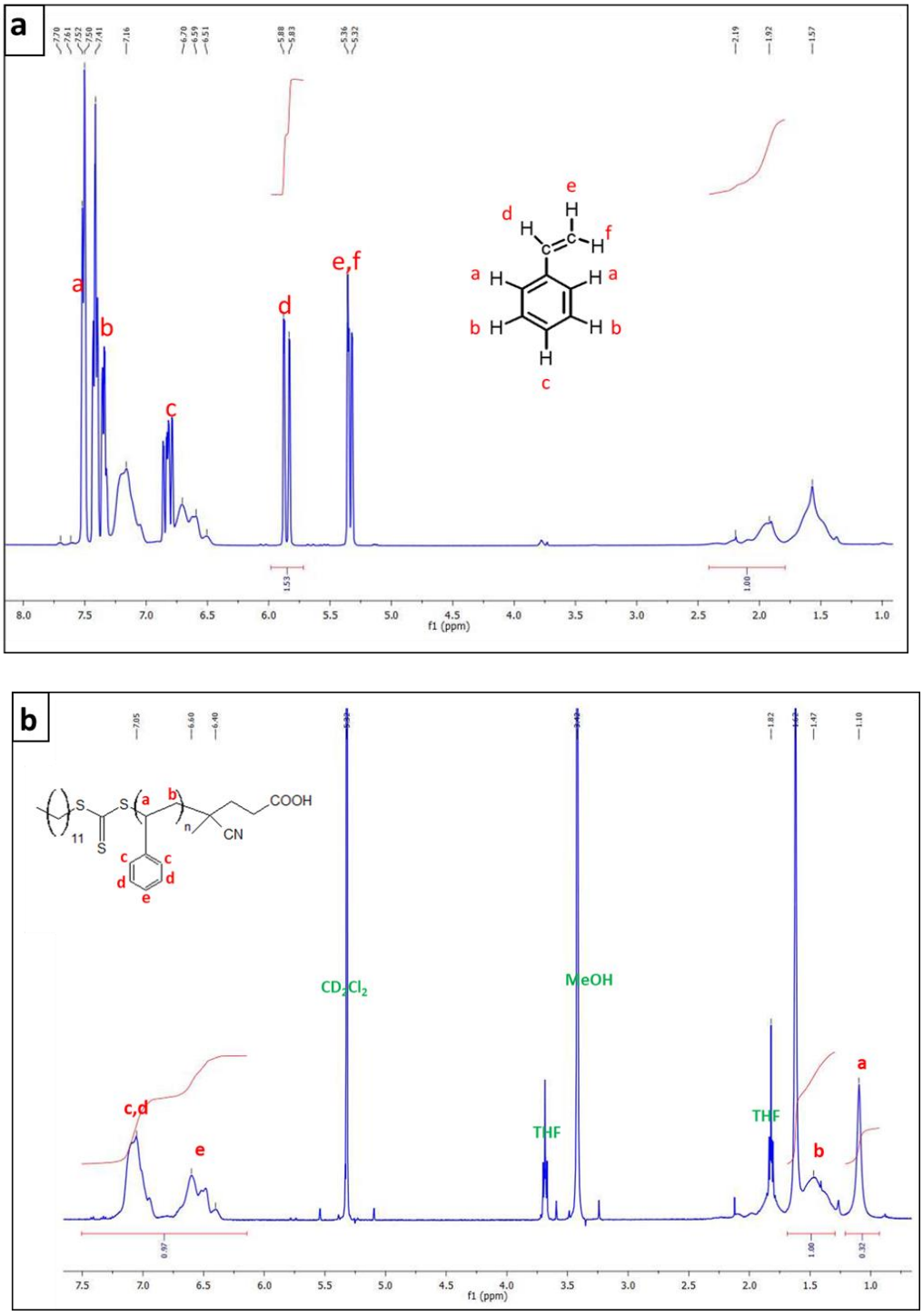

Figure 2. ^{1}H NMR spectrum of the PS macro-CTA in CD_2Cl_2 before (a) and after (b) precipitation.

The molecular weight of the homopolymer was determined only by size exclusion chromatography (SEC) since the large size of the hPS chains makes that the CTA chain-end protons of the methyl group (at 3.35 ppm) were not visible from the NMR spectrum.

Figure 3 represents the SEC chromatograms of two purified PS homopolymers (THF at 35°C using PS standard) with different molecular weights: S15 (red, M_n = 54.7 kg.mol^{-1}, Đ = 1.19) and S7 (black, M_n= 28.2 kg.mol^{-1}, Đ = 1.09). In order to characterize the controlling/living nature of the chain growth polymerization, different kinetic representations of the experimental results were plotted such as conversion of monomer *vs.* reaction time, experimental molecular weight (SEC) *vs.* conversion and ln(Mo/M) *vs.* time. The linear relationship shows the controlled and living nature of RAFT polymerization (see **Figure 4**).

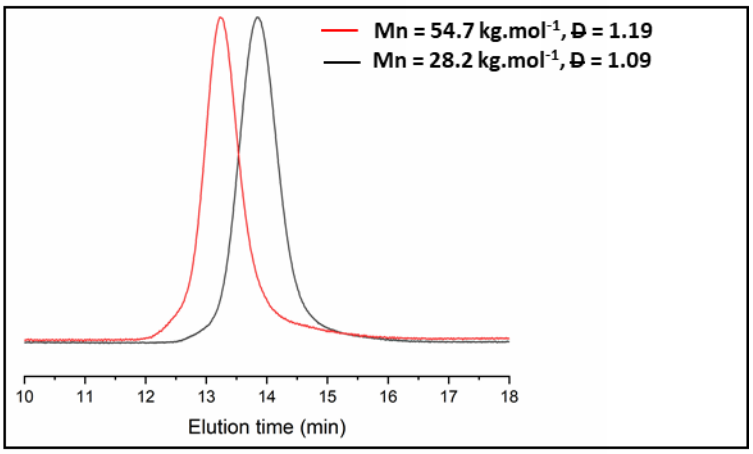

Figure 3. SEC traces in THF of two hPS macro-CTAs of different molecular weights (red is S15 and black is S7 from table 1).

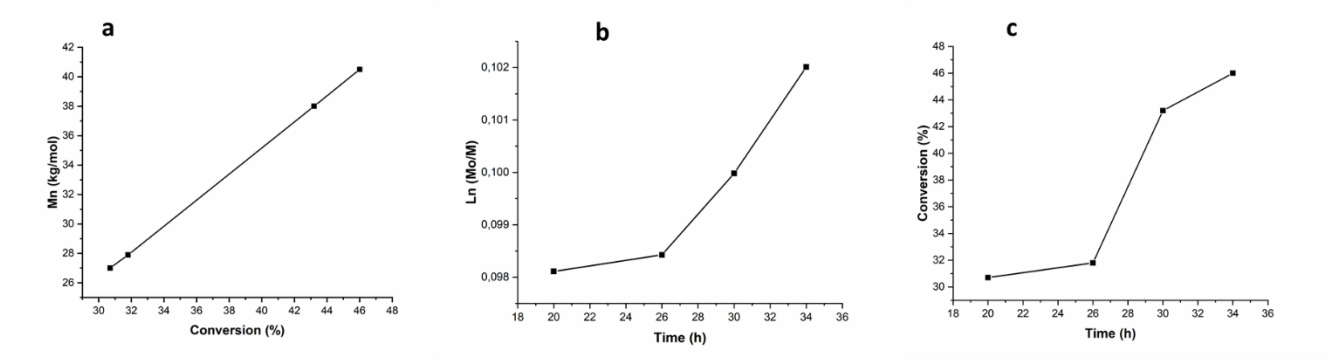

Figure 4. Kinetic plots (a) molecular weight M_n (SEC) *vs*. conversion, (b) ln(M_o/M) *vs*. time, (c) conversion *vs.* time for RAFT polymerization of PS macro-CTA (S13 Table 1).

As discussed in the previous part, the synthesis in solution of PS homopolymers is more complicated than in bulk. For instance, to illustrate the effect of a high temperature on ~~Đ~~, **Figure 5** represents the SEC chromatogram of S12 (in **Table 1**) synthetized at 110°C for 62h. Here, a high conversion value was obtained (90%) but, unfortunately, the loose of control of the polymerization is clearly evidenced by the generation of several polymer chains with different molecular weights.

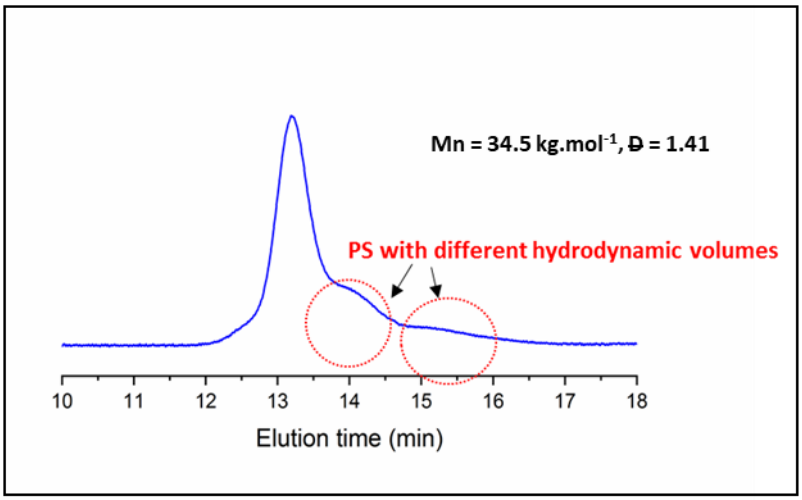

Figure 5. SEC trace in THF of the S12 macro-CTA .

3. Polystyrene-*block*-poly(2-vinylpyridine) (PS-*b*-P2VP)

3.1. Synthesis of PS-*b*-P2VP by RAFT polymerization

Smart BCP chains are highly-desirable for the manufacture of next-generation membranes able to self-regulate their permeability *via* the flexible adjustment of the pore size based on the "open/close" switch of the stimuli-responsive block. To address this issue, P2VP was incorporated as middle block of the targeted ABC-type BCP due to its capability to respond to a change in the environment and particularly in pH. Indeed, P2VP is one of the well-known pH sensitive polymer having a pKa value of approximately 4.5[7] that allows for a change in its conformation by the protonation and deprotonation of the nitrogen group.[8] Under neutral or alkaline conditions, the nitrogen group is deprotonated and the insoluble P2VP can shrink in water (open state). Conversely, under acidic conditions (pH < 5), the protonated P2VP can swell in water due to the electrostatic repulsion between protonated nitrogen groups (close state).[9] Moreover, PS and P2VP are strongly incompatible with an interaction parameter $\chi_{PS\text{-}P2VP} \approx 0.1$.[10] Such a high incompatibility is mandatory to produce nanostructured BCP membranes even for low degrees of P2VP polymerization.

The synthesis of the PS-*b*-P2VP macro-CTA was performed in 1,4-dioxane by mixing the 2VP monomer with the previously synthesized PS macro-CTA and AIBN (see **Scheme 3**). The reaction medium was purged with nitrogen and heated to 70°C.

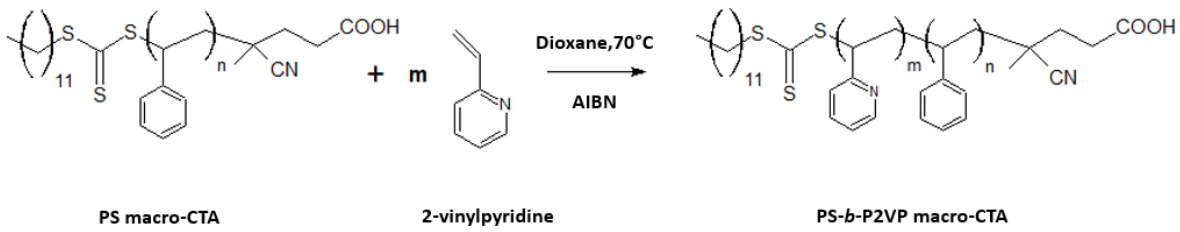

Scheme 3. PS-*b*-P2VP macro-CTA synthesis by RAFT polymerization.

About certain amount of time (see **Table 2**), the reaction was stopped by lowering the temperature of the reaction mixture into an ice bath. The targeted diblocks will have a high PS volume fraction, f_{PS}, and low dispersity value.

Polymer	Macro-CTA	Reaction time (h)	$M_{n,\ P2VP,theo}$ [a] (kg/mol)	$M_{n,RMN}$ [b] (kg/mol)	$M_{n,RMN}$ [c] (PS : P2VP) (kg/mol)	vol.fraction [d]	Conversion [e] (%)	Mn (SEC) Kg/mol	Mw/Mn [f]
SV1	S4	1	5.2	39.9	26.4 : 5.6	0.84 : 0.16	1.8	31.1	1.18
SV2	S7	7	20.1	38.4	28.2 : 10.2	0.75 : 0.25	12.4	34.5	1.20
SV3	S7	7	16.6	34.6	28.2 : 6.4	0.83 : 0.17	10.2	41.8	1.14
SV4	S13	4	17.3	80.1	40.5 : 39.6	0.54 : 0.47	12.4	45.8	1.41
SV5	S14	4.5	17.0	77.4	49.9 : 23.3	0.70 : 0.30	10.5	46.2	1.45
SV6	S15	4	30.9	89.7	54.7 : 35	0.63 : 0.37	19	57.6	1.56
SV7	S13	3.5	15.5	68.8	40.5 : 28.3	0.61 : 0.39	11	51.0	1.50

Reaction temperature : 70°C. [a] Theoretical average molar mass : $M_{n,theo}$ = ([2VP]/|CTA] x conversion) x M_{2VP} + M_{CTA} , where M_{2VP} and M_{CTA} are the molar masses of and CTA respectively. [b] molar mass determined by ^{1}H NMR sepectroscopy. [c] molar mass of each block determined by ^{1}H NMR spectroscopy. [d] volume fractions determined by ^{1}H NMR spectroscopy. [e] conversion determined by ^{1}H NMR spectroscopy. [f] polydispersity value determined by SEC

Table 2. PS-*b*-P2VP macro-CTAs prepared by RAFT polymerization.

3.2. Characterization of PS-*b*-P2VP by ^{1}H NMR and SEC

^{1}H NMR spectroscopy (400MHz) in CD_2Cl_2 was used to determine the monomer conversion during the reaction. To do this, an aliquot was withdrawn from the solution before the precipitation of the PS-*b*-P2VP chains three times in heptane to eliminate the remaining monomer. For instance, the resulting brown PS-*b*-P2VP macro-CTA corresponding to SV3 in gave rise to a yield of ~26% after to be dried overnight at RT under vacuum. For this PS-*b*-P2VP macro-RAFT agent, the conversion was calculated by ^{1}H NMR to be 10.2 % by comparing the integrated aromatic proton signals of the P2VP ring at 8.25 ppm to those of the 2VP monomer at 8.53 ppm.

After precipitation in heptane, the ^{1}H NMR spectrum of the SV3 BCP (red) shows additional peaks that are not observed on the corresponding hPS CTA spectrum (blue) (see **Figure 6**). These characteristic peaks of P2VP units were indexed as follows: δ = 8.25 (1H,m Ph), 6.61-7.06 (8H,m,Ph) and 1.27-2.30 (6H,m,CH-CH2). From the ^{1}H NMR spectrum, the molecular weight of SV3 and its PS volume fraction were determined to be 34.6 kg.mol^{-1} and 0.83, respectively.

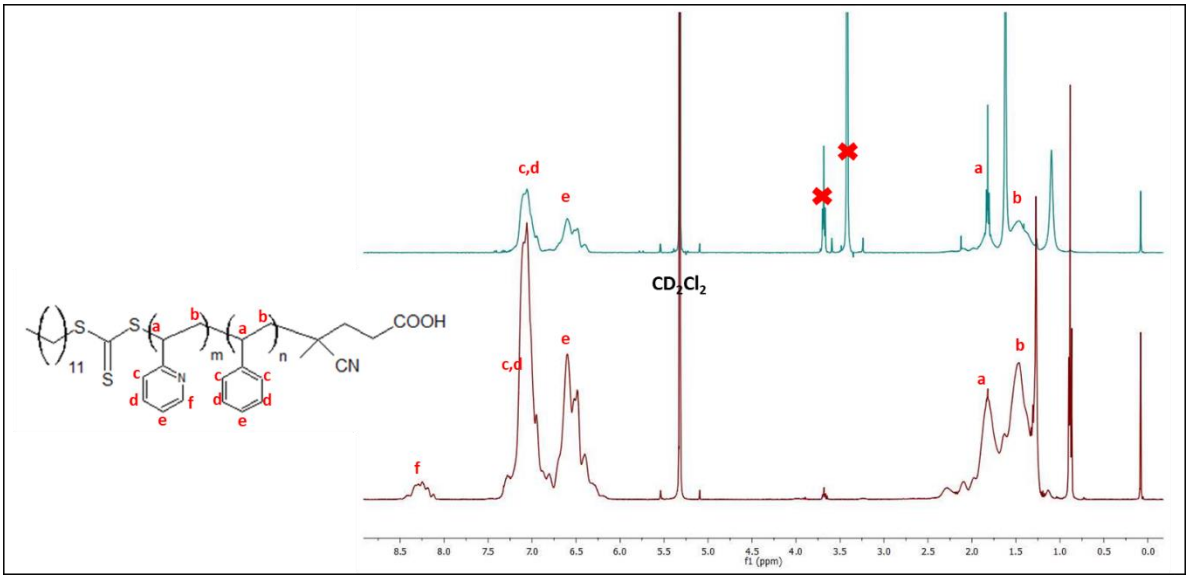

Figure 6. ^{1}H NMR spectra of the PS (in blue) and PS-*b*-P2VP (in red) macro-CTAs in CD_2Cl_2.

Figure 7 represents the SEC traces in THF using PS standard of the SV3 BCP (blue) and its corresponding hPS CTA (red, given for comparison). The monomodal blue curve indicates the absence of any residual hPS chains during the synthesis of the SV3 BCP having a molecular weight of ~41.8 Kg.mol^{-1}. In addition, the SEC trace shows that the SV3 chains have a relatively narrow molecular weight distribution (Đ = 1.14).

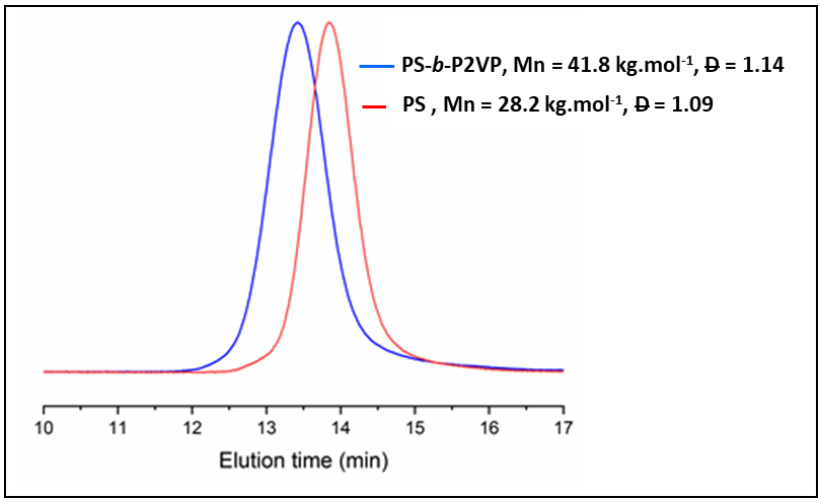

Figure 7. SEC traces of the PS (S7 in red) and PS-*b*-P2VP (SV3 in blue) macro-CTAs in THF.

4. Polystyrene-*block*-poly(2-vinylpyridine)-block-poly(*N*-isopropylacrylamide) (PS-*b*-P2VP-*b*-PNIPAM)

4.1. Synthesis of the PS-*b*-P2VP-*b*-PNIPAM macro-CTA by RAFT polymerization

The synthesis of linear ABC triblock teroplymers was performed as follows: PS-*b*-P2VP macro-RAFT agent, NIPAM and AIBN were dissolved in 1,4-dioxane. The solution was purged with nitrogen and placed in preheated oil bath at 70°C for certain amount of time (see **Scheme 4**).

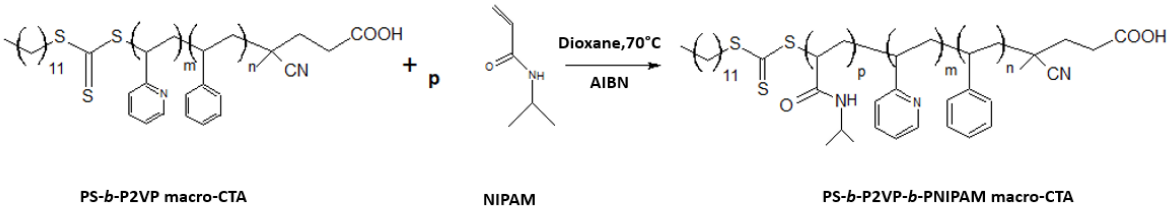

Scheme 4. PS-*b*-P2VP-*b*-PNIAM macro-CTA synthesis by RAFT polymerization.

The polymerization was stopped by placing the reaction vessel into ice bath and an aliquot was afterwards withdrawn. 1,4-Dioxane was removed with a rotary evaporator after which the PS-*b*-P2VP-*b*-PNIPAM chains were dissolved in a small amount of THF. The ABC triblock terpolymer was precipitated first from cold diethyl ether, in order to eliminate the unreacted NIPAM monomer, and then in heptane. Importantly, all the resulting PS-*b*-P2VP-*b*-PNIPAM terpolymers prepared *via* this route inherently contained PNIPAM dead chains that can be observed from their SEC chromatogram.

Here a side synthesis of free hPNIPAM takes place due to the poor accessibility of the CTA at the end chains of the PS-*b*-P2VP macro-CTA. This poor accessibility of the CTA, mainly due to a weak diffusion of both the initiator and NIPAM in presence of high molecular weight PS-*b*-P2VP chains, makes that the monomers preferentially react with the initiator before they ever

get a chance to polymerize with the PS-*b*-P2VP macro-CTA. Such a phenomenon gives rise to the formation of undesired PNIPAM chains in the reaction medium.

To properly separate the PS-*b*-P2VP-*b*-PNIPAM terpolymer from the undesired PNIPAM chains, a liquid-liquid extraction in dichloromethane/water was performed since hPNIPAM is soluble in water at temperature T < 32°C while the PS-*b*-P2VP-*b*-PNIPAM terpolymer is soluble in dichloromethane. Although this technique allowed the separation of the terpolymer from the homopolymer chains, several cycles of extraction were required to completely remove the unattached PNIPAM homopolymers, which results in a decrease of ~15% in the final yield.

In order to avoid this decrease of yield, we opted for liquid solid extraction namely Soxhlet extraction. Chen *et al.*[11] used Soxhlet extractor to remove the unreacted PNIPAM chains within functionalized silica nanoparticles.

Soxhlet extraction is based on a continuous extraction generally used for analysis of pesticides in food and soil materials. [12] The principle of Soxhlet extraction is based on continuous solvent reflux, where the solid component (polymer powder) is placed in suitable thimble (generally in cellulose) and is ground to a fine powder prior extraction to increase the area of the immersion liquid. The extractor containing the product in the thimble is connected to a round bottom flask containing the solvent that is heated to the boiling point. The subsequent steam in formation rises through the branch pipe of the extractor prior to be condensed and drops in the extractor. At this stage, the solvent enters in contact with the solid for extraction, and the siphon is then filled with solvent and at a certain amount and is siphoned back to the flask. The cycle is repeated until the solid is highly purified (see **Figure 8**).[13]

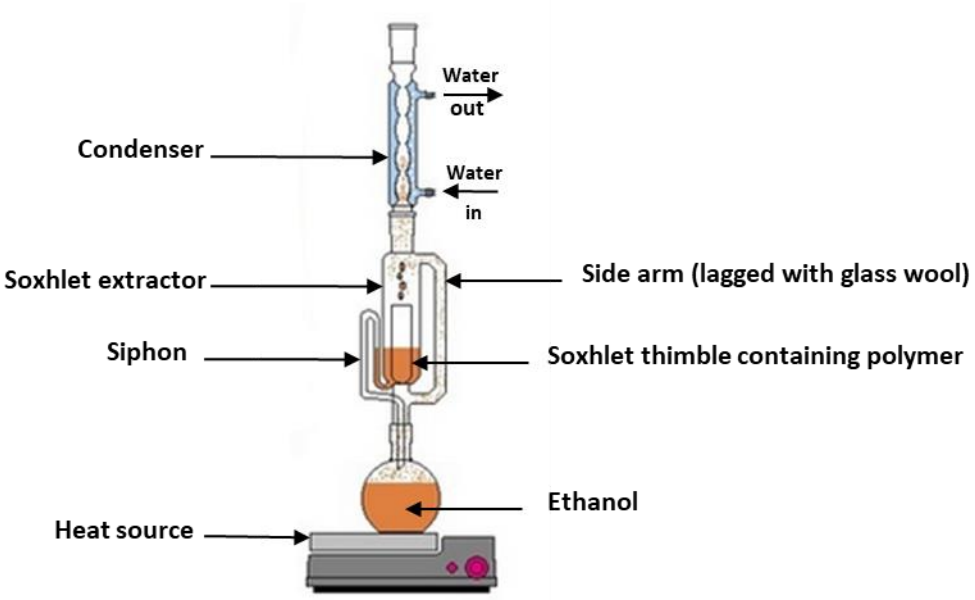

Figure 8. Soxhlet extraction set-up. [12]

Soxhlet extraction of PS-*b*-P2VP-*b*-PNIPAM terpolymers was performed in ethanol at 95°C for 4 days. For instance, the yield of NIPAM monomer transformation into PNIPAM was found to be 40% for the SVN7 terpolymer presented in **Table 3**.

Polymer	macro-CTA	M/CTA/AIBN	Reaction time (h)	Temperature (°C)	$M_{n,RMN}$ [a] (Kg/mol)	$M_{n,RMN}$ [b] (PS : P2VP : PNIPAM) (Kg/mol)	vol.fraction [c]	Conversion [d] (%)	Mn (SEC) (Kg./mol)	Mw/Mn [e]
SVN1	SV2	301 / 1 / 0.1	5	70	51.8	28.2 : 10.1 : 13.5	0.56 : 0.18 : 0.26	61	46 500	1.22
SVN2	SV5	301 / 1 / 0.05	3	110	80	40.5 : 33.8 : 5.7	0.53 : 0.40 : 0.07	26	54 600	1.4
SVN3	SV8	301 / 1 / 0.05	16	70	82.1	40.5 : 37.2 : 4.4	0.51 : 0.43 : 0.05	23	66 400	1.14
SVN4	SV6	286 / 1 / 0.2	5	70	88.9	49.9 : 23.3 : 15.7	0.58 : 0.25 : 0.17	47	63.4	1.43
SVN5	SV7	286 / 1 / 0.2	8	70	92.8	54.7 : 33.5 : 4.3	0.61 : 0.34 : 0.05	25	80.2	1.31
SVN6	SV7	286 / 1 / 0.2	8	70	92.1	54.7 : 31.1 : 6.3	0.61 : 0.32 :0.07	27	50.2	1.31
SVN7	SV3	301 / 1 / 0.1	5	70	42.5	28.2 : 5.8 : 8.5	0.68 : 0.13 : 0.19	56	26.4	1.32

[a] molar mass determined by ^{1}H NMR sepectroscopy [b] molar mass of each block determined by ^{1}H NMR spectroscopy. [c] volume fractions determined by ^{1}H NMR spectroscopy. [d] conversion determined by ^{1}H NMR spectroscopy. [e] polydispersity value determined by SEC

Table 3. Series of PS-*b*-P2VP-*b*-PNIPAM triblock terpolymers synthesized by RAFT polymerization.

After Soxhlet extraction in ethanol of PS-*b*-P2VP-*b*-PNIPAM chains, we noticed a decrease in P2VP ratio, meaning that the starting PS-*b*-P2VP macro-CTA contained some unattached P2VP hompolymers that dissolved in ethanol. This phenomenon indicates that the length of the synthesized BCP macro-CTA was already too long to incorporate properly the 2VP monomer.

4.2. Characterization of PS-*b*-P2VP-*b*-PNIPAM by ^{1}H NMR and SEC

The conversion of the synthesized PS-*b*-P2VP-*b*-PNIPAM macro-CTA corresponding to SVN7 in **Table 3** was calculated by ^{1}H NMR to be 56%. This percentage value was determined by comparing the integrated proton signals of the PNIPAM groups at 3.99 ppm to those of the NIPAM monomer. **Figure 9** shows the ^{1}H NMR spectrum in CD_2Cl_2 of the synthesized SVN7 triblock terpolymer (blue) as well as its associated hPS (green) and PS-*b*-P2VP (red) macro CTA spectra where the additional peaks arising from the PNINAM block were indexed as follows: δ = 3,99 (1H, s, CH), 1.13 (6H,m,CH3-). The (blue) ^{1}H NMR spectrum revealed that PS-*b*-P2VP-*b*-PNIPAM chains consisted of PS (28.2 kg/mol, f_{PS} = 0.68), P2VP (5.8 kg/mol, f_{P2VP} = 0.13) and PNIPAM (8.5 kg/mol, f_{PNIPAM} = 0.19).

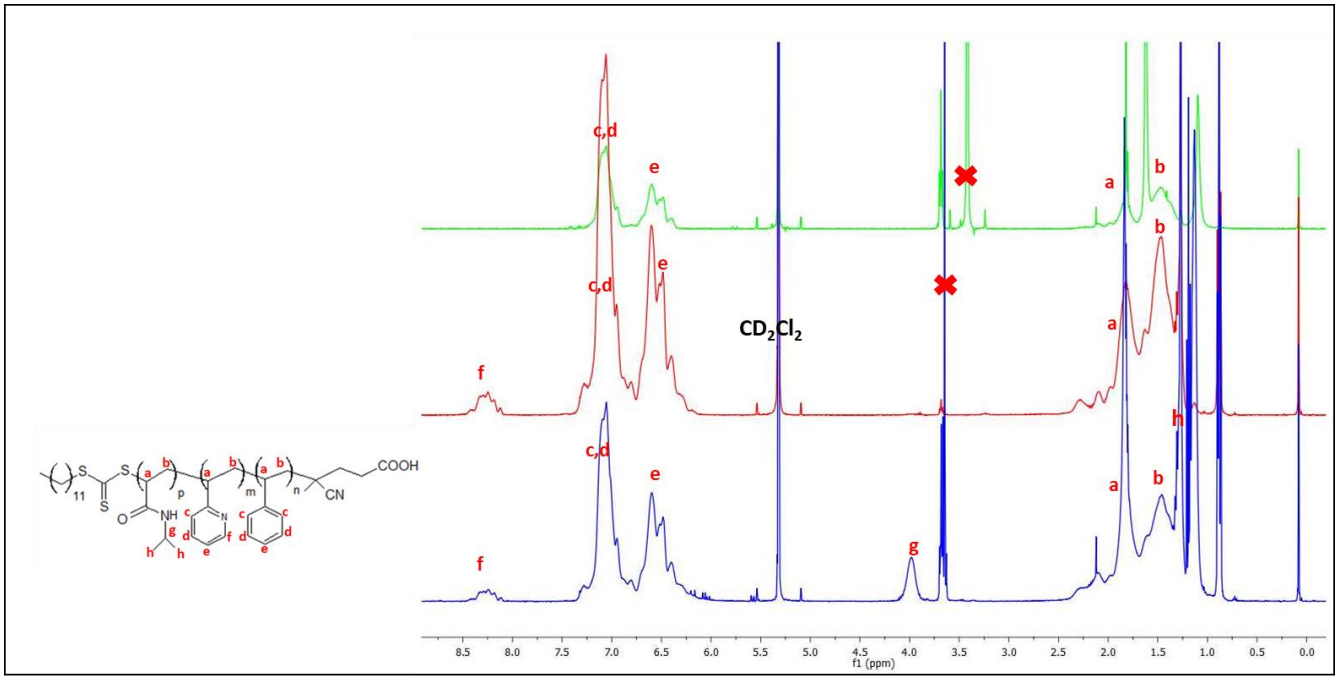

Figure 9. ^{1}H NMR spectra in CD_2Cl_2 of hPS (green), PS-*b*-P2VP (red) and PS-*b*-P2VP-*b*-PNIPAM (blue).

The SEC elugrams in THF corresponding to the SVN7 triblock terpolymer before (blue) and after (black) purification by Soxhlet extraction as well as the data (red) arising from the residual hPNIPAM concentrated in ethanol at the end of the extraction are shown in **Figure 10.a**. The presence of a shoulder (at low molecular weight side) on the blue curve evidences the presence of residual PNIPAM chains within the crude product, and makes that the molecular weight distribution of the blend is large (Đ = 1.79). After purification by Soxhlet extraction, a black curve with a monomodal profile can be observed. This SEC curve indicates that the purified SVN7 chains have a relatively narrow molecular weight distribution (Đ = 1.32) after the extraction of the undesired PNIPAM homopolymer giving rise to the red trace (Đ = 1.29). **Figure 10.b.** represents the SEC traces of the PS homopolymer (red), PS-*b*-P2VP (green) and PS-*b*-P2VP-b-PNIPAM (blue) chains synthesized by RAFT polymerization. All the polymers were obtained with relatively narrow molecular weight distributions (Đ < 1.32). The shift of the SEC curves toward higher molecular weights, resulting from the difference in the hydrodynamic volumes of polymers, fully supports the successful preparation of targeted ABC-type BCP chains.

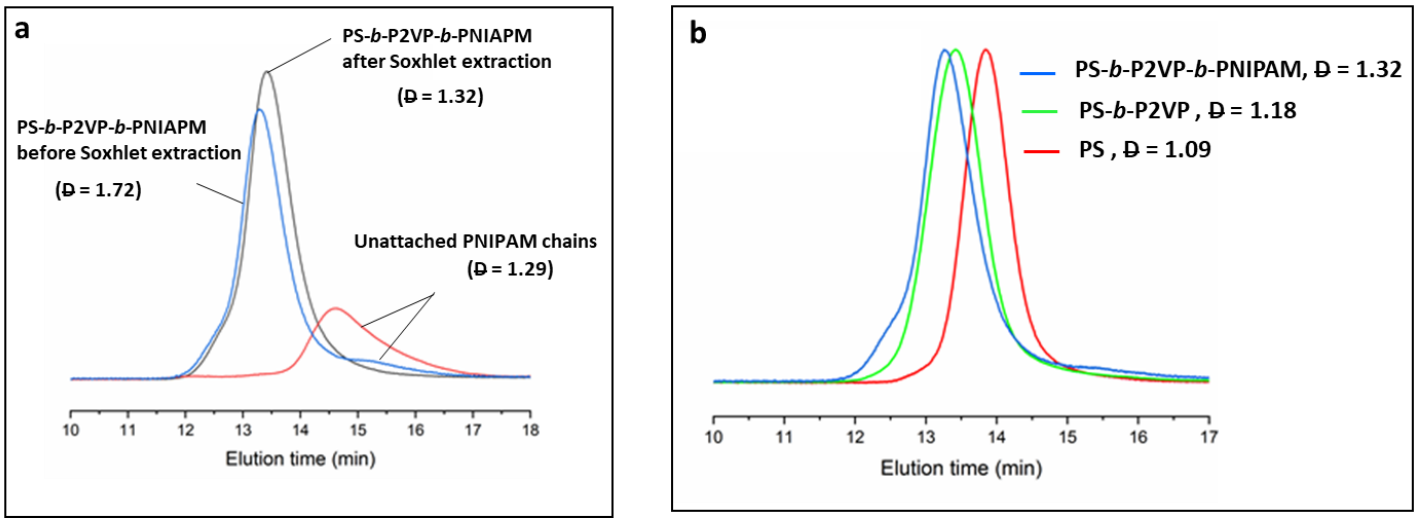

Figure 10. (a) SEC traces in THF of unattached PNIPAM chains (in red) eliminated by Soxhlet extraction and SEC traces of PS-*b*-P2VP-*b*-PNIPAM before- (in blue) and after Soxhlet extraction (in black). (b) SEC traces of PS (red), PS-*b*-P2VP (green) and PS-*b*-P2VP-*b*-PNIPAM (red).

Figure 11 represents the 2D DOSY (diffusion ordered spectroscopy) NMR spectra (600 MHz, $CDCl_3$) of the hPS (red), PS-*b*-P2VP (green) and PS-*b*-P2VP-*b*-PNIPAM (blue) chains. The protons assigned to each block are aligned along the same line, confirming a good purity of the polymers since all the signals arise from the same macromolecule having a diffusion coefficient of 5.01 x 10^{-11} $m^2.s^{-1}$. The diffusion coefficients of the PS and PS-*b*-P2VP chains are bigger than that of the ABC triblock terpolymer since they are found to be 6.60 x 10^{-11} $m^2.s^{-1}$ and 8.31 x 10^{-11} $m^2.s^{-1}$, respectively.

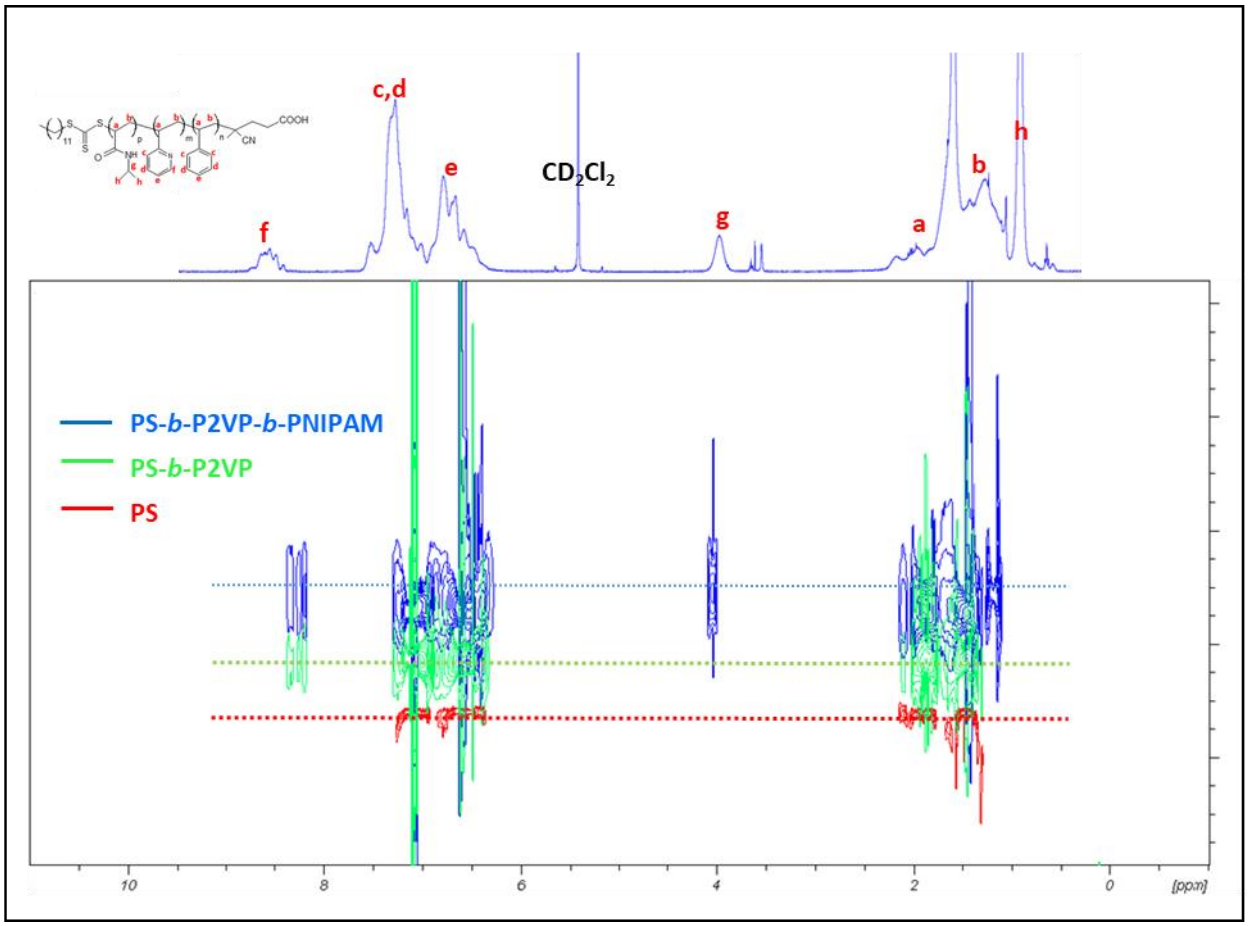

Figure 11. Overlaid ^{1}H NMR 2D DOSY spectra in $CDCl_3$ of hPS (red), PS-*b*-P2VP (green) and PS-*b*-P2VP-*b*-PNIPAM (blue).

5. Synthesis of linear CBA triblock terpolymers: effect of the block sequence order

As discussed previously, the synthesis of PS-*b*-P2VP-*b*-PNIPAM triblock terpolymer by RAFT polymerization required several purification steps due to the presence of free PNIPAM chains. In order to face this issue, another strategy was followed based in the change of the block sequence order. Here instead of beginning the terpolymer synthesis with a PS-macro CTA, we rather started the polymerization with a PNIPAM macro-RAFT agent, following by P2VP and PS, in order to prepare a linear CBA triblock terpolymer.

It was reported in the literature[10] that in case of linear ABC triblock terpolymers, the accessible morphologies within the phase diagram can be crucially influenced by the sequence order of the blocks. As the junction points are equivalent for a CBA-type BCP and its ABC homologue, the phase behavior of these triblock terpolymers would be basically the same. In fact, a linear CBA triblock terpolymer will differ from the ABC-type BCP only in the location of the RAFT agent end chains. Consequently, starting the polymerization with short PNIPAM chains could be a good alternative to purity and livingness issues reported previously. In addition, the change of the block sequence order and therefore the location of the RAFT agent end chains could be a good point of comparison of both the phase behavior and filtration performance of the BCP membranes.

RAFT polymerization is ideal for the synthesis of low molecular weights.[3] Besides, PNIPAM homopolymer has already been synthesized by RAFT in the literature with a low molecular weight and low dispersity value.[14] The aim of this section was the synthesis of linear CBA triblock terpolymer (*i.e.*, PNIPAM-*b*-P2VP-*b*-PS) by RAFT polymerization with a high PS volume fraction (targeted compositions: $f_{PNIPAM} = 0.1$, $f_{P2VP} = 0.2$ and $f_{PS} = 0.7$).

5.1. Synthesis and characterization of the PNIPAM macro-CTA

The RAFT polymerization was started by filling a ground flask with NIPAM, DDMAT, AIBN and dimethylformamide (DMF) used as solvent. The reaction mixture was stirred until full dissolution of solid components and purged with nitrogen. The reaction vessel was then sealed and placed in a preheated oil bath at 70°C for 2h30. The reaction was stopped by plunging the reaction vessel into an ice bath (see **Scheme 5)**. The crude product was precipitated three times

in cold diethyl ether and dried at room temperature under vacuum overnight to recover the PNIPAM macro-CTA.

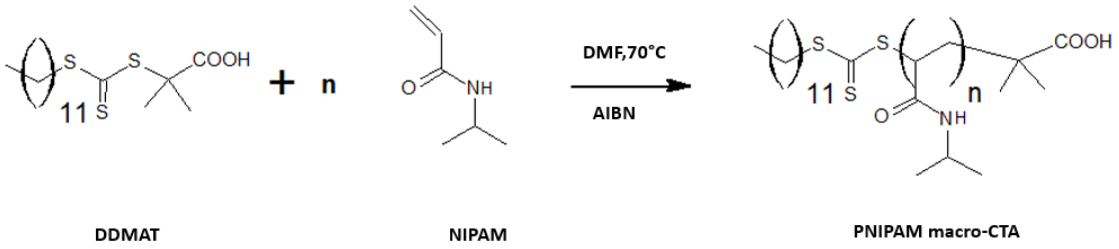

Scheme 5. Synthesis route for the PNIPAM macro-CTA by RAFT polymerization.

The molecular weight of the PNIPAM-macro CTA was determined by ^{1}H NMR spectroscopy by the following equation :

$$M_{n,\,RMN} = \frac{3 \int 3.98\ ppm}{\int 0.88\ ppm} \times M_{o,\,NIPAM} + M_{o,\,DDMAT}$$

Where ∫ represent the peak integral of the amide group of PNIPAM at 3.98 ppm and the peak integral of methyl group of end chain of DDMAT at 0.88 ppm. $M_{o,NIPAM}$ and $M_{o,DDMAT}$ are the molecular weight of NIPAM monomer and RAFT agent DDMAT respectively.

Conversely to PS-macro CTA discussed previously, the molecular weight of PNIPAM-macro CTA could be determined by NMR spectroscopy since the end chain of DDMAT were visible from the spectrum (see **Figure 12**, triplet zoomed in orange corresponding to 3H). The molecular weight of the synthesized hPNIPAM determined by ^{1}H NMR spectroscopy in CD_2Cl_2, $M_{n,NMR}$ was of ~7 kg.mol^{-1} while the one established by SEC, $M_{n,SEC}$, in THF using PS standard was of ~4.9 kg.mol^{-1}, Đ = 1.02.

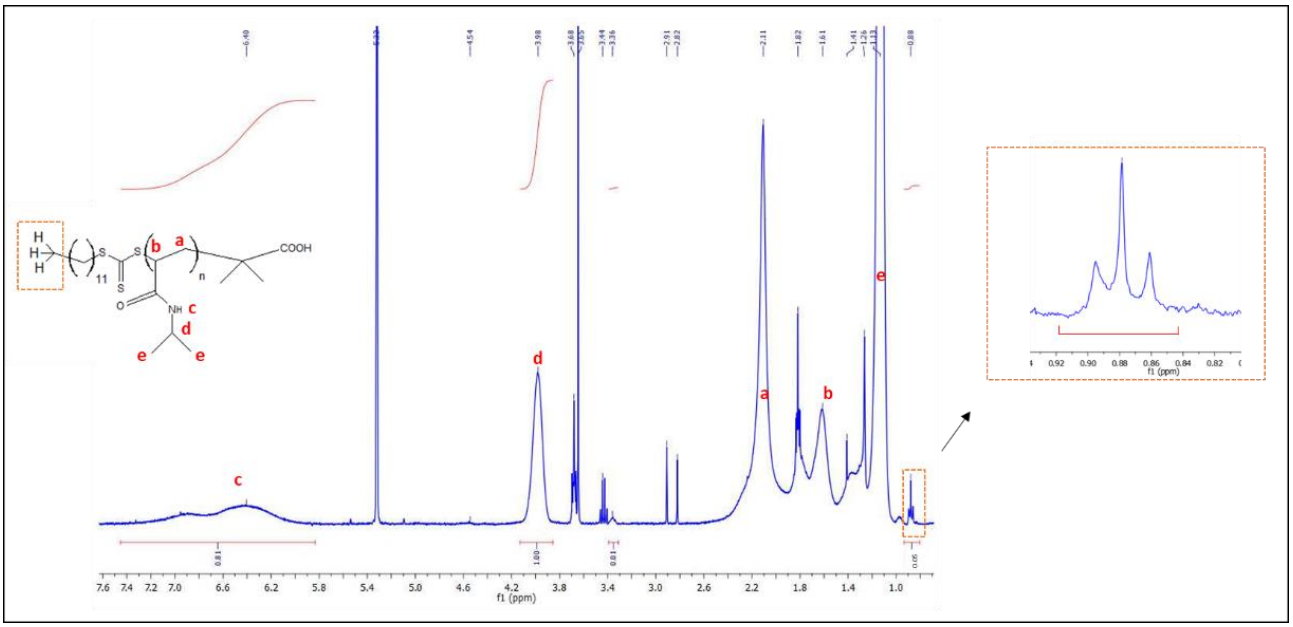

Figure 12. ^{1}H NMR Spectrum in CD_2Cl_2 of the PNIPAM macro-CTA.

5.2. Synthesis and characterization of the PNIPAM-*b*-P2VP macro-CTA

Starting from a PNIPAM macro-CTA, the controlled synthesis of BCPs containing 2VP by RAFT was previously described Zeng *et.al.*[15]. In this work, the same synthesis route was used to prepare PNIPAM-*b*-P2VP chains with low dispersity. For that purpose, the PNIPAM macro-CTA was mixed with 2VP and AIBN, and the reaction was performed in mass for 5h at 70°C prior to recover the PNIPAM-*b*-P2VP chains by twice precipitation in hexane (see **Scheme 6**).

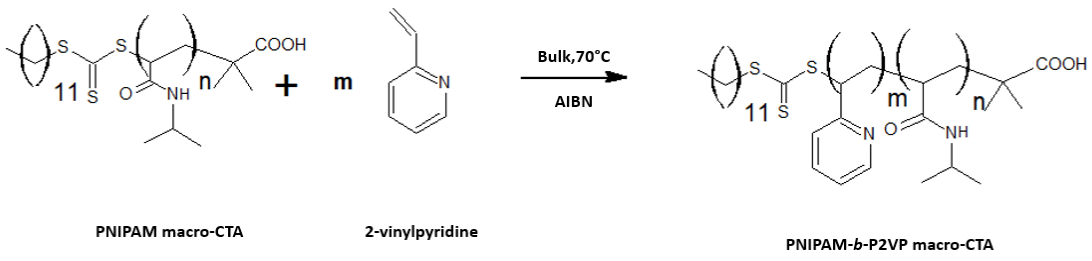

Scheme 6. PNIPAM-*b*-P2VP macro-CTA synthesis by RAFT polymerization.

Interestingly, the presence of a small shoulder at low molecular weight on the (blue) SEC trace presented in **Figure 13** makes that the crude product exhibits a higher dispersity value (Đ = 1.96) than the PS-*b*-P2VP chains. Due to its position on the SEC elugram, this shoulder unambiguously can be attributed to the unreacted PNIPAM chains. To eliminate hPNIPAM, the crude product was rinsed with cold water and lyophilized. This purification step was effective since a lower dispersity value (Đ = 1.3) can be observed on the (black) SEC trace of the recovered PNIPAM-*b*-P2VP chains due to a good shoulder attenuation (see **Figure 13**).

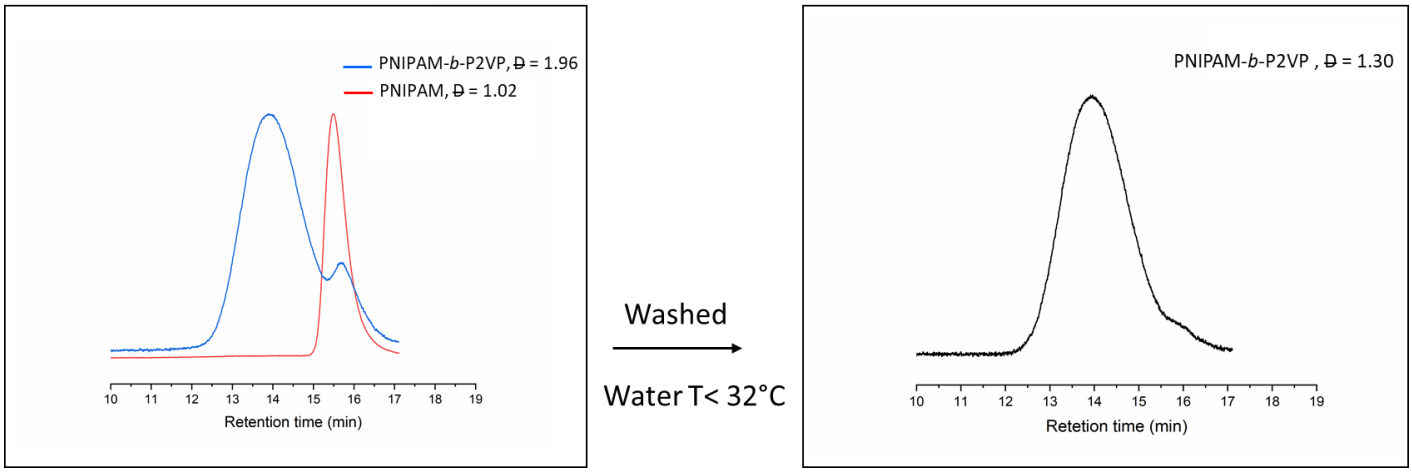

Figure 13. Superimposed SEC traces of PNIPAM-*b*-P2VP diblock and hPNIPAM (in the left) and SEC trace of the purified PNIPAM-*b*-P2VP chains in THF (in the right).

It is noteworthy that the undesired side reaction can be attributed to a reinitiation problem of the PNIPAM radicals on the 2VP monomer since the PNIPAM macro-CTA has a low molecular weight (M_n < 7 kg/mol). This is probably due to a difference in the reactivities of the species that was also reported by Bivigou-koumba *et.al* [1] for polymerization of styrene from a PNIPAM macro-CTA where a slow initiation and fragmentation of the intermediate radials as well as irreversible termination reactions were encountered. This behavior differs from the free radical polymerization of NIPAM occurring during the preparation of the PS-*b*-P2VP-*b*-PNIPAM terpolymer since the lower availability of the RAFT agent at the end of the PS-*b*-P2VP chains was identified as the main problem to explain this undesired reaction.

5.3. Synthesis and characterization of the PNIPAM-*b*-P2VP-*b*-PS macro-CTA

The first strategy for the incorporation of the PS block within the previously synthesized CB-type BCP consisted on the growing chain *via* RAFT polymerization (see **Scheme 7**). Here the PNIPAM-*b*-P2VP macro-CTA was mixed with styrene, AIBN and 1,4-dioxane. After degassing the reaction was plunged in preheated oil bath at 70°C for 48h.

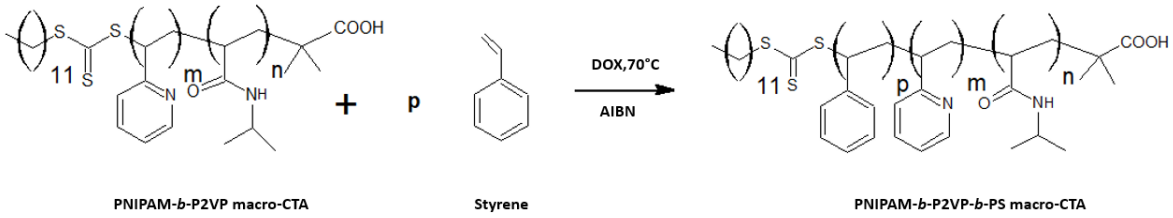

Scheme 7. PNIPAM-b-P2VP-b-PS synthesis by RAFT polymerization

The growing of PS block was slow and AIBN initially present in the reaction vessel was fully consumed about 24h. Therefore, the reaction was reinitiated by adding the same amount of AIBN, resulting in damaged RAFT end chains of the synthesized CBA triblock terpolymer.

To avoid this phenomenon, another synthesis strategy based on the RAFT emulsion polymerization was followed. Here we inspired from the work of Nieswandt *et al.* [16] based on the synthesis of the P3VP-*b*-PS BCP by this method. The reaction named surfactant-free RAFT emulsion polymerization known as a feasible and robust route towards the polymerization of a variety of vinyl monomers[16]. It was reported that the synthesis of PS by radical polymerizations has been found to be slow. Conversely, RAFT emulsion polymerization in water has been proven to be a feasible approach to accelerate styrene polymerization. In their study, Nieswandt and coworkers described the RAFT synthesis of P3VP-*b*-PS chains using a polymerization-induced self-assembly (PISA) approach, based on the chain extension of homopolymer-macro RAFT agents with co-monomer to eventually achieve the desired BCP.[16]

To follow this approach, in a flask containing the PNIPAM-*b*-P2VP macro-CTA dissolved in dimethylformamide (DMF) and water, AIBN dissolved in a small amount of DMF was first

added to the solution followed by styrene. After purging the headspace of the solution mixture with nitrogen, the reaction was allowed to proceed overnight under stirring at 800 rpm. After removing the DMF/H_2O mixture, the resulting PISA-latex was dissolved in THF and subsequently precipitated twice in diethyl ether prior to be washed in heptane.

Figure 14. represents the SEC traces of the CBA triblock terpolymer synthesized by RAFT emulsion polymerization (in blue), PNIPAM-*b*-P2VP diblock (in red) and PNIPAM homopolymer (in black). The shift to high molecular weight evidences the difference in hydrodynamic volumes of polymers and support the preparation of the synthesized CBA triblock terpolymer. A high molecular weight PNIPAM-*b*-P2VP-*b*-PS triblock terpolymer, with high PS volume fraction was synthesized, with $M_{n,SEC}$ = 115.1 kg.mol^{-1}, Đ = 1.17 and f_{PS} = 0.51.

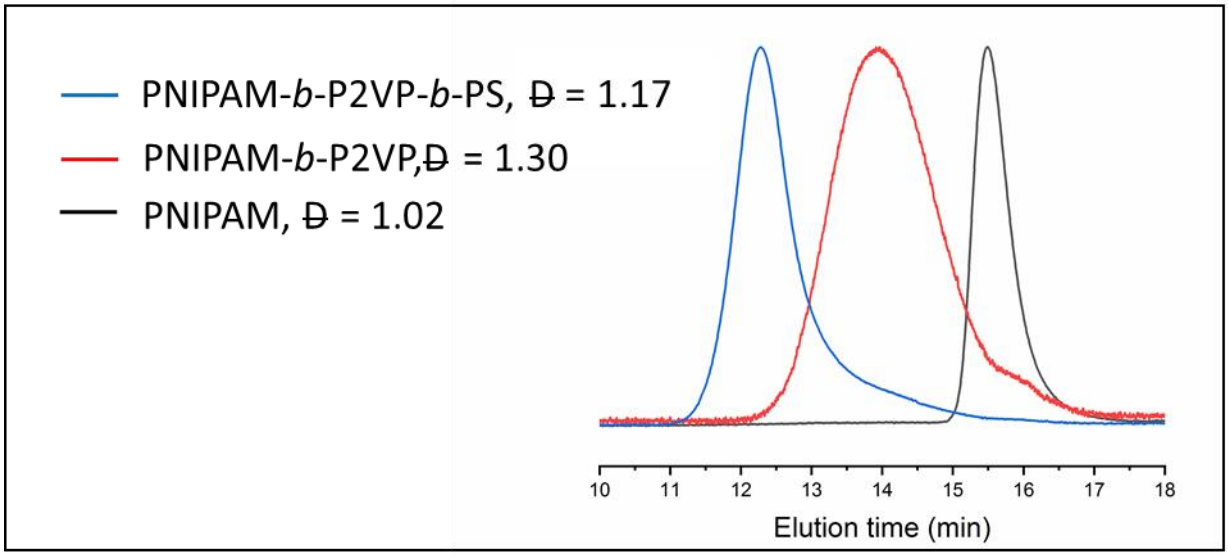

Figure 14. SEC traces of CBA macro-CTA by RAFT emulsion polymerization.

The synthesis of CBA triblock terpolymer by RAFT polymerization in this study was not successful. Starting with PNIPAM with low molecular weight and accessible end chains is more favorable in synthesis of block copolymer by RAFT polymerization, but in this case the reactivity of 2VP caused retardation of polymerization. The chain extension of styrene using the synthesized PNIPAM-*b*-P2VP as macro-CTA was slow, resulting in loss of livingness and control of the polymerization.

However, the chain extension of styrene *via* surfactant-free RAFT emulsion polymerization was more promising method, resulting in pure CBA linear triblock terpolymer with low dispersity values (Đ = 1.17), without any unattached dead chains.

6. Conclusion

In this chapter, linear PS-*b*-P2VP-*b*-PNIPAM triblock terpolymer was synthesized for the first time by RAFT polymerization. Different series of well-defined dual stimuli-responsive ABC triblock terpolymers were obtained with different molecular weight and compositions. The main issues reported during the synthesis were the purity and the livingness of polymers, specially the unattachement of hPNIPAM chains to the diblock, essentially due to its chain length.

Liquid-solid Soxhlet extraction was a successful purification technique to eliminate the remaining PNIPAM chains and obtain pure ABC triblock terpolymer by RAFT polymerization with high molecular weight.

Synthesis of polymer with low molecular weight is more favorable in RAFT polymerization. The change of monomer sequence order in this study and the use of acrylamide group with low molecular weight as starting block was not advantageous due to retardation polymerization. The use of other RAFT agent with the AIBN leaving R-group could be a solution to get a better control. Styrene chain extension was slow and several re-initiations were needed to obtain high PS volume fraction. The other technique tested was surfactant-free RAFT emulsion polymerization. The CBA triblock terpolymer obtained was pure with low dispersity value, however, this technique was not compatible with the aim of this study since it generates in situ formation of micellar structures through initial chain growth in aqueous solution.[16]

For the rest of this study, we preferred to work with synthesized ABC triblock terpolymer by RAFT polymerization with different composition, study their self-assembly behavior in bulk and finally membrane fabrication.

7. References

1. Bivigou-Koumba, A. M., Kristen, J., Laschewsky, A., Müller-Buschbaum, P. & Papadakis, C. M. Synthesis of Symmetrical Triblock Copolymers of Styrene and *N* -isopropylacrylamide Using Bifunctional Bis(trithiocarbonate)s as RAFT Agents. *Macromol. Chem. Phys.* **210**, 565–578 (2009).
2. Cetintas, M. *et al.* Free-standing thermo-responsive nanoporous membranes from high molecular weight PS-PNIPAM block copolymers synthesized via RAFT polymerization. *Polym. Chem.* **8**, 2235–2243 (2017).
3. Perrier, S. 50th Anniversary Perspective: RAFT Polymerization—A User Guide. 15 (2017).
4. Moad, G. Mechanism and Kinetics of Dithiobenzoate-Mediated RAFT Polymerization - Status of the Dilemma. *Macromol. Chem. Phys.* **215**, 9–26 (2014).
5. Jin, C., Liu, C., Jiang, B. & in, Q. Synthesis and characterization of high molecular weight and low dispersity polystyrene homopolymers by RAFT polymerization. *E-Polym.* **12**, (2012).
6. Sha, Y. *et al.* Synthesis of site-specific charged metallopolymers via reversible addition-fragmentation chain transfer (RAFT) polymerization. *Polymer* **187**, 122095 (2020).
7. Topham, P. D., Howse, J. R., Fernyhough, C. M. & Ryan, A. J. The performance of poly(styrene)-block-poly(2-vinyl pyridine)-block-poly(styrene) triblock copolymers as pH-driven actuators. *Soft Matter* **3**, 1506 (2007).
8. Wang, S. & Zhao, J. First-order conformation transition of single poly(2-vinylpyridine) molecules in aqueous solutions. *J. Chem. Phys.* **126**, 091104 (2007).
9. Borchert, U. *et al.* pH-Induced Release from P2VP−PEO Block Copolymer Vesicles. *Langmuir* **22**, 5843–58s47 (2006).

10. Antoine, S. Synthesis of linear and star miktoarm ABC terpolymers and their self-assembly in thin films. 162.
11. Chen, J., Liu, M., Chen, C., Gong, H. & Gao, C. Synthesis and Characterization of Silica Nanoparticles with Well-Defined Thermoresponsive PNIPAM via a Combination of RAFT and Click Chemistry. *ACS Appl. Mater. Interfaces* **3**, 3215–3223 (2011).
12. Stamm, O., Latscha, U., Janecek, P. & Campana, A. Development of a special electrode for continuous subcutaneous pH measurement in the infant scalp. *Am. J. Obstet. Gynecol.* **124**, 193–195 (1976).
13. Dabbs, D. M., Mulders, N. & Aksay, I. A. Solvothermal removal of the organic template from L 3 ("sponge") templated silica monoliths. *J. Nanoparticle Res.* **8**, 603–614 (2006).
14. Zeng, J. *et al.* Synthesis of poly(N-isopropylacrylamide)-b-poly(2-vinylpyridine) block copolymers via RAFT polymerization and micellization behavior in aqueous solution. *J. Colloid Interface Sci.* **322**, 654–659 (2008).
15. Zeng, J. *et al.* Synthesis of poly(N-isopropylacrylamide)-b-poly(2-vinylpyridine) block copolymers via RAFT polymerization and micellization behavior in aqueous solution. *J. Colloid Interface Sci.* **322**, 654–659 (2008).
16. Nieswandt, K., Georgopanos, P., Abetz, C., Filiz, V. & Abetz, V. Synthesis of Poly(3-vinylpyridine)-Block-Polystyrene Diblock Copolymers via Surfactant-Free RAFT Emulsion Polymerization. *Materials* **12**, 3145 (2019).

CHAPTER 3

Self-assembly of double-stimuli responsive PS-*b*-P2VP-*b*-PNIPAM triblock terpolymer membranes

Table of content

1. Introduction

Nowadays, one of the biggest challenge in membrane technology is the preparation of advanced materials combining high selectivity, high permeability and good fouling-resistance. An ideal membrane should be endowed with self-cleaning capabilities and should be composed of a macroporous substructure and a dense skin layer having a high-areal density of isopores to insure high permeability and high selectivity, respectively.

In this strategy, the block copolymers (BCPs) have attracted more attention in the manufacture of isoporous membranes with improved selectivity and permeability. Thanks to their ability to self-assemble into a large diversity of morphologies, they offer the possibility to adapt the size and chemistry of the membrane pores, resulting in a variety of pores geometries and a great flexibility in their functionalization.[1] Furthermore, the incorporation of stimuli-responsive pores into the membrane is one of the promising approach to help cleaning and overcome fouling issues. In this approach, the use of BCPs with stimuli-responsive characters can prevent the common problem of fouling (*e.g.*, thermal, pH, light, magnetic or electrical, etc.). Upon the application of one of these external stimuli, the pore sizes can be adjusted (*e.g.*, increased), resulting in a high back flush speeds and higher shear forces that lead to much more efficient physical cleaning.[2]

Non-solvent induced phase separation (NIPS) technique was introduced for the first time in the 1960s[3] to fabricate integrally asymmetric structure, and since that time it is still a promising approach that attracts lots of interest from the membrane community to prepare membranes with varied pore sizes ranging from nanometer to micrometer.[4] In this work, the phase behavior of the previously synthesized polystyrene-*block*-poly(2-vinylpyridine)-*block*-poly(*N*-isopropylacrylamide) (PS-*b*-P2VP-*b*-PNIPAM) triblock terpolymer was studied in membrane configuration. The NIPS technique was combined to a solvent vapor annealing (SVA) process to produce pH- and thermo-sensitive membranes.

In this chapter, we will detail the transformation of a poorly defined phase generated by NIPS on the top surface of asymmetric PS-*b*-P2VP-*b*-PNIPAM thick films into a well-ordered perforated lamellar (PL) structure when exposed to a chloroform vapor.

2. Self-assembly of PS-*b*-P2VP-*b*-PNIPAM triblock terpolymers

As reported in **Chapter 2**, the synthesis of linear PS-*b*-P2VP-*b*-PNIPAM triblock terpolymer was realized by RAFT polymerization. The three different polymer blocks were used for their intrinsic properties. For such reasons, the synthesized terpolymers were prepared of a high PS volume fraction in order to obtain mechanically robust membranes by phase inversion. P2VP was introduced to generate smart nanopores able to regulate their size under pH environment changes.[5] Indeed, the deprotonation of the pyridine groups under pH values above 5, results in a shrinkage of the P2VP block, and so an increase of the nanochannel porosity. Conversely, the swelling of the P2VP block under pH values below 5 makes that the nanopores close. To produce double stimuli-responsive nanochannels, the gold standard thermo-responsive PNIPAM has been also incorporated within the ABC-type BCP. Here, the lower critical temperature (LCST) of PNIPAM occurring at 32°C enables to control both the size and the hydrophilic/hydrophobic character of the pores by adjusting the water temperature.

The study of the self-assembly of the PS-*b*-P2VP-*b*-PNIPAM triblock terpolymer within double-sensitive membranes is detailed in the following section. For that purpose, the NIPS process was combined to the SVA technique in order to produce a well-defined perforated lamellar structure.

2.1. Non-solvent induced phase separation (NIPS)

2.1.1. Membranes preparation

Non-solvent induced phase separation (NIPS) technique was used for the first time by Loeb and Sourirajan in 1960 to prepare a reverse osmosis membrane with an asymmetric structure.[3] NIPS process is described as a controlled precipitation of a polymer solution by immersion in a coagulation bath.

In general, NIPS process is simple and based on three steps (see **Figure 1**). First, a polymer is dissolved in a solvent or solvents mixture that is/are miscible with the non-solvent. The polymer solution is then casted as a film and afterward immersed in a coagulation bath, that is nearly always water. As the solvent(s) and the non-solvent (water) are miscible, they exchange such that the solvent(s) diffuses out in water and water diffuses into the polymer solution. This solvents exchange continues until the polymer solution coagulates as a solid porous film.[6] The resulting membrane is composed of a dense skin layer and a macro/microporous substructure. On one hand, the dense surface is formed due to the solidification of the polymer top layer as soon as the cast membrane is in contact with the coagulation bath which is induced by a fast solvent outflow. On the other hand, the porous sub-layer morphology is formed from the liquid-liquid demixing during which the solution phase separates into a polymer rich-phase[5] and a polymer poor-phase.[7] In this case, the solvent/non-solvent diffusion rate as well as the solidification rate will define the final structure of the porous substructure.[8] Strathmann *et al.*[9] and Smolders *et al.*[10] reported in their work that if the solvent/non-solvent mutual diffusion is high, instantaneous demixing occurs with the formation of a macrovoid structure, while a bicontinuous structure is observed in the case where the diffusion rate is low enough to go through delayed demixing.

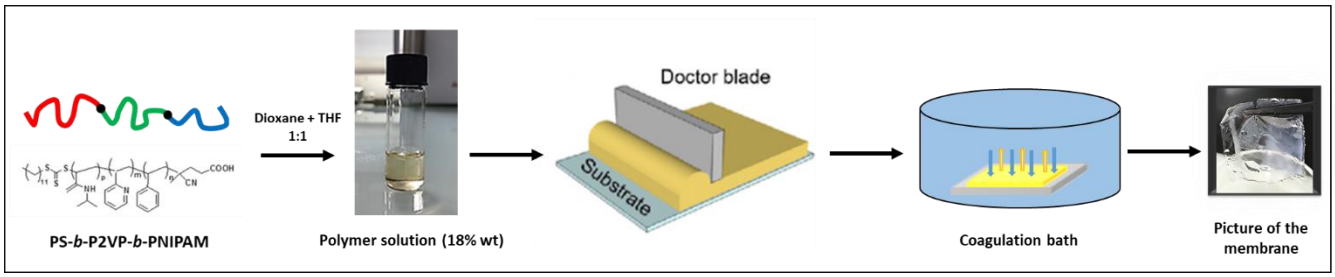

Figure 1. Non-solvent induced phase separation (NIPS) process used for the preparation of PS-*b*-P2VP-*b*-PNIPAM membranes.

The final membrane morphology depends on several parameters such as the type of polymers, molecular weights, polymer concentrations, the choice of solvent/solvents mixture, type of non-solvent, evaporation time, relative humidity, temperature of polymer solution and non-solvent bath.

In this chapter, the previously synthesized PS-*b*-P2VP-*b*-PNIPAM (**SVN7** from **Chapter 2**) composed of a high PS volume fraction (28.2 kg/mol, f_{PS} = 0.68), P2VP (5.8 kg/mol, f_{P2VP} = 0.13) and PNIPAM (8.5 kg/mol, f_{PNIPAM} = 0.19) was selected for the rest of this study.

The terpolymer was dissolved in a di-solvent mixture of 1,4-dioxane (DOX) and tetrahydrofuran (THF) (50/50 by weight). The choice of solvents is one of the most important parameters for NIPS, due to the significant effects on the final material properties.[11] In this study, THF and DOX are miscible with water and are selective solvents for the three blocks. THF was chosen since it is frequently used for the preparation of block copolymer membranes, due to its high volatility and its ability to create ordered structures.[11–13] DOX is a good solvent for the three polymers and evaporate slower than THF.

After the complete dissolution of the PS-*b*-P2VP-*b*-PNIPAM in the DOX/THF di-solvent mixture, the polymer solution (18 wt.%) was casted onto (3x3 cm) silicon substrates by using a tape casting technique with a 250 μm gap. DOX and THF were allowed to evaporate during 30s at room temperature (RT), thus forming a dense air surface layer with a kinetically trapped nanoporous structure. The prepared PS-*b*-P2VP-*b*-PNIPAM membrane was immersed into a deionized water bath at RT for 5 min to induce the polymer precipitation. In this step, the miscible solvent mixture and the non-solvent exchange to give rise to a so-called integral-asymmetric membrane. When the viscous polymer film is transferred to the non-solvent, PS precipitates and a matrix is formed due to the poor affinity of PS with water.[14] In order to facilitate the removal of the terpolymer membranes from the substrate, the silicon pieces were treated by an oxygen plasma in a home-made chamber prior to their use (plasma conditions: 45W mTorr O_2, 10 min). A sacrificial poly(poly(3,4-ethylenedioxythiophene) polystyrene sulfonate (PEDOT: PSS) was then inserted by spin-coating between the substrate and the PS-*b*-P2VP-*b*-PNIPAM thick films.

In this work, the polymer concentration was kept to 18 wt.% in order to avoid any problem related to polymer solution viscosity. Indeed, it was reported that a higher polymer concentration (~25 wt.%) results in higher viscosity solution which prevents the non-solvent penetration, resulting in the formation of a dense structure.[7]

The evaporation time before the polymer film immersion in water was about 30s to allow the formation of a dense top layer. This is in accordance with previous results since Jung *et al.*[15] reported that an irregular membrane layer composed of few nanopores and macropores was formed within PS-*b*-P2VP membranes for a shorter evaporation time (~20s). Conversely, by increasing it by 5s, perpendicular and parallel cylinders were formed. The authors also demonstrated that the best result was obtained for an evaporation time of 30s, since hexagonally packed cylinders with a perpendicular orientation take place. For longer evaporation time, the homogeneous layer is still present but the cylinders are not hexagonally assembled anymore.

2.1.2. Membranes characterization

Atomic force microscopy (AFM Nano-Observer, CSInstruments) was used to study the local surface morphology of the films. Silicon cantilevers (PPP-NCH, Nanosensors) with a typical tip radius of ~5 nm were used. The resonance frequency of the cantilevers was about 235 kHz. Prior AFM measurements, PS-*b*-P2VP-*b*-PNIPAM thick films were treated with a fluorine based plasma in a home-made chamber to improve the AFM topographic image contrast (plasma conditions: 45W, 75 mTorr CF_4 and 90s).

Scanning electron microscopy (SEM) was used to analyze the membranes cross section and top surface. SEM pictures were obtained using a Hitachi S4800 operating under 0.1-30 kV working voltage.

Figure 2 shows two representative top surface morphologies of PS-*b*-P2VP-*b*-PNIPAM thick films generated by NIPS (as cast) for a solvent evaporation time of 30s. Interestingly, for similar NIPS process conditions, the membrane top surfaces exhibit different morphologies: one is highly porous while the other one appears denser (*i.e.*, less porous). In **Figure 2.a** is presented a highly porous top surface membrane exhibiting a rough surface (R_{rms} = 10.8 nm) and a mean center-to-center pore spacing, *p*, of ~68 nm as extracted from the 2D-fast Fourier transform (FFT). This poorly-ordered phase generated by NIPS on the material top surface is mainly due to the presence of a large amount of solvent within the skin layer when the sample was transferred in the water bath. In contrast, a denser membrane top surface with R_{rms} = 23.8 nm and *p* = 12 nm can be observed from on **Figure 2.b**. Here, it appears that the remaining solvents (mainly THF) contained in the as-cast polymeric membrane have been evaporated faster to leave a denser top surface. Note that the two top surface morphologies were generated by the

same NIPS conditions (*i.e.*, similar polymer solution concentration, evaporation time and immersion time in the coagulation bath) but not made the same day, thereby indicating that the external temperature and the relative humidity variations play an important role on the NIPS process reproducibility. Such results demonstrate that the preparation of asymmetric and isoporous copolymer thick films by NIPS require extensive optimization.

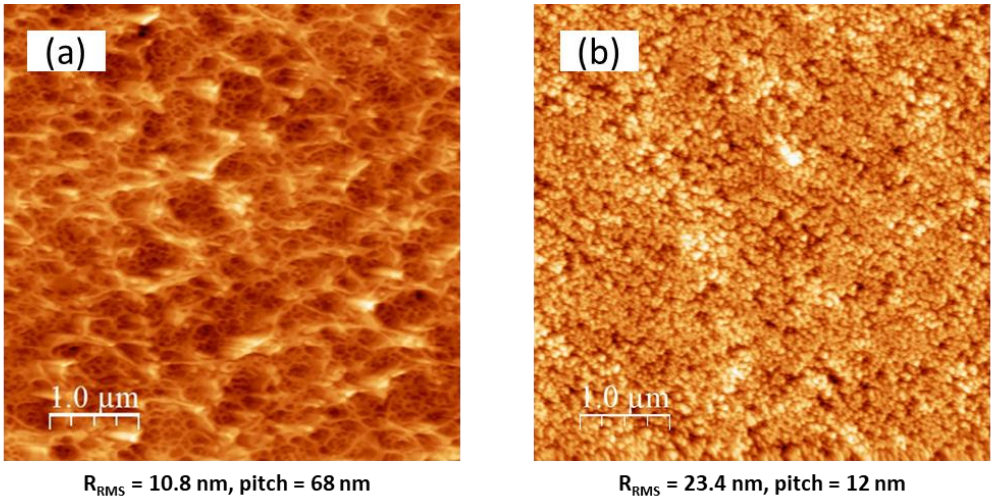

Figure 2. (a) and (b) AFM topographic images of NIPS-made (as cast) PS-*b*-P2VP-*b*-PNIPAM thick films.

To produce well-ordered nanochannels within the membrane skin layer, the NIPS process was combined to a SVA treatment as previously performed.[16–18] In the following section, it is detailed the top surface reconstruction of PS-*b*-P2VP-*b*-PNIPAM thick films by SVA treatment.

2.2. Solvent vapor annealing (SVA)

The solvent vapor annealing process is based on the exposure of the BCP film to vapors of one or more solvents at temperature below the bulk glass temperature (T_g) of the different blocks to form a swollen and mobile polymer film on the substrate. The process takes place in a closed chamber continuously filled with solvent vapor(s). SVA is highly effective over other techniques such as thermal annealing requiring large timescales, particularly for high molecular

weight BCPs. SVA is highly dependent on several parameters such as the χ-parameters, the degree of polymerization (N), the BCP composition, and more importantly the type of solvent and SVA treatment time.[19] Indeed, the importance of solvent choice is related to the reconstruction of the surface during the SVA treatment. In general, when the BCP film is cast from a solvent onto a substrate, it becomes kinetically trapped in a non-equilibrium, disordered and ill-defined structure. The solvent chosen must drive sufficiently the mobility of the polymer chains to allow for a structural reorganization.[20]

2.2.1. Membranes preparation

In this study, the self-assembly of PS-*b*-P2VP-*b*-PNIPAM terpolymers was stimulated by exposing films for different times (ranging from 0h to 7h) to a continuous stream of chloroform ($CHCl_3$) as represented in **Figure 3**. Chloroform is a good solvent for the three polymers and can drive the chain mobility. The vapor was produced by bubbling nitrogen gas through the liquid solvent as described in previous works.[21–23] The continuous flow system was used to control the $CHCl_3$ vapor pressure in the chamber by dilution with a separate N_2 stream so that a solvent vapor consisted of 32 sccm $CHCl_3$ vapor and 8 sccm N_2 (total 40 sccm). The morphology of the solvent-annealed PS-*b*-P2VP-*b*-PNIPAM thick film was frozen by fast removal of the chamber lid.

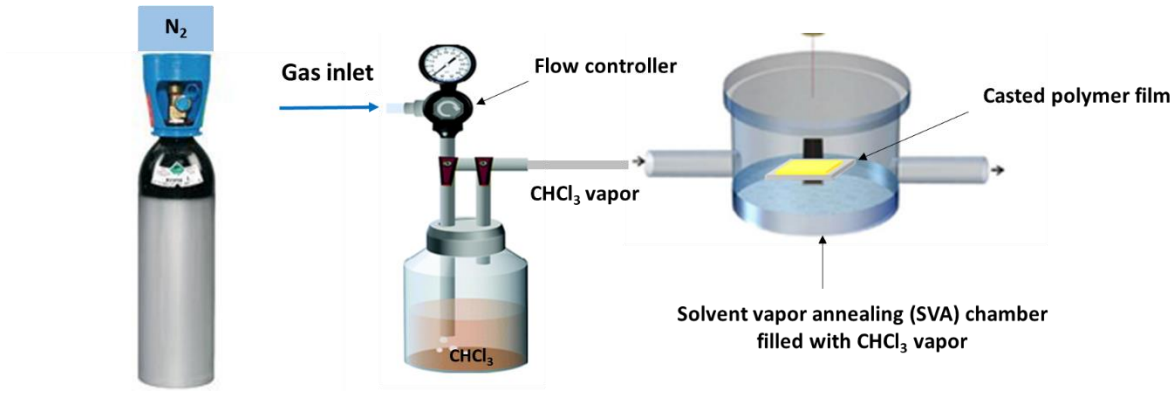

Figure 3. Schematic representation of solvent vapor annealing (SVA) setup used in this work. Adapted from [24, 25**].**

2.2.2. Membranes characterization

Figure 4 shows the AFM topographic images of several membrane top surfaces generated by NIPS-SVA from three different PS-*b*-P2VP-*b*-PNIPAM (SVN) terpolymers with the respective volume fractions (determined by ^{1}H NMR): S:V:N = 56:18:26 (51.8 kg/mol, Đ = 1.22) (see **Figure 4.a**), S:V:N = 61:34:5 (92.8 kg/mol, Đ = 1.31) (see **Figure 4.b**), and S:V:N = 68:13:19 (42.5 kg/mol, Đ = 1.32) (see **Figure 4.c**). Here, the solvent was allowed to evaporate for 30s during the NIPS process, and the three different PS-*b*-P2VP-*b*-PNIPAM membranes were then exposed to a $CHCl_3$ vapor during 6h. Under such conditions, the use of CF_4 plasma etching reveals that the equilibrium structure formed on the membrane top surfaces consists of an alternation of long range-ordered PS (bright) and P2VP/PNIPAM (dark) out-of-plane lamellae.

In all cases, the combination of the NIPS and SVA techniques result in a full reconstruction of the membrane top surfaces into a lamellar morphology where the period varies as follows: (a) 55.7 nm, (b) 53.1nm and (d) 41 nm. Note that the PS-*b*-P2VP-*b*-PNIPAM chains with the largest PNIPAM composition (S:V:N = 56:18:26) are ordered into out-of-plane lamellae with short-range order which should be taken account to explain its larger periodicity.

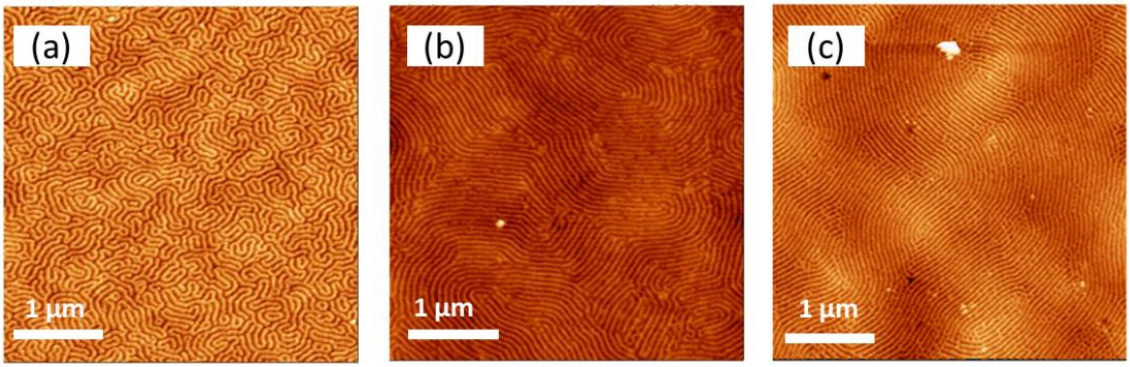

Figure 4. AFM topographic images of several membrane top surfaces generated by NIPS-SVA (30s-$CHCl_3$, 6h) from three different PS-*b*-P2VP-*b*-PNIPAM (SVN) terpolymers: (a) S:V:N = 56:18:26 (51.8 kg/mol, Đ = 1.22), (b) S:V:N = 61:34:5 (92.8 kg/mol, Đ = 1.31) and (c) S:V:N = 68:13:19 (42.5 kg/mol, Đ = 1.32).

To better understand the phase behavior of the PS-*b*-P2VP-*b*-PNIPAM chains during the SVA process, AFM topographic images, taken for different times of exposure to a chloroform stream, are presented in **Figure 5**. When the PS-*b*-P2VP-*b*-PNIPAM (S:V:N = 68:13:19) membrane is solvent-annealed during 30min, the top surface roughness and the pore size start to decrease, in comparison with the as-cast surface morphology (see **Figure 2a**). Indeed, a smooth top surface membrane (R_{rms} = 0.7 nm) with pores having a mean period of ~47 nm are produced from a solvent-annealed ($CHCl_3$, 30 min) PS-*b*-P2VP-*b*-PNIPAM thick film. By increasing SVA treatment to one hour, the period of the nanostructure formed on the membrane top surface decreased again to ~42 nm (very close to the equilibrium period of 41 nm, see **Figure 4.c**) and a narrower first-order peak is observed on the power spectral density (PSD) profile (see **Figure 5.c**). The presence of a high-order peak located at 2k (where k is the spatial frequency) confirms an increase of the long-range order of pores on the membrane top surface.

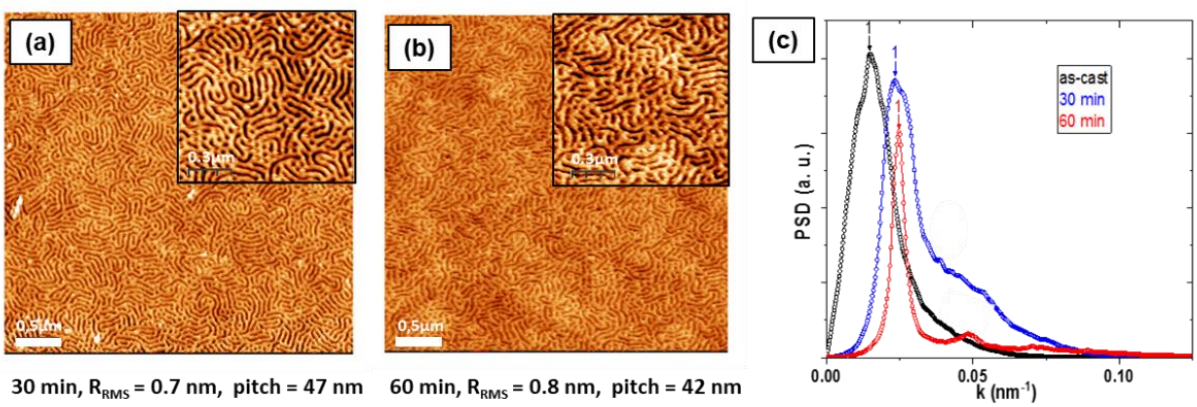

Figure 5. (a) and (b) AFM topographic images of PS-*b*-P2VP-*b*-PNIPAM (S:V:N = 68:13:19) thick films treated by SVA for 30min and 60min in a $CHCl_3$ vapor. (c) Power spectral density (PSD) profiles of NIPS-made (as cast) and SVA treated thick films (30min and 60min).

SEM image presented in **Figure 6.a** shows the representative top view of a PS-*b*-P2VP-*b*-PNIPAM thick film generated by NIPS. A dense top surface layer with poorly defined domains is produced when the mixture of di-solvents is allowed to evaporate from the PS-*b*-P2VP-*b*-PNIPAM material for 30s. The cross-sectional view presented in **Figure 6.b**. indicates this 500 nm thick dense top layer with closed pores has formed on microporous substructure exhibiting a (spinodal) open network morphology (see the part bellow the dotted line in **Figure 6.b**).

Cross-sectional SEM images of solvent-annealed (6h, $CHCl_3$) PS-*b*-P2VP-*b*-PNIPAM thick films taken close to the top surface and in middle of the material are shown in **Figure 6.c** and **d**, respectively. These images reveal that after the SVA treatment, the microporous open network generated by NIPS has been transformed into an ordered lamellar phase (see **Figure 6.d**).

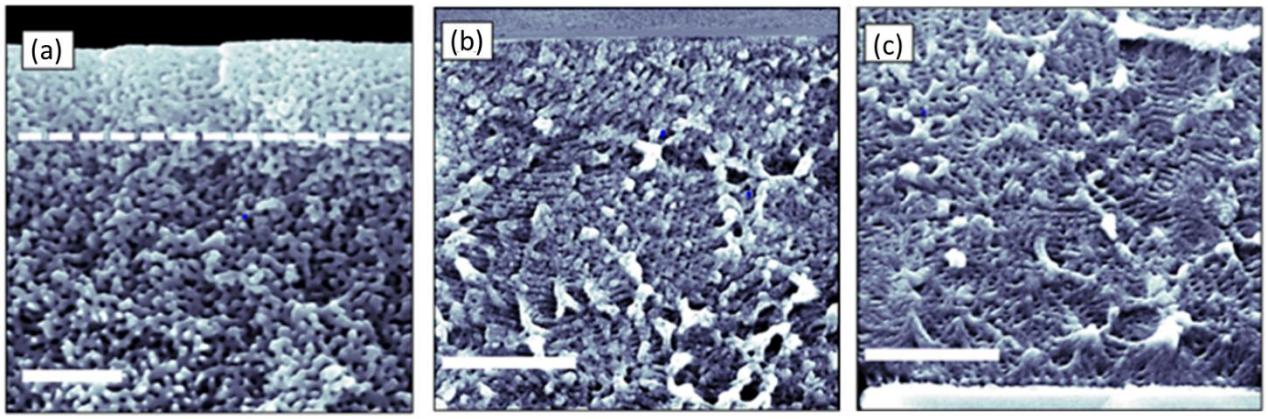

Figure 6. (a) Cross-sectional SEM view of an asymmetric PS-*b*-P2VP-*b*-PNIPAM thick film generated by NIPS showing a 500 nm thick top layer with a poorly defined phase delimited from the sponge-like substructure by a dashed line. (b) Cross-sectional SEM views of a solvent-annealed (6h, $CHCl_3$) PS-*b*-P2VP-*b*-PNIPAM thick film generated by NIPS-SVA showing the formation of a symmetric membrane composed with a lamellar phase in the top and in the (c) bottom interfaces. Scale bars: 500 nm.

In the following part, the filtration performances of the prepared PS-*b*-P2VP-*b*-PNIPAM membranes were studied as a function of temperature and pH variations.

3. Double stimuli-responsive membranes

The water permeability of the different PS-*b*-P2VP-*b*-PNIPAM thick films was studied using a dead-end filtration set-up by measuring the flux of Milli-Q pure water at different pressures (0–2 bar). The membrane was cut into a round shape with a diameter of 2.5 cm supported by a high permeable hydrophilic polyvinylidene fluoride (PVDF) material. It was subsequently placed in an Amicon type filter cell (Amicon 8010 stirred cell) with a volume of 10 mL. The cell was connected to a pressure vessel filled with Milli-Q pure water, where pressure was applied using compressed air line. The cell and the vessel were heated to specific temperatures ranging from 15 °C to 46°C by placing them inside a stainless steel electronic bath filled with water (see

Figure 7). To ensure a stable temperature, the cell was stored at a specific temperature for half an hour before the measurement.

Figure 7. Schematic representation of the dead-end filtration setup used in this work.

3.1. Thermo-responsive PS-*b*-P2VP-*b*-PNIPAM thick films

In order to investigate the thermo-responsive properties of the membrane, we studied membrane permeability at temperature below (15°C) and above (45°C) the LCST of PNIPAM (32°C). The water permeability ($L.h^{-1}.m^{-2}.bar^{-1}$) was calculated as the ratio of the flux over the applied pressure drop as shown in the following equation:

$$\text{Permeability} = \frac{V}{(A.t.\Delta P)} = J/\Delta \text{P}$$

Where V is the permeate volume (L), A is the membrane area (m^2), t is the time (h), J is the permeate flux ($L.h^{-1}.m^{-2}$) and ΔP is the pressure drop across the membrane (bar). For temperature higher than 20°C, the permeability was normalized for the temperature dependent changes in viscosity of the water passing at elevated temperature. For that purpose, the permeability results were corrected by multiplying the results with the relative change in the dynamic viscosity of water given at a specific temperature compared to that of water at 20°C.

In this section, we will detail the water permeability values obtained as a function of the annealing time and temperature.

Table 1 and 2 summarize the normalized water permeability rates of NIPS-SVA made PS-*b*-P2VP-*b*-PNIPAM thick films.

The NIPS-made PS-*b*-P2VP-*b*-PNIPAM thick films showed different disordered morphologies: one composed of completely open pores (refereed hereafter as case 1) and the other with closed pores (case 2).

Annealing time ($CHCl_3$)	Temperature (°C)	Permeability normalized to 20°C (L/h*m²*bar)
0	Blow LCST*	112
0	Above LCST**	194
30min	Blow LCST	25 ± 20
30min	Above LCST	96 ± 27
1h	Blow LCST	21
1h	Above LCST	115
6h	Blow LCST	24
6h	Above LCST	119

Below LCST* = 23°C
Above LCST** = 38 °C

Table 2. Membrane permeability rates as a function of the annealing time and temperature obtained from open porous NIPS-made membranes (see Fig. 2a).

Annealing time ($CHCl_3$)	Temperature (°C)	Permeability normalized to 20°C ($L.m^{-2}.h^{-1}.bar^{-1}$)
0	Below LCST*	0
0	Above LCST**	0
30min	Below LCST	7 ± 2
30min	Above LCST	50 ± 9
2h	Below LCST	2 ± 1
2h	Above LCST	18 ± 4
6h	Below LCST	2 ± 1
6h	Above LCST	18 ± 4

Below LCST* = 15.2°C
Above LCST** = 46.0 °C

Table 1. Membrane permeability rates as a function of the annealing time and temperature obtained from closed porous NIPS-made membranes (see Fig. 2b).

In the first case, the NIPS-made membrane is composed of highly open pores generated during the solvent exchange. The water permeability value recorded at 23°C is maximized to 112 $L.h^{-1}.m^{-2}.bar^{-1}$ when the nanostructure formed was composed of highly disordered and large open pores as shown in **Table 1**. After the SVA treatment, the membranes surface reconstruction induced by the polymer chain mobility in $CHCl_3$ vapors results in decrease of permeability at temperature below LCST to 25 $L.h^{-1}.m^{-2}.bar^{-1}$ accompanied by a pronounced thermo-responsive character at temperature above LCST (~ 96 $L.h^{-1}.m^{-2}.bar^{-1}$). By increasing the SVA treatment of the prepared membrane to 1h and 6h, the permeability remains the same (~ 115 $L.h^{-1}.m^{-2}.bar^{-1}$). This is mainly due to the polymer chain mobility that reaching the thermodynamic equilibrium. This is in agreement with informations extracted from AFM topograpgic images, where the period decreases until a thermodynamic equilibrium, and thus the permeability does not change even until 6h.

In the second case, the as-cast membrane is composed of completely closed pores. Not surprisingly, no permeability was recorded in this case as shown in **Table 2**. However, after 30 min exposition to $CHCl_3$ vapors, the membrane surface reconstruction allows to reach a water permeability of 7 $L.h^{-1}.m^{-2}.bar^{-1}$ at temperature below LCST (at 15°C). By heating up the membrane above the PNIPAM LCST (at 46°C), the permeability was measured to be 7 times higher (50 $L.h^{-1}.m^{-2}.bar^{-1}$), thereby confirming the thermo-responsive character of the terpolymer thick film generated by the collapsed state of the PNIPAM blocks. After 2h of exposure to $CHCl_3$ vapors, the water permeability at 15°C decreased by 70 % to

2 $L.h^{-1}.m^{-2}.bar^{-1}$, which is due to the membrane top surface reconstruction as discussed previously. Finally, the permeability value for a terpolymer membrane exposed to a $CHCl_3$ vapor for 6h, was quite similar to the one measured at 2h at temperatures below and above the PNIPAM LCST. Such results are in accordance with membrane top surface reconstruction observed by AFM, where the period of the nanostructure formed on the membrane top surface was close to the equilibrium period. We can note that the morphology changes of porous nanodomains are due to the mobility of polymer chains driven by the $CHCl_3$ vapors.

From these results, we can conclude that the NIPS-made thick films are not stable and can generate different top surface organizations. However, the combination of the NIPS process with a SVA treatment generate the same overall qualitative trend in term of permeability. Starting from an initial membrane morphology genetrated by NIPS, the permeability at temperature below LCST starts to decrease and stabilizes when for a SVA treatment of 1h. The thermo-responsive behavior caused by the difference in pore size between the open and close states of PNIPAM-based nanodomains is more pronouced in well organised top surface. Finally, we can note that the morphology change of porous nanodomains strongly influences the overall membrane permeability since we observe that the water transport properties, at temperature above LCST, through poorly ordered membrane top surfaces (SVA, 30 min, 96 L. $L.h^{-1}.m^{-2}.bar^{-1}$) are lower than that through highly ordered lamellae (SVA, 6h, 115 $L.h^{-1}.m^{-2}.bar^{-1}$).

The corrected and uncorrected permeability values of the NIPS-SVA made PS-*b*-P2VP-*b*-PNIPAM annealed 30 min in $CHCl_3$ is presented in **Figure 8**. The thermo-responsive behavior is a consequence of the chain collapse of PNIPAM above its LCST. The linear relation between flux and pressure for 20°C and 46°C demonstrate the mechanical stability of the membrane. Indeed, if the membrane exhibited any compaction or rupture, there would be deviation from linearity. The slope of the line for viscosity corrected flux at 46°C (~ 56 $L.h^{-1}.m^{-2}.bar^{-1}$) is considerably higher than the one at 20°C (~ 7 $L.h^{-1}.m^{-2}.bar^{-1}$) which clearly reveals the thermo-responsive character of the membrane.

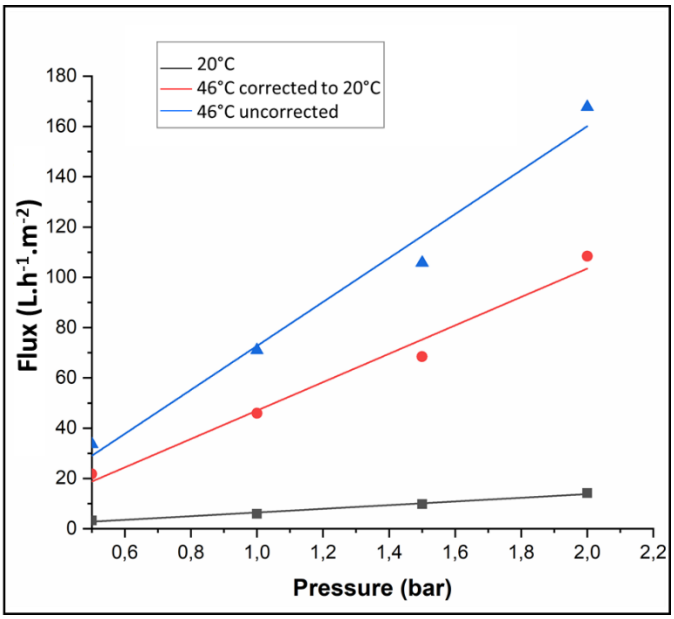

Figure 8. Membrane permeability rates (annealed 30 min in $CHCl_3$) at 20°C and 46°C as a function of pressure.

Since the studied PS-*b*-P2VP-*b*-PNIPMA is reported as a double stimuli-responsive triblock terpolymer, it was important to show the pH-responsive character in addition to the thermo-responsive state. Therefore, the following section is devoted to this aspect.

3.2. pH-responsive PS-*b*-P2VP-*b*-PNIPAM thick films

In order to show the double stimuli-responsiveness of the prepared PS-*b*-P2VP-*b*-PNIPAM membranes, pH-dependent water flux was measured at acidic (pH = 3) and basic (pH = 9.5) environment at temperatures below (11 °C) and above (42°C) the PNIPAM LCST. By changing the pH, the nitrogen group in P2VP can be protonated and deprotonated, and thus allowing the tuning of the pore size. Hydroxide sodium solution was used for increasing the pH value and hydrochloric acid solution for decreasing it. Before water permeability measurements at different pH values, the NIPS-made PS-*b*-P2VP-*b*-PNIPAM thick film was exposed to $CHCl_3$ vapor for 2h. As discussed previously, the as cast membranes were not sufficiently stable and can show different membrane surface constructions (either highly porous or completely closed pores). SVA treatment of about 30 min showed a beginning of membrane top surface

reconstruction and depending on the as cast configuration, the membrane did not reach the thermodynamic equilibrium. However, with about 2h of $CHCl_3$ exposure, the membrane roughness decreased and the periodicity of the pores was quite similar to the membrane treated for 6h, which is the thermodynamic equilibrium in this case. For a question of time, we chose to work with membranes treated during 2h instead of 6h.

The highest water flux of the PS-*b*-P2VP-*b*-PNIPAM membrane was measured at pH of 9.5 and water temperature of 42°C, and it was found to be 8.8 $L.h^{-1}.m^{-2}$ for a pressure drop of 1 bar. By decreasing the temperature below the PNIPAM LCST (to 10°C), it was found to 1.2 $L.h^{-1}.m^{-2}$ at 1bar. At acidic pH, P2VP is protonated and the pore size decreases, thereby the water flux goes down as represented in **Figure 9**.

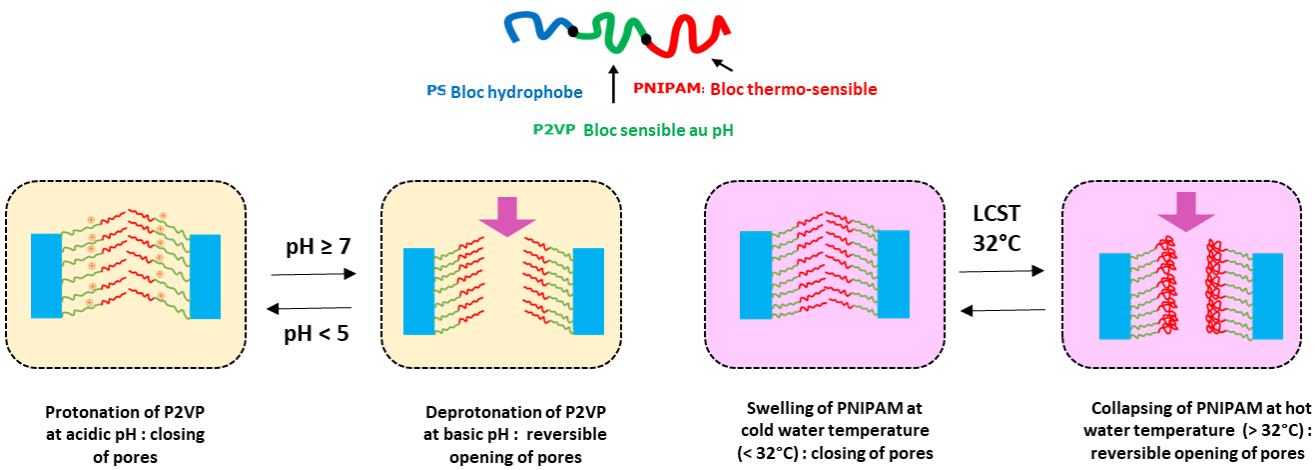

Figure 9. Schematic representation of (left) protonation/deprotonation of the P2VP block depending of pH and (right) swelling/stretching of the PNIPAM block depending of temperature.

At pH of 3, the pores are almost closed, which leads to a very small flux (0.8 $L.h^{-1}.m^{-2}$ at 10 °C and 5.1 $L.h^{-1}.m^{-2}$ at 42°C) (see **Figure 10.a**). From these results, we can conclude that the prepared PS-*b*-P2VP-*b*-PNIPAM membrane shows a double stimuli-responsive behavior to pH and temperature variations. The flux variation under different pH environments is less pronounced than the one observed with temperature, this is may be due to the chain length of P2VP (5.8kg/mol) which is smaller than the one of PNIPAM (8.5 kg/mol).

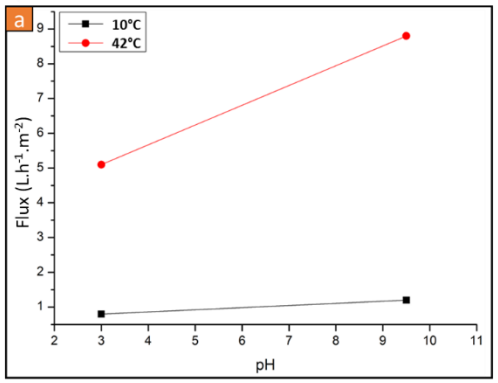

PS-*b*-P2VP-*b*-PNIPAM	pH	Flux ($L.h^{-1}m^2$) at 10-11°C	Flux ($L.h^{-1}m^2$) at 42°C
$M_{n,NMR}$ (PS : P2VP : PNIPAM) = 28.2 k : 5.8 k : 8.5 k	3	0.8	5.1
Φ_{PS} = 0.68, Φ_{P2VP} = 0.13, Φ_{PNIPAM} = 0.19	9.5	1.2	8.8

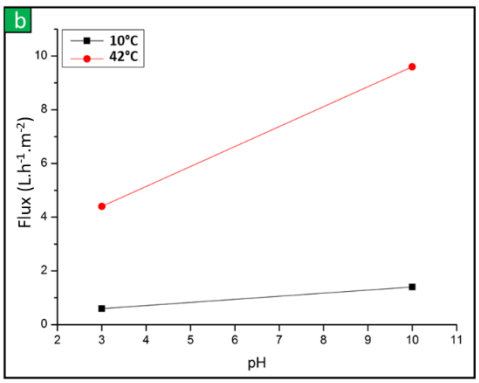

PS-*b*-P2VP-*b*-PNIPAM	pH	Flux ($L.h^{-1}m^2$) at 10-11°C	Flux ($L.h^{-1}m^2$) at 42°C
$M_{n,NMR}$ (PS : P2VP : PNIPAM) = 54.7 k : 31.1 k : 6.3 k	3	0.6	4.4
Φ_{PS} = 0.61, Φ_{P2VP} = 0.31, Φ_{PNIPAM} = 0.07	10	1.4	9.6

Figure 10. Water flux variations as a function of pH for two different NIPS-SVA made PS-*b*-P2VP-*b*-PNIPAM thick films. Water fluxes for different environments as well the molecular weight and compositions of the ABC-type BCPs used to produce the membranes are given in their respective Table.

Another PS-*b*-P2VP-*b*-PNIPAM triblock terpolymer system with a higher P2VP ($M_{n,NMR}$ = 31.1 kg/mol, Φ_{P2VP} = 0.31) volume fraction was tested in order to verify that this less pronounced pH effect is related to the chain length. Surprisingly, the results were similar as presented in **Figure 10.b.** Indeed, the highest water flux was observed for a basic and hot water solution. It was measured to be of ~ 9.6 $L.h^{-1}.m^{-2}$ at pH =10 and 42°C. The lowest water flux value was observed for the opposite case (~ 0.6 $L.h^{-1}.m^{-2}$ at pH =3 and 10°C). The water permeability observed in this case are slightly higher than with the other terpolymer composed with smaller P2VP volume fraction ($M_{n,NMR}$ = 5.8 kg/mol, Φ_{P2VP} = 0.13). These results show that the prepared membranes are pH- and thermo-responsive but the pH responsiveness is less

pronounced. This is due to the P2VP block length but more importantly to its position within the terpolymer chain.

The use of polymers containing stimuli-responsive character is a promising approach to facilitate the cleaning process of the membranes and thus limiting the fouling. Furthermore, it was reported that membranes endowed with a good temperature cyclability (*i.e.*, good reversibility of the water permeability as a function of temperature cycles) offer new possibilities for the development of advanced easy-to-clean membranes.[2] To this end, we detail the cyclability of the pH- and thermo-responsive PS-*b*-P2VP-*b*-PNIPAM membranes upon temperature variations in the following section.

3.3. Reversible PS-*b*-P2VP-*b*-PNIPAM thick films

The cyclability of the membranes was tested by measuring the permeability for four temperature cycles (*i.e.*, switching between 13°C and 43°C) for three different NIPS-SVA made PS-*b*-P2VP-*b*-PNIPAM membranes (see **Figure 11)**. Here the corrected permeability values show that the thermo-responsive behavior is a consequence of the chain collapse of PNIPAM above its LCST.

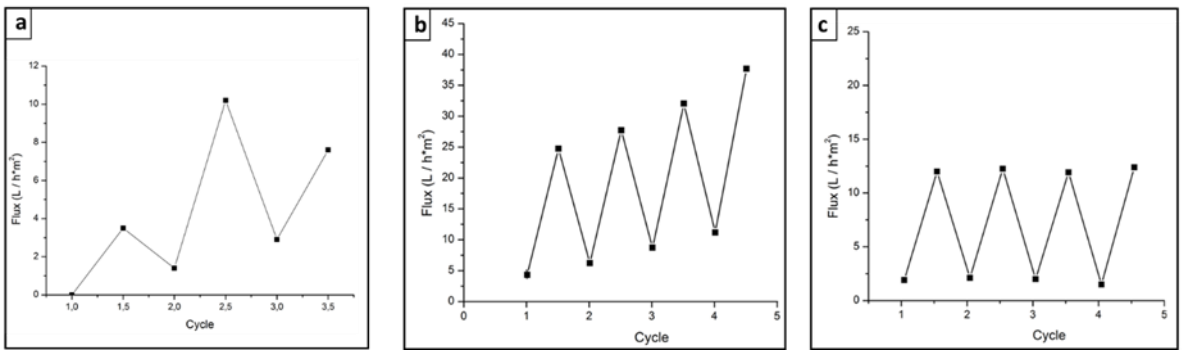

Figure 11. Reversibility of thermo-responsive behavior of three PS-*b*-P2VP-*b*-PNIPAM membranes showing different stabilities.

Figure 11.a presents a freshly prepared membrane exposed to a $CHCl_3$ vapor for 2h and directly tested by measuring the permeability for four temperature cycles. The membrane was conditioned at 2 bar at temperature below the PNIPAM LCST for 10 min before each cycle. This membrane was not reversible since it shows unstable variations of permeability for each cycle, with an important increase of permeability during the second cycle. From this result, we can conclude that the filtration at high temperature played a role in the permeability and the freshly prepared membrane was not stable.

In **Figure 11.b** is presented another membrane that was stored in water few hours to allow hydration and stabilization of pores and then conditioned at 45°C before reversibility measurements. We can observe an increase of permeability during the last cycle which is probably due to the high pressure drop applied during the filtration (1.5bar). From these results, we can note that the conditioning at temperature above the PNIPAM LCST as well as the storage in water conduce to a more reversibly stable membrane.

Finally, a fully reversible membrane with the same permeability values for each temperature cycle was obtained in the following conditions: applied filtration pressure about 1bar, storage of the membrane in water and conditioning at 43°C (see **Figure 11.c**).

We can conclude that the conditioning step is important to generate fully reversible double stimuli-responsive PS-*b*-P2VP-*b*-PNIPAM membranes.

The determination of the pore size distribution (PSD) is a critical factor characterizing the membrane filtration performances. It plays a major influence on the membrane permeability and in turn the filtrate flux. In this study, an approach based on solute rejection using gold nanoparticles was used to evaluate the rejection of nanostructured NIPS-SVA made PS-*b*-P2VP-*b*-PNIPAM thick films.

4. Pore size distribution of PS-*b*-P2VP-*b*-PNIPAM thick films

Aqueous solutions containing monodisperse gold nanoparticles (Au-NPs) with different sizes ranging from 5 to 20 nm were used to evaluate the pore size of the prepared double stimuli-responsive thick films. This strategy is based on the evaluation of the rejection factor that can be determined by the following equation:

$$R = 1 - \frac{C_{\text{Perm.}}}{C_{\text{Feed}}}$$

Where R is the rejection factor (%), $C_{\text{perm.}}$ and C_{Feed} are the concentrations of the permeate and of the feed respectively. The ideal case in this study would be composed of high rejection factor at temperature below the PNIPAM LCST due to its swollen state and low rejection factor at temperature above LCST.

The filtrations were performed at 2 bar with the same filtration setup used to determine the water permeability. The Au-NPs solutions were diluted 10 times in Milli-Q ultrapure water. UV-visible spectrometer (Shimadzu, UV-2401 PC) was used to measure the concentrations in the feed, permeate and retentate solutions by recording its UV-visible spectrum over the 400-800 spectral range.

Figure 12.a presents the UV-visible spectra of the feed, retentate and permeate of rejection of 5 nm Au-NPs. A rejection of ~ 57% was achieved at 2 bar for the NIPS-SVA made (2h, $CHCl_3$) PS-*b*-P2VP-*b*-PNIPAM thick film, suggesting first that the prepared thick film is not dominated by any macro defects, and consequently that the water transport occurs through the perforated lamellar P2VP-PNIPAM nanodomains. By heating-up the rejection factor decreased to ~51% confirming the shrinking of PNIPAM chains and a small opening of the membrane pores (see **Figure 12.b**).

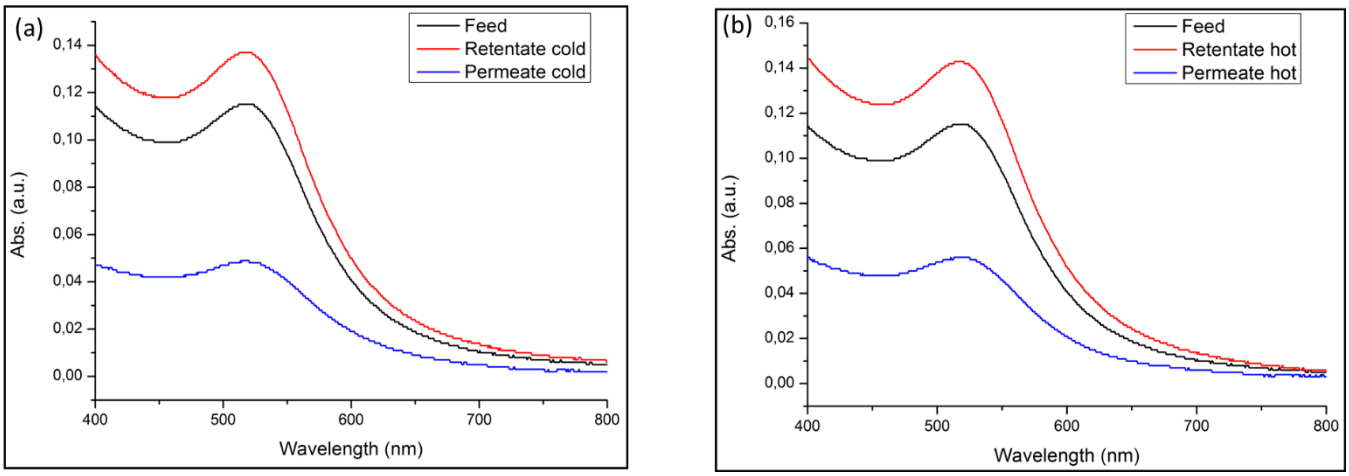

Figure 12. UV-visible spectra of the feed, retentate and permeate recorded over the 400-800 nm spectral range at a (a) low and (b) high temperature. All the UV-visible spectra consist of a peak centered at approximatively 520 nm corresponding to the surface polariton generated by the 5 nm Au-NPs.

This rejection rate gives a first information regarding the pore size that are bigger than 5 nm and confirms the thermo-responsive character of the material.

10 nm Au-NPS were filtrated at 46°C. Here, a higher rejection of ~ 81% was recorded at temperature below LCST (see **Figure 13.a**), indicating that the prepared thick film has pore size distribution higher than 5nm but not equal to 10 nm, otherwise the rejection would be 100%. Surprisingly, the rejection factor at temperature above LCST has increased to ~ 97% as shown in **Figure 13.b**, no absorption at 520 nm in the UV-visible spectrum can be achieved, indicating that the 10 nm gold NPs are completely blocked and that the pore size are smaller than in the cold state, which is not in accordance with the PNIPAM behavior.

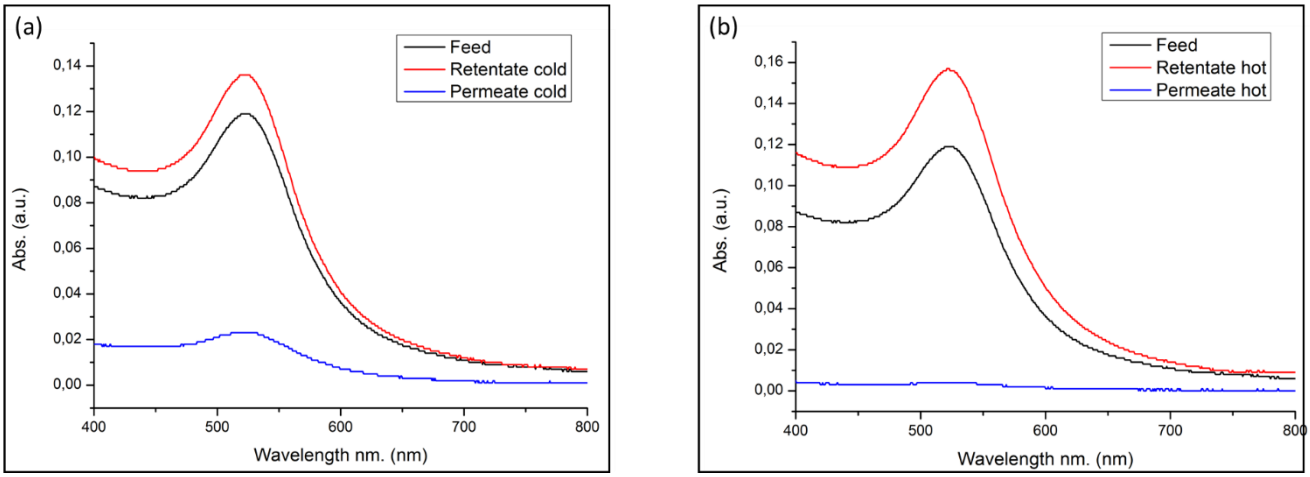

Figure 13. UV-visible spectra of the feed, retentate and permeate recorded over the 400-800 nm spectral range. (a) At low temperature, all the UV-visible spectra consist of a peak centered at approximatively 520 nm corresponding to the surface polariton generated by the 10 nm Au-NPs. (b) At high temperature, no absorption peak is observed at 520 nm on permeate spectra, which indicates a rejection of the 10 nm Au-NPs.

We assumed that Au-NPs solutions were not stable at high temperature and the nanoparticles aggregate.Dynamic light scattering was performed on 5 nm and 10 nm Au-NPs in order to verify their stability in hot water. As shown in **Figure 14**, the three NPs of different sizes did not show any change in their hydrodynamic diameter between cold and hot temperature and show a good stability of the solutions.

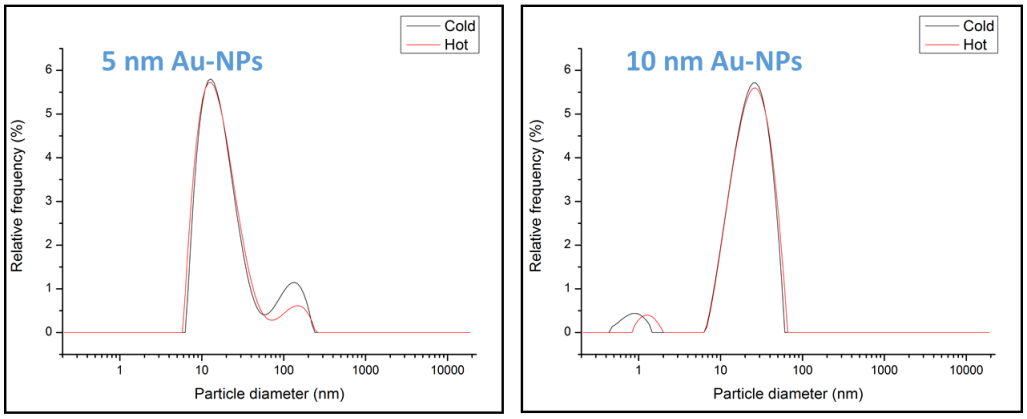

Hydrodynamic Diameter	5nm Au-NPs	10nm Au-NPs
Cold	19 nm	22 nm
Hot	16 nm	22 nm

Figure 14. Hydrodynamic size calculated by DLS measurements of commercial 5 nm and 10 nm gold nanoparticles solutions.

From these results, we can conclude that the pore size distribution of the NIPS-SVA made PS-*b*-P2VP-*b*-PNIPAM membrane is higher than 10 nm at temperature below 32°C and that the prepared material is not dominated by the formation of macro defects. However, the 10 nm gold nanoparticles filtration was not in accordance with the thermo-responsive behavior of the PNIPAM and was not successful.

5. Conclusion

In this chapter, we presented the study of self-assembly of the previously synthesized PS-*b*-P2VP-*b*-PNIPAM triblock terpolymer by RAFT polymerization. For that purpose, we used a combination of the non-solvent induced phase separation (NIPS) technique with a solvent vapor annealing (SVA) treatment to produce an out-of-plane lamellar phase.

We showed that the NIPS-made (as-cast) membranes were not stable and presented two completely different morphologies: either highly porous or completely closed membrane surface. These results are in accordance with the high influence of external parameters (specifically the external temperature and relative humidity in our case) on the final morphology.

The use of a SVA treatment showed a full reconstruction of the membrane surface. Indeed, by varying the exposure time to $CHCl_3$ vapors (from 0 to 6h), the membrane surface morphology, roughness and pore periodicity decreased to reach thermodynamic equilibrium resulting in a highly ordered out-of-plane lamellar phase (SVA, 6h in $CHCl_3$) with a period ~41 nm.

The water permeability of the double stimuli-responsive membrane was studied at temperatures below (< 20°C) and above (> 35°C) the PNIPAM LCST. Depending on the NIPS-made membrane *i.e.*, the starting point (either highly permeable or completely closed membrane) the water permeability measurements were in accordance with PNIPAM collapsed and swollen states, presenting in all cases an increase in water permeability at temperature higher than 32°C, thereby confirming the presence of a thermo-sensitive effect of the prepared membranes. Moreover, the thermo-sensitive behavior was fully reversible, if the membrane conditioning was adapted.

The double stimuli-responsive behavior was also confirmed by water permeability measurement in different pH environments. It was found that the pH-sensitive character is less pronounced at cold temperature due to the P2VP chain length and probably its position within the terpolymer. Finally, the pore size distribution of the prepared thick film is higher than 10 nm since the rejection factor was less than 100% at cold temperature. However, the pore size distribution of the material was not confirmed at hot temperature.

6. References

1. Zhu, G.-D. et al. Preparation of isoporous membranes from low χ block copolymers via co-assembly with H-bond interacting homopolymers. J. Membr. Sci. **589**, 117255 (2019).
2. Cetintas, M. et al. Free-standing thermo-responsive nanoporous membranes from high molecular weight PS-PNIPAM block copolymers synthesized via RAFT polymerization. Polym. Chem. **8**, 2235–2243 (2017).
3. Saline Water Conversion—II. vol. 38 (AMERICAN CHEMICAL SOCIETY, 1963).
4. Guillen, G. R., Pan, Y., Li, M. & Hoek, E. M. V. Preparation and Characterization of Membranes Formed by Nonsolvent Induced Phase Separation: A Review. Ind. Eng. Chem. Res. **50**, 3798–3817 (2011).
5. Liu, D., Wei, C., Yan, G. & Sun, G. 'Schizophrenic' behavior of poly (N-isopropylacrylamide)-b-poly (2-vinylpyridine) in aqueous solutions. Polym. Test. **65**, 97–102 (2018).
6. Baig, M. I., Durmaz, E. N., Willott, J. D. & Vos, W. M. Sustainable Membrane Production through Polyelectrolyte Complexation Induced Aqueous Phase Separation. Adv. Funct. Mater. **30**, 1907344 (2020).
7. Jung, J. T. et al. Understanding the non-solvent induced phase separation (NIPS) effect during the fabrication of microporous PVDF membranes via thermally induced phase separation (TIPS). J. Membr. Sci. **514**, 250–263 (2016).
8. McKelvey, S. Phase separation, vitrification, and the manifestation of macrovoids in polymeric asymmetric membranes. J. Membr. Sci. **112**, 29–39 (1996).
9. Strathmann, H., Kock, K., Amar, P. & Baker, R. W. The formation mechanism of asymmetric membranes. Desalination **16**, 179–203 (1975).
10. Smolders, C. A., Reuvers, A. J., Boom, R. M. & Wienk, I. M. Microstructures in phase-inversion membranes. Part 1. Formation of macrovoids. J. Membr. Sci. **73**, 259–275 (1992).

11. Cetintas, M. & Kamperman, M. Self-assembly of PS-b-PNIPAM-b-PS block copolymer thin films via selective solvent annealing. Polymer **107**, 387–397 (2016).
12. Rangou, S. et al. Self-organized isoporous membranes with tailored pore sizes. J. Membr. Sci. **451**, 266–275 (2014).
13. Qiu, X. et al. Selective Separation of Similarly Sized Proteins with Tunable Nanoporous Block Copolymer Membranes. ACS Nano **7**, 768–776 (2013).
14. Abetz, V. Isoporous Block Copolymer Membranes. Macromol. Rapid Commun. **36**, 10–22 (2015).
15. Jung, A., Rangou, S., Abetz, C., Filiz, V. & Abetz, V. Structure Formation of Integral Asymmetric Composite Membranes of Polystyrene -block- Poly(2-vinylpyridine) on a Nonwoven: Structure Formation of Integral Asymmetric Composite Membranes …. Macromol. Mater. Eng. **297**, 790–798 (2012).
16. Aissou, K. et al. Asymmetric Solvent-Annealed Triblock Terpolymer Thick Films Topped by a Hexagonal Perforated Lamellar Nanostructure. Macromol. Rapid Commun. 2100585 (2021) doi:10.1002/marc.202100585.
17. Aissou, K. et al. Bicontinuous Network Nanostructure with Tunable Thickness Formed on Asymmetric Triblock Terpolymer Thick Films. Macromolecules **52**, 4413–4420 (2019).
18. Aissou, K. et al. Periodic Bicontinuous Structures Formed on the Top Surface of Asymmetric Triblock Terpolymer Thick Films. ACS Macro Lett. **8**, 923–930 (2019).
19. Yang, Q. & Loos, K. Perpendicular Structure Formation of Block Copolymer Thin Films during Thermal Solvent Vapor Annealing: Solvent and Thickness Effects. Polymers **9**, 525 (2017).
20. Sinturel, C., Vayer, M., Morris, M. & Hillmyer, M. A. Solvent Vapor Annealing of Block Polymer Thin Films. Macromolecules **46**, 5399–5415 (2013).

21. van Zoelen, W., Asumaa, T., Ruokolainen, J., Ikkala, O. & ten Brinke, G. Phase Behavior of Solvent Vapor Annealed Thin Films of PS- b -P4VP(PDP) Supramolecules. Macromolecules **41**, 3199–3208 (2008).
22. Gu, X., Gunkel, I., Hexemer, A. & Russell, T. P. Solvent vapor annealing of block copolymer thin films: removal of processing history. Colloid Polym. Sci. **292**, 1795–1802 (2014).
23. Aissou, K., Choi, H. K., Nunns, A., Manners, I. & Ross, C. A. Ordered Nanoscale Archimedean Tilings of a Templated 3-Miktoarm Star Terpolymer. Nano Lett. **13**, 835–839 (2013).
24. Tu, K.-H. et al. Universal pattern transfer methods for metal nanostructures by block copolymer lithography. Nanotechnology **26**, 375301 (2015).
25. Hulkkonen, H., Salminen, T. & Niemi, T. Automated solvent vapor annealing with nanometer scale control of film swelling for block copolymer thin films. Soft Matter **15**, 7909–7917 (2019).

CHAPTER 4

Upgrading PS-*b*-P2VP-*b*-PNIPAM ultrafiltration membranes by blending with amphiphilic block copolymers

Table of contents

1. Introduction

As discussed in **Chapter 3**, amphiphilic block copolymers (BCPs) are excellent candidates for membrane preparation since well-defined nanostructures with highly desirable functionalities (*i.e.*, isoporosity, hydrophilicity, and fouling reduction) can be produced on the material top surface. Depending on the block volume fractions and the Flory-Huggins interaction parameters between the different pairs (*i.e.*, A/B, B/C and A/C), more than 20 ordered morphologies have been reported[1] from the microphase-separation of linear ABC triblock terpolymers, including lamellae, cylinders, spheres, and more complex continuous phases (*e.g.*, perforated lamellae and gyroid).[2] One of the critical challenges in BCP self-assembly is the extension of the available suite of geometries to more complicated ones. Therefore, the combination of two (or more) distinctly BCPs, also referred as blend of BCPs is a promising approach to design novel superstructures with controlled morphologies.[3]

In this thesis, we are interested in the manufacture of fouling resistant membranes. To this end, we chose the direct incorporation of hydrophilic polymers with strong water affinity such as the pH-responsive P2VP and the thermo-responsive PNIPAM within the double stimuli-responsive PS-*b*-P2VP-*b*-PNIPAM membrane to build fouling-resistant nanopores.

To increase the membrane hydrophilicity (so as to reduce the interactions between the foulants and materials), the previously synthesized PS-*b*-P2VP-*b*-PNIPAM has been blended with other amphiphilic BCPs. To this end, a poly(ethylene oxide) (PEO)-containing ABC-type BCP and a PNIPAM-containing AB-type BCP were loaded to the PS-*b*-P2VP-*b*-PNIPAM membranes to possibly improve their fouling resistance.

This chapter will be devoted to the study of the self-assembly of blended PS-*b*-P2VP-*b*-PNIPAM with two different amphiphilic BCPs: PS-*b*-P2VP-*b*-PEO and PS-*b*-PNIPAM. The combination of the non-solvent induced phase separation (NIPS) technique and the solvent-vapor annealing (SVA) process was used to produce asymmetric blended PS-*b*-P2VP-*b*-PNIPAM thick films with improved hydrophilicity.

2. Fabrication of blended PS-*b*-P2VP-*b*-PNIPAM thick films by NIPS

NIPS was used to prepare asymmetric blended PS-*b*-P2VP-*b*-PNIPAM thick films. The following described procedure was applied for all the prepared materials (*i.e.*, blends of PS-*b*-P2VP-*b*-PNIPAM chains with the two PEO-based ABC-type terpolymers and the PS-*b*-PNIPAM BCP discussed later on).

PS-*b*-P2VP-*b*-PNIPAM terpolymer was mixed with the selected terpolymer as blend in the targeted ratio. The polymer mixture powder was dissolved in a di-solvent mixture of 1,4-dioxane (DOX) and tetrahydrofuran (THF) (50/50 by weight). Before casting the polymer solution, the silicon substrate has been prepared in advance according to this procedure: the silicon substrate (3x3cm) surface was treated by an oxygen plasma (45W mTorr O_2, 10 min) in order to prevent the polymer from sticking. A hydrophilic "sacrificial" poly(poly(3,4-ethylenedioxythiophene) polystyrene sulfonate (PEDOT: PSS) was then spin-coated on the silicon substrate in order to facilitate the removal of the polymeric membrane once immersed in water.

The polymer mixture solution (18 wt.%) was casted using a tape casting technique with a 250μm gap. DOX and THF were evaporated for 30s at room temperature (RT) to form a dense top layer. The membrane was then plunged into a deionized water bath for 5 min to induce the polymer precipitation (see **Figure 1**).

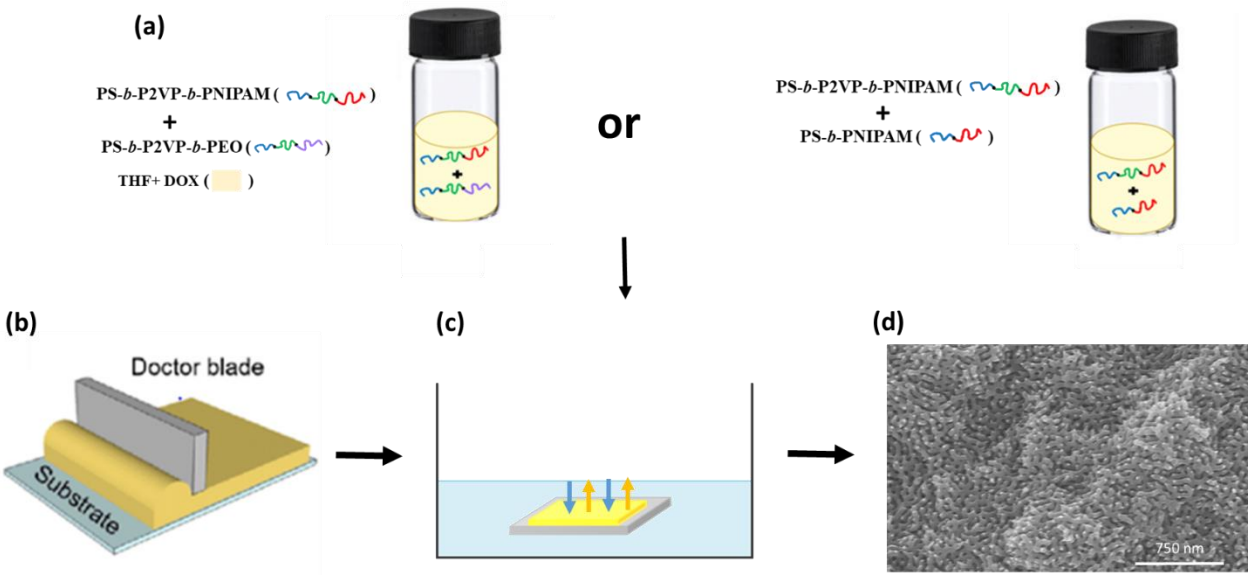

Figure 1. Schematic representation of the NIPS technique used for preparation of blended PS-*b*-P2VP-*b*-PNIPAM membranes. (a) Polymer solution mixture, (b) polymer solution casting, (c) immersion in coagulation bath and (d) cross-sectional view of blended membrane obtained by NIPS showing sponge-like sublayer.

The choice of polymer concentration, solvent mixture and evaporation time were proved to be good conditions to generate asymmetric PS-*b*-P2VP-*b*-PNIPAM thick films, so they were applied here as point of comparison. However, in the previous chapter, we noted that the NIPS process generated an instable poorly ordered membrane surface mainly due to external temperature and relative humidity issues. In order to avoid any problem related to these parameters, the membranes to be studied were prepared the same day.

3. Surface reconstruction of blended PS-*b*-P2VP-*b*-PNIPAM thick films by SVA

Solvent vapor annealing treatment is a promising technique for the generation of well-organized PS-*b*-P2VP-*b*-PNIPAM membrane surfaces.

In this chapter, the self-assembly of the blended PS-*b*-P2VP-*b*-PNIPAM system with other block copolymers was stimulated by exposing films for different times (ranging from 0h to 6h) to a continuous stream of chloroform ($CHCl_3$). Nitrogen gas was bubbled continuously through the liquid solvent in order to generate continuous flow and insure a good control of $CHCl_3$ vapor pressure in the chamber. The solvent vapor was diluted with a separate N_2 stream so that a solvent vapor consisted of 32 sccm $CHCl_3$ vapor and 8 sccm N_2 (total 40 sccm). The morphology of the solvent-annealed PS-*b*-P2VP-*b*-PNIPAM thick films was frozen by a fast removal of the chamber lid. Chloroform was already studied on the self-assembly of PS-*b*-P2VP-*b*-PNIPAM and it was shown that it can drive the membrane reconstruction until full equilibrium. Furthermore, it was demonstrated that it is a suitable solvent for the PS-*b*-P2VP-*b*-PEO terpolymer.[4]

3.1. Characterization techniques

The following characterization techniques were used for all the blended PS-*b*-P2VP-*b*-PNIPAM thick films presented in this chapter.

❖ Surface morphology

The surface morphology of the blended PS-*b*-P2VP-*b*-PNIPAM thick-films were characterized by Atomic force microscopy (AFM Nano-Observer, CSInstruments) in tapping mode. Silicon cantilevers (PP-NCH-Nanosensers) with a typical tip radius of ~5 nm were used. The resonance frequency of the cantilevers was about 235 kHz. In order to improve the AFM contrast, the blended thick films were treated with a fluorine plasma in a home-made chamber. The plasma conditions were as followed: 45 W, 75 mTorr CF_4, and 90s.

Scanning electron microscopy (SEM) was used to analyze the membranes cross section and top surface. SEM pictures were obtained using a Hitachi S4800 operating under 0.1-30 kV working voltage.

- **Water flux performances**

The water permeability of the different blended PS-*b*-P2VP-*b*-PNIPAM thick films was studied using a dead-end filtration set-up by measuring the flux of Milli-Q pure water at different pressures (0–2 bar). Hydrophilic polyvinylidene fluoride (PVDF) was used to support the round shape blended membranes with a diameter of 2.5 cm. Amicon type filter cell containing the supported membrane was connected to a pressure vessel filled with Milli-Q pure water. A stainless steel electronic bath filled with water was used to heat up the temperature and measure the water permeability from 23°C to 45°C. All the measured permeability at temperature below or above than 20°C, the results were corrected by multiplying them with the relative change in the dynamic viscosity of water at 20°C.

4. Phase behavior of blends of PS-*b*-P2VP-*b*-PNIPAM and PS-*b*-P2VP-*b*-PEO: effect of the molecular weight

Amphiphilic copolymers composed of both hydrophobic and hydrophilic materials are largely used as additives to be blended with different types of host polymers.[5] The principle of blending block copolymers lies in that the hydrophilic segments tend to segregate within the nanopores, and improve consequently the membrane hydrophilicity. The hydrophobic ones, for their part, are mixed with the membrane skeleton by chain entanglement which improve their compatibility with host polymers.[6] Surface segregation of amphiphilic copolymers in the phase inversion process has long been used to improve membrane hydrophilicity as long as the copolymers used are sparsely dosed into the casting solutions.[6] Indeed, membrane properties, such as high flux, high solute rejection and fouling resistance can be tuned by controlling the ratio of hydrophobicity and hydrophilicity.[7] The use of diblock and triblock copolymers result in more complex morphologies able to muscularly sway transport properties of the membrane. However, in order to insure the successful blending of BCPs and improve the targeted membrane properties, the selected polymers must be miscible at any blend ratio.[6]

The BCP self-assembly is highly dependent on several parameters such as: polymer types, blocks order, their respective molecular weight, volume fractions, Flory-Huggins χ-parameters, etc. In this chapter part, two commercial PS-*b*-P2VP-*b*-PEO triblock terpolymers (noted hereafter SVO) having different molecular weights (69,5 kg/mol and 112 kg/mol) were used as additives in different ratios to be blended with the double stimuli responsive PS-*b*-P2VP-*b*-PNIPAM chains in order to manufacture fouling resistant membranes with improved hydrophilicity. Here the effect of the molecular weight as well as the effect of the blend percentage on the self-assembly of the PS-*b*-P2VP-*b*-PNIPAM terpolymer will be evaluated. For the rest of this study, the previously synthesized double stimuli-responsive terpolymer (**SVN7** from **Chapter 2**) composed of PS (28.2 kg/mol, f_{PS} = 0.68), P2VP (5.8 kg/mol, f_{P2VP} = 0.13) and PNIPAM (8.5 kg/mol, f_{PNIPAM} = 0.19) was selected (see **Table 1**).

Both PEO-containing ABC-type terpolymers were purchased from Polymer source and have a low dispersity (Đ < 1.10). The small molecular weight SVO system consisted of PS (45 kg/mol, ϕ_{PS} = 56), P2VP (16 kg/mol, ϕ_{P2VP} =23) and PEO (8.5 kg/mol, ϕ_{PEO} = 12) while the large one was composed of PS (75 kg/mol, ϕ_{PS} = 69), P2VP (21 kg/mol, ϕ_{P2VP} = 18) and PEO (16 kg/mol, ϕ_{PEO} = 14), where ϕ represents the different volume fractions. PS_{45k}-*b*-$P2VP_{16k}$-*b*-$PEO_{8.5k}$ and PS_{75k}-*b*-$P2VP_{21k}$-*b*-PEO_{16k} will be called hereafter SVO_{8k} and SVO_{16k}, respectively, where the subscripts represent the molecular weight of each block and k means kg/mol (see **Table 1**).

	Composition (kg/mol)				
Polymer	**PS**	**P2VP**	**PEO**	**PNIPAM**	**Đ**
SVO_{16k}	75	21	16	_	1.04
SVO_{8k}	45	16	8.5	_	1.05
SVN7	28.2	5.8	_	8.5	1.32

Table 1. Molecular weight of each block and dispersity of selected PS-*b*-P2VP-*b*-PEO and PS-*b*-P2VP-*b*-PNIPAM triblock terpolymers.

The following part is devoted to the study of the self-assembly of blended PS-*b*-P2VP-*b*-PNIPAM terpolymer with a high molecular weight SVO_{16k} system in membrane configuration generated by the NIPS-SVA technique.

4.1. Asymmetric PS-*b*-P2VP-*b*-PNIPAM thick films blended with SVO_{16k} chains

PEO is a hydrophilic polymer with low toxicity suitable for medical and biological applications.[8] Thanks to its affinity with water, PEO is well-known for improving the antifouling properties of a membrane which is desirable characteristic with respect of durability.[9] Several studies demonstrated that surface modifications with PEO reduced significantly the adsorption of proteins. Regarding this aspect, great efforts have been invested in the use of PEO coating to improve fouling resistance.[8]

Thanks to the hydroxyl end-group, the PEO block can be easily added as a third block to PS-*b*-P2VP system to improve the membrane properties (see **scheme 1**).[10]

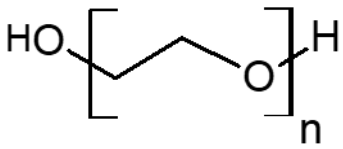

Scheme. 1 Chemical structure of poly(ethylene oxide) (PEO).

Before starting the study of the blended PS-*b*-P2VP-*b*-PNIPAM/SVO systems, we first compared water permeability performances of PS-*b*-P2VP-*b*-PNIPAM and SVO_{16K}. As it was reported in **Chapter 3**, NIPS process generated unstable membrane morphologies, either highly porous or completely closed depending on the external parameters. However, SVA treatment allowed a full membrane surface reconstruction, resulting in stable and reproducible membrane morphologies. From this results, an asymmetric NIPS-made SVO_{16K} was prepared and exposed to $CHCl_3$ vapor for 6h. The permeability of the prepared membrane was then recorded using a dead-end filtration set-up by measuring the flux of Millli-Q water from 0.5 to 2 bar and at temperatures below and above the PNIPAM LCST (32°C). **Figure 2.a** presents the permeability rate of the SVO_{16k} membrane while **Figure 2.b** corresponds to the one obtained for a PS-*b*-P2VP-*b*-PNIPAM membrane.

Water permeability of the NIPS-SVA made SVO_{16K} membrane at temperature below 32°C was noted to be 7 time higher than that of the PS-*b*-P2VP-*b*-PNIPAM one due to the presence of PEO chains. However, it was measured to be lower than the one of the double-stimuli

responsive system at temperature above the PNIPAM LCST, which is expected since PEO polymer is not thermosensitive. These results show that the PEO-containing ABC-type terpolymer will not negatively impact the hydrophilicity of the blended systems.

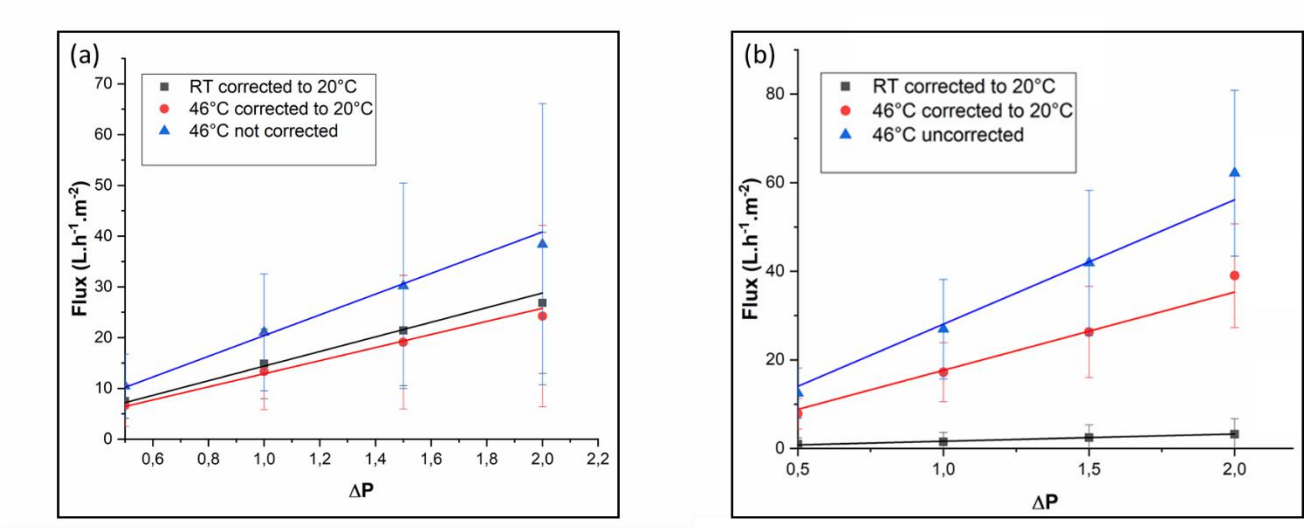

Temperature (°C)	Permeability (L.h^{-1}.m^{-2}.bar)
15°C corrected to 20°C	14 ± 8
46°C corrected to 20°C	12 ± 10
46°C not corrected	20 ± 16

Temperature (°C)	Permeability (L.h^{-1}.m^{-2}.bar)
23°C corrected to 20°C	2 ± 1
46°C corrected to 20°C	18 ± 4
46°C not corrected	28 ±6

Figure 2. Water permeability rates of the (a) PS-*b*-P2VP-*b*-PEO and (b) PS-*b*-P2VP-*b*-PNIPAM membranes generated by NIPS-SVA (annealed 6h in $CHCl_3$) at 20°C and at 46°C as a function of pressure.

Note that the selected commercial SVO_{16k} was composed of a high PS volume fraction to reinforce the membrane mechanical properties and with a small PEO volume fraction to fit with the PNIPAM domain size. PS-*b*-P2VP-*b*-PNIPAM was blended with 75 wt.%, 50 wt. % and 25 wt. % of SVO_{16K}, and three membranes (one for each blend ratio) were prepared by NIPS process and treated with $CHCl_3$ vapors for 6h. **Figure 3**. presents the AFM topographic images of the obtained membranes. We can see that the blended PS-*b*-P2VP-*b*-PNIPAM membranes with 75% and 50% SVO_{16K} show a poorly-ordered top surface. While the membrane top surface, corresponding to the blend with the lower amount of SVO_{16k}, exhibits a less defective nanostructure.

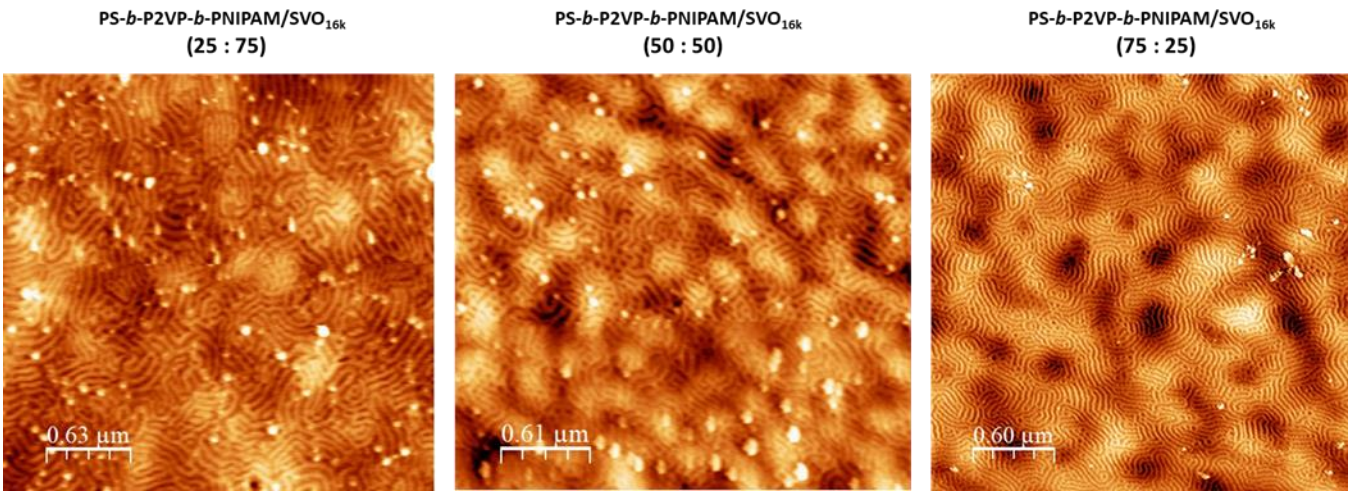

Figure 3. AFM topographic images of PS-*b*-P2VP-*b*-PNIPAM/ SVO_{16k} thick films with different blend ratios.

From these results, we can note that the optimum blend ratio of SVO_{16k} with the double stimuli-responsive PS-*b*-P2VP-*b*-PNIPAM triblock terpolymer was about 25 wt.%. It was reported that overdosed additives, specifically amphiphilic BCP may not be compatible with the casting solutions and can ruin the phase inversion process as well as the membrane performances.[6]

Table 2. summarizes the normalized water permeability rates of NIPS-SVA made blended PS-*b*-P2VP-*b*-PNIPAM/SVO_{16k} thick films measured at temperatures below (15°C) and above (46°C) the PNIPAM LCST. The as-cast membranes loaded with 50 wt.% and 25wt.% of SVO_{16k} present different water permeability values. The permeability value of the membrane with the highest SVO blend ratio was established to be of ~135 $L.h^{-1}.m^{-2}.bar^{-1}$ at 15°C. By increasing the water temperature above the PNIPAM LCST, the water permeability is found to be ~2 times higher (245 $L.h^{-1}.m^{-2}.bar^{-1}$ at 46°C). The second membrane with the lowest amount of SVO_{16k}, has a water permeability value of ~2 $L.h^{-1}.m^{-2}.bar^{-1}$ at 15°C . However, this value is 10 times increased at 46°C (22 $L.h^{-1}.m^{-2}.bar^{-1}$) which indicates that the thermo-responsive character of the membrane is more pronounced in this case.

After exposure to $CHCl_3$ vapors, the permeability of both membranes decreased due to the surface reconstruction. After a SVA treatment of 6h, both membranes present water permeability values not higher than 10 $L.h^{-1}.m^{-2}.bar^{-1}$ at 46°C. From these results, we can conclude that PS-*b*-P2VP-*b*-PNIPAM thick films blended with 25 wt.% of SVO_{16k} chains shows the best membrane surface reconstruction generated by SVA. In this case, the

hydrophilicity of the membrane did not increase but the thermo-responsive character was conserved. Higher ratio percentages result in a less well-ordered morphology on the NIPS-SVA made membrane top surface, and conduce to a decrease in the material thermo-responsive character.

Annealing time ($CHCl_3$)	Temperature (°C)	50% SVO_{16k} Permeability normalized to 20°C ($L.h^{-1}.m^{-2}.bar^{-1}$)	25% SVO_{16k} Permeability normalized to 20°C ($L.h^{-1}.m^{-2}.bar^{-1}$)
0	15°C	135 ± 164	2.00 ± 0.004
0	46°C	245 ± 146	22 ± 7
30min	15°C	181 ± 88	12 ± 5
30min	46°C	213 ± 182	29 ± 9
2h	15°C	6 ± 4	2 ± 1
2h	46°C	15 ± 2	9 ± 1
6h	15°C	3 ± 2	4 ± 3
6h	46°C	7 ± 3	10 ± 2

Table 2. Membrane permeability rates as a function of the annealing time and temperature. Results were obtained from blends of PS-*b*-P2VP-*b*-PNIPAM chains with 50 wt.% and 25 wt. % of SVO_{16k}.

Another PEO-containing ABC-type terpolymer having a lower molecular weight was also blended with the PS-*b*-P2VP-*b*-PNIPAM chains to evaluate the effect of the molecular weight on the BCP self-assembly.

4.2. Asymmetric PS-*b*-P2VP-*b*-PNIPAM thick films blended with SVO_{8k} chains

Erukhimovich *et al.*[11] reported in their work that the addition of a short third block in diblock copolymer can influence the segregation and change the stretching of the other two blocks. Jung *et al.*[10] showed that short PEO (< 10 Kg/mol) has a strong influence on the structure formation of PS-*b*-P2VP membranes. A repulsion interaction between PEO and the other blocks tend to induce a decrease of interfacial curvature where the system adopts a morphology in which the components are stronger segregated.

In this study, the same previously synthesized $PS_{28.2k}$-*b*-$P2VP_{5.8k}$-*b*-$PNIPAM_{8.5k}$ was blended with 25 wt % of SVO_{8k}. Here the hydrophilic end-block of both systems have the same molecular weight about 8.5 kg/mol (see **Table 1**).

Figure 4.presents the AFM topographic images of NIPS-SVA made blended PS-*b*-P2VP-*b*-PNIPAM/SVO_{8k} thick films. The membrane surface reconstruction is similar to the one of pure double stimuli-responsive terpolymer. The as cast (SVA = 0h) to surface membrane showed a poorly ordered micelle-like nanoparticles generated as a result of solvent exchange during NIPS process (**Figure 4.a)**. After 30 min of exposure to $CHCl_3$ vapors, the membrane surface exhibits poorly ordered core/shell P2VP/PNIPAM nanodomains (**Figure 4.b)**.

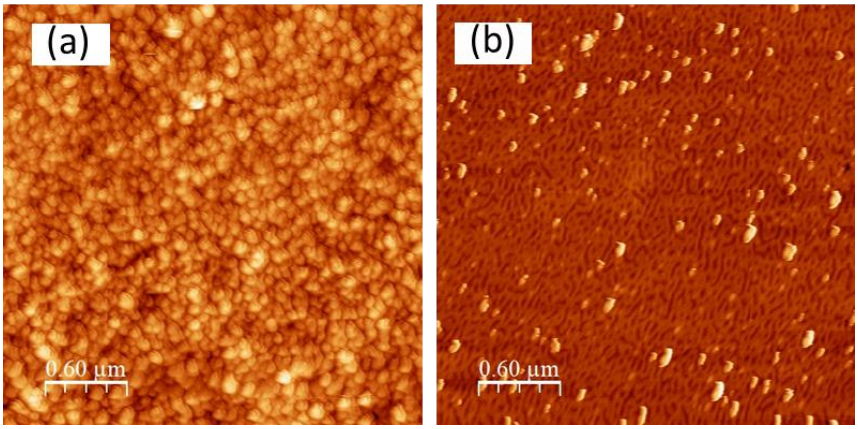

Figure 4. AFM topographic images of solvent-annealed PS-*b*-P2VP-*b*-PNIPAM membranes blended with 25 wt.% SVO_{8k}. Membranes were treated with $CHCl_3$ vapors for different times: (a) 0h and (b) 30min

Filtration performances of the blended PS-*b*-P2VP-*b*-PNIPAM/SVO_{8k} were measured at pressure drop between 0.5 and 2 bar for two temperatures (15°C and 46°C) as shown in **Table 3**.

The NIPS-made (as-cast) PS-*b*-P2VP-*b*-PNIPAM/SVO_{8k} membrane showed small increase of water permeability values ~ 3 $L.h^{-1}.m^{-2}.bar^{-1}$ at 15°C comparing to the one of the non-blended polymer (0 $L.h^{-1}.m^{-2}.bar^{-1}$) even if the AFM topographic image (see **Figure 4.a**) showed completely closed pores. This small permeability difference is mainly due to the presence of PEO chains.

A higher water permeability was measured to be ~157 $L.h^{-1}.m^{-2}.bar^{-1}$ (at 15°C) for 30 min of exposure to $CHCl_3$ vapors, which is roughly 22 times higher than the one recorded for the

PS-*b*-P2VP-*b*-PNIPAM system. At this point the reconstruction of the membrane surface and the segregation of the PEO block within the P2VP/PNIPAM pores allowed an increase of water permeability. After a SVA treatment of 6h, the permeability decreased to ~5 $L.h^{-1}.m^{-2}.bar^{-1}$ at 15°C, which is in accordance with the previous results, where the reorganization of the membrane surface resulted in decrease of permeability values at temperature above the PNIPAM LCST. However, at 46°, the water permeability increased to ~ 21 $L.h^{-1}.m^{-2}.bar^{-1}$ which is higher than the one reported for the non-blended membrane.

Annealing time ($CHCl_3$)	Temperature (°C)	25% SVO_{8k} Permeability normalized to 20°C ($L.h^{-1}.m^{-2}.bar^{-1}$)	PS-*b*-P2VP-*b*-PNIPAM Permeability normalized to 20°C ($L.h^{-1}.m^{-2}.bar^{-1}$)
0	15°C	2.9 ± 0.3	0
0	46°C	52.1 ± 6.2	0
30min	15°C	157.7 ± 11.0	7.0 ± 2.0
30min	46°C	298.1 ± 4.0	50.0 ± 9.0
2h	15°C	5.3 ± 1.2	2.0 ± 1.0
2h	46°C	17.2 ± 0.4	18.0 ± 4.0
6h	15°C	4.8 ± 1.0	2.0 ± 1.0
6h	46°C	21.0 ± 0.3	18.0 ± 4.0

Table 3. Permeability rates of blended (25wt.% of SVO_{8k}) and unblended PS-*b*-P2VP-*b*-PNIPAM membranes as a function of the SVA duration and temperature.

The overall hydrophilicity of the double stimuli-responsive membrane has increased by using 25wt.% of SVO_{8k} chains. This blend percentage as well as the addition of terpolymer with short PEO block, having exact molecular weight as PNIPAM block ($Mn_{,PEO} = Mn_{,PNIPAM} = 8.5$ kg/mol) seemed to be more compatible, resulting in successful segregation of the hydrophilic PEO polymer with membrane pores composed of P2VP/PNIPAM. Despite the increase of overall wettability of the membrane, the thermo-responsive behavior was conserved.

In order to improve the hydrophilicity as well as the thermo-repsonsive behavior of the membrane, another AC-type BCP composed of PS-*b*-PNIPAM was studied. Here, the addition of short hydrophilic thermo-responsive polymer is expected to increase the membrane permeability, thanks to its perfect compatibility with the double stimuli-responsive ABC-type terpolymer end-block, as well as the membrane fouling resistance. Indeed, if the transtition

between swelling and stretching state of PNIPAM (also reprensenting the "close/open" state of membrane pores) is increased, the membrane self-cleaning is then increased.

In the following section, we will detail the self-assembly of PS-*b*-P2VP-*b*-PNIPAM/PS-*b*-PNIPAM, also reffered as ABC/AC thick films.

5. Self-assembly of PS-*b*-P2VP-*b*-PNIPAM membranes blended with PS-*b*-PNIPAM chains

Poly(*N*-isopropylacrylamide) (PNIPAM) is a hydrophilic polymer, and one of the best known thermo-responsive polymer exhibiting a lower critical solution temperature in water ranging from 31°C to 33°C.[12] In membrane technology, the combination of PNIPAM with other polymers has been largely investigated to develop smart surfaces with a controllable wetting behavior.[13]

The selected PS-*b*-PNIPAM diblock copolymer was synthesized by RAFT polymerization in presence of 2-(dodecylthiocarbonothioylthio)-2-methylpropionic acid (DDMAT) as RAFT agent and azobisisobutyronitrile (AIBN) as initiator. Polystyrene macro RAFT agent was prepared first, and then extended with NIPAM to produce PS-*b*-PNIPAM with low dispersity, Đ = 1.10 (see **Chapter 5** for synthesis details). The synthesized AC-type BCP consisted of a high PS volume fraction (22 kg/mol, f_{PS} = 0.81) and PNIPAM (6.7 kg/mol, f_{PNIPAM} = 0.19) (see **Table 4**).

	Composition (kg/mol)			
Polymer	PS	P2VP	PNIPAM	Đ
SVN7	28.2	5.8	8.5	1.32
SN	22	_	6.7	1.10

Table 4. Molecular weight of each block and dispersity of selected PS-*b*-P2VP-*b*-PNIPAM terpolymer and PS-*b*-PNIPAM diblock copolymer.

NIPS technique was used to produce asymmetric PS-*b*-P2VP-*b*-PNIPAM blended with 20 wt.% of PS-*b*-PNIPAM. In **Figure 5.a** is presented an AFM topographic image of the NIPS-made ABC/AC thick film. The rough membrane surface (R_{rms} = 25.9 nm) was composed of poorly-ordered features with a period of ~12.3 nm, that was transformed into highly open porous surface with P2VP-PNIPAM/PNIPAM pores having a period of ~57.1 nm after exposure to $CHCl_3$ vapors for 2h as shown in **Figure 5.b.**

The membrane surface reconstruction of a NIPS-SVA made PS-*b*-P2VP-*b*-PNIPAM/PS-*b*-PNIPAM thick film exposed to chloroform vapors for 6h is shown in **Figure 5.c**. Once again the SVA treatment allowed an improvement of the long-range ordered nanostructure. The membrane top surface is composed of well-organized pores having a mean period of ~ 45 nm.

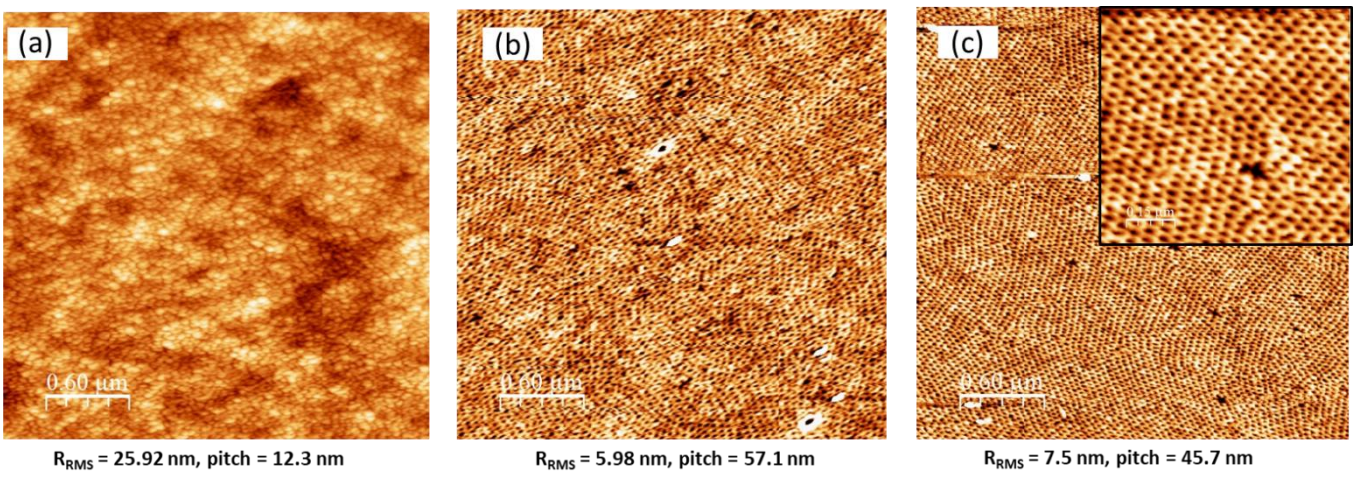

Figure 5. AFM topographic images of NIPS-made PS-*b*-P2VP-*b*-PNIPAM/PS-*b*-PNIPAM thick films exposed to a CHCl3 vapor for different times: (a) 0 min (as-cast) (b) 2h and (c) 6h.

The cross-sectional SEM view in **Figure 6.b** shows an asymmetric PS-*b*-P2VP-*b*-PNIPAM/ PS-*b*-PNIPAM thick film prepared by NIPS process and SVA treatment for 2h. The prepared thick film consisted of a dense skin layer (see the part above the dotted line) and a microporous substructure morphology.

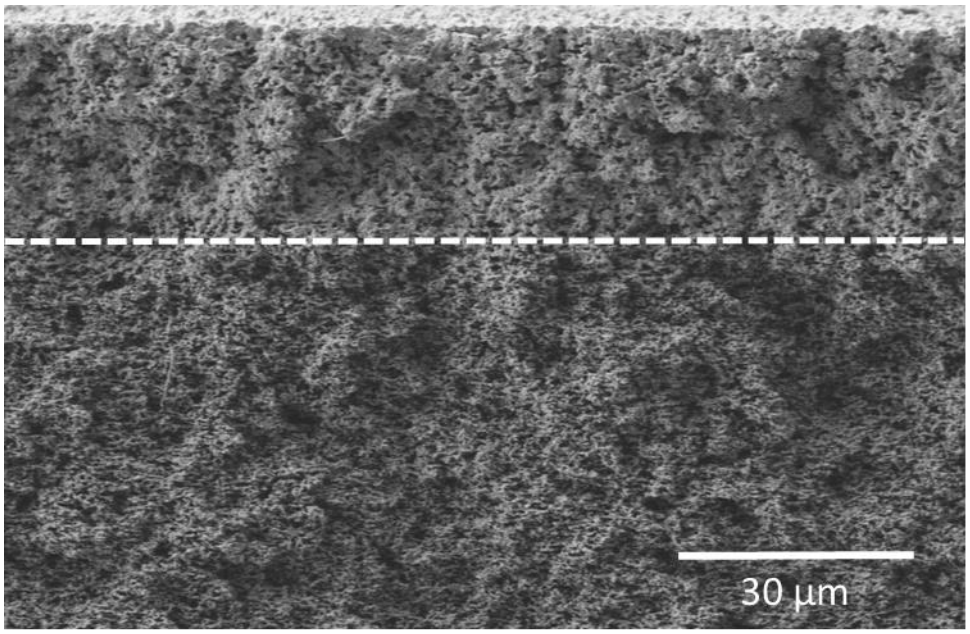

Figure 6. Cross-sectional SEM view of blended (20 wt. %) PS-*b*-P2VP-*b*-PNIPAM/PS-*b*-PNIPAM thick film generated by NIPS-SVA (2h, $CHCl_3$).

The water permeability values of the NPS-SVA made ABC/AC thick films obtained for different SVA durations are presented in **Table 5**. The SVA treatment was successful in term of membrane surface reconstruction but also it allows, for the first time in this study, an important increase of the water permeability for the PS-*b*-P2VP-*b*-PNIPAM/PS-*b*-PNIPAM thick films. After SVA treatment for 6h in $CHCl_3$ vapor, the water permeability of the blended membrane was measured to be ~30 $L.h^{-1}.m^{-2}.bar^{-1}$ at 15°C. By heating up the water temperature to 46°C, the permeability increased by ~ 2.5 times (81 $L.h^{-1}.m^{-2}.bar^{-1}$).

The use of PS-*b*-PNIPAM as blend ratio with small PNIPAM volume fraction has leaded to a drastic increase of membrane surface reconstruction resulting in perforated lamellar phase on the membrane top surface, which is relevant for challenging separation applications. [14]

Annealing time ($CHCl_3$)	Temperature (°C)	20% PS-*b*-PNIPAM Permeability normalized to 20°C ($L.h^{-1}.m^{-2}.bar^{-1}$)
0	< 20°C	0
0	Above LCST	0
10min	< 20°C	209
10min	Above LCST	353
30min	< 20°C	4 ± 1
30min	Above LCST	30 ± 8
2h	< 20°C	$1 \pm 0,3$
2h	Above LCST	22 ± 5
6h	< 20°C	30 ± 9
6h	Above LCST	81 ± 10

Table 5. Membrane permeability rates as a function of the annealing time and temperature obtained from PS-*b*-P2VP-*b*-PNIPAM thick films blended with 20 wt% of PS-*b*-PNIPAM chains.

6. Conclusion

In this chapter, double stimuli-responsive PS-*b*-P2VP-*b*-PNIPAM membranes were blended with different amphiphilic copolymers in order to increase their hydrophilicity and their potential fouling resistance. Different molecular weight PEO-containing ABC-type BCPs were first studied in different blend ratios in order to evaluate the effect of the molecular weight as well as the effect of the blend percentage on the final self-assembled terpolymer thick films.

As the combination of the NIPS process with a SVA treatment generated well organized double stimuli-responsive membrane composed of lamellar morphology (reported in **Chapter 3**). The same techniques were used to produce blended membranes with improved hydrophilicity and achieve new morphologies *via* a blending strategy.

Firstly, blend ratio of PS-*b*-P2VP-*b*-PEO triblock terpolymer was studied and it was reported that high blend percentage > 25 wt. % leaded to disturbed phase inversion process and poorly organized morphologies. Furthermore, NIPS-SVA PS-*b*-P2VP-*b*-PNIPAM membranes blended with 50 wt. % of PEO-containing ABC-type terpolymer showed poor permeability value at temperatures below and above the PNIPAM LCST.

Secondly, the molecular weight effect of blended PEO-based terpolymer was studied and it was observed that a short PEO block with equal molecular weight to the PNIPAM one (8.5 kg/mol) showed less packing frustration within the membrane pores (*i.e.*, blended and unblended membranes exhibit the same morphology). Moreover, by blending the PS-*b*-P2VP-*b*-PNIPAM membranes with SVO_{8k} chains, it is observed an increase of the water permeability both below and above the PNIPAM LCST in comparison with the neat material. Here, the water permeability is increased thanks to the presence of the PEO blocks within the membranes pores since PEO allows for an increase of the pore hydrophilicity, thereby reducing the capillary forces occurring within the nanodomains. In other words, a full reconstruction of the membrane top surface into a highly ordered lamellar phase was observed accompanied with increase of the hydrophilicity as well as the thermo-responsiveness.

A PS-*b*-PNIPAM BCP was also loaded within the pH and thermo-responsive PS-*b*-P2VP-*b*-PNIPAM membranes with a low percentage (20 wt. %). This made that, for the first time in this work, the water permeability of the blended membranes generated by NIPS-SVA (6h, $CHCl_3$) has increased to ~80 $L.h^{-1}.m^{-2}.bar^{-1}$ at temperature above the PNIPAM LCST.

The full compatibility between the PNIPAM blocks has increased the transition between collapsed and stretched state of PNIPAM resulting in increase of water permeability and of thermo-responsive character of the membrane.

Finally, the combination of the NIPS-SVA process is a promising technique for the generation of membrane top surfaces having a well-ordered morphology. The blend of the double stimuli-responsive PS-*b*-P2VP-*b*-PNIPAM terpolymer with an amphiphilic BCP, and particularly the AC-type BCP, created a new film morphology having well-ordered nanodomains. This membrane reconstruction increased the wettability of the thick film and its thermo-responsive behavior, which is one of the desired properties in the manufacture of fouling-resistant membranes.

7. References

1. Abetz, V. & Simon, P. F. W. Phase Behaviour and Morphologies of Block Copolymers. in *Block Copolymers I* (ed. Abetz, V.) vol. 189 125–212 (Springer-Verlag, 2005).

2. Algarni, F. *et al.* Thermo-Responsive Membranes from Blends of PVDF and PNIPAM-*b* -PVDF Block Copolymers with Linear and Star Architectures. *Macromolecules* **54**, 10235–10250 (2021).

3. Radjabian, M. *et al.* Structure Formation of Binary Blends of Amphiphilic Block Copolymers in Solution and in Bulk. *Macromol. Chem. Phys.* **218**, 1600587 (2017).

4. Aissou, K. *et al.* Asymmetric Solvent-Annealed Triblock Terpolymer Thick Films Topped by a Hexagonal Perforated Lamellar Nanostructure. *Macromol. Rapid Commun.* 2100585 (2021) doi:10.1002/marc.202100585.

5. Rajasekhar, T., Trinadh, M., Veera Babu, P., Sainath, A. V. S. & Reddy, A. V. R. Oil–water emulsion separation using ultrafiltration membranes based on novel blends of poly(vinylidene fluoride) and amphiphilic tri-block copolymer containing carboxylic acid functional group. *J. Membr. Sci.* **481**, 82–93 (2015).

6. Chen, Y., Wei, M. & Wang, Y. Upgrading polysulfone ultrafiltration membranes by blending with amphiphilic block copolymers: Beyond surface segregation. *J. Membr. Sci.* **505**, 53–60 (2016).

7. Nunes, S. P. & Car, A. From Charge-Mosaic to Micelle Self-Assembly: Block Copolymer Membranes in the Last 40 Years. *Ind. Eng. Chem. Res.* **52**, 993–1003 (2013).

8. Hahn, J. *et al.* Structure formation of integral-asymmetric membranes of polystyrene -*block* -Pol *y* (ethylene oxide). *J. Polym. Sci. Part B Polym. Phys.* **51**, 281–290 (2013).

9. Harder, P., Grunze, M., Dahint, R., Whitesides, G. M. & Laibinis, P. E. Molecular Conformation in Oligo(ethylene glycol)-Terminated Self-Assembled Monolayers on Gold and Silver Surfaces Determines Their Ability To Resist Protein Adsorption. *J. Phys. Chem. B* **102**, 426–436 (1998).

10. Jung, A. *et al.* Formation of Integral Asymmetric Membranes of AB Diblock and ABC Triblock Copolymers by Phase Inversion. *Macromol. Rapid Commun.* **34**, 610–615 (2013).

11. Erukhimovich, I., Abetz, V. & Stadler, R. Microphase Separation in Ternary ABC Block Copolymers: Ordering Control in Molten Diblock AB Copolymers by Attaching a Short Strongly Interacting C Block. *Macromolecules* **30**, 7435–7443 (1997).

12. Jain, K., Vedarajan, R., Watanabe, M., Ishikiriyama, M. & Matsumi, N. Tunable LCST behavior of poly(N-isopropylacrylamide/ionic liquid) copolymers. *Polym. Chem.* **6**, 6819–6825 (2015).

13. Kanidi, M., Papagiannopoulos, A., Skandalis, A., Kandyla, M. & Pispas, S. Thin films of PS/PS- *b* -pnipam and ps/pnipam polymer blends with tunable wettability. *J. Polym. Sci. Part B Polym. Phys.* **57**, 670–679 (2019).

14. Aissou, K. *et al.* Bicontinuous Network Nanostructure with Tunable Thickness Formed on Asymmetric Triblock Terpolymer Thick Films. *Macromolecules* **52**, 4413–4420 (2019).

CHAPTER 5

Materials and methods

Table of contents

1. Used products

❖ **Monomers**

N-isopropylacrylamide (NIPAM, >99%, Sigma-Aldrich) was purified by recrystallization in a mixture of toluene/hexane (50/50, v/v). Styrene (St, >98%, Sigma-Aldrich) was stirred with inhibitor removal resin about 30 min prior to use. 2-Vinylpyridine (2VP, >97%, Sigma-Aldrich) was passed throw a column of activated alumina in order to remove the *tert*-butylcatechol present in the monomer.

❖ **RAFT agents**

4-Cyano-4-[(dodecylsulfanylthiocarbonyl)sulfanyl]pentanoic acid (CDPA, >97%, RAFT agent, Sigma-Aldrich), 4-Cyano-4-[dodecylsulfanylthiocarbonyl)sulfanyl]pentanol (CDP ≥ 96.5%, RAFT agent, Sigma-Aldrich) and 2-dodecylthiocarbonylthio-2-methyl propionic acid (DDMAT, >97%, RAFT agent, Sigma-Aldrich) were used without further purification.

❖ **Initiator**

2,2′-Azobis (2-methylpropionitrile) (AIBN, >99%, Sigma-Aldrich) was purified by recrystallization from methanol before being used.

❖ **Polymers**

Polystyrene-*block*-poly(2-vinylpyridine)-*block*-poly(ethylene oxide) PS_{45k}-*b*-$P2VP_{26k}$-*b*-$PEO_{8.5k}$ and PS_{75k}-*b*-$P2VP_{21k}$-*b*-PEO_{16k} (where the subscripts represent the number averages molecular weight of each block, k means kg/mol) were purchased from Polymer source.

❖ **Solvents**

1,4-dioxane (DOX, >99%), tetrahydrofuran (THF, >99%), heptane, dimethylformamide (DMF, >99%), diethyl ether (>99%) and NMR solvents: deuterated dichloromethane (CD_2Cl_2) and chloroform deuterated ($CDCl_3$) were purchased from Sigma-Aldrich and used as received.

2. Analysis techniques

2.1. Polymers characterization

2.1.1. ^{1}H nuclear magnetic resonance (NMR) spectroscopy

^{1}H NMR spectra were recorded at room temperature on Bruker Avance spectrometers operating at 400 MHz using either deuterated dichloromethane (CD_2Cl_2).

2.1.2. Diffusion ordered spectroscopy (DOSY)

2D DOSY spectra were recorded at room temperature on Bruker Avance spectrometers operating at 600 MHz using deuterated chloroform ($CDCl_3$).

2.1.3. Size exclusion chromatography (SEC)

Size exclusion chromatography SEC was carried out on a Viscotek device (Malvern Instruments, Worcestershire, U.K) with a triple detector array. The SEC apparatus was equipped with two PLgel 5μm 500Å columns, THF as eluent with a flow rate at 1mL/min at 35°C, PS standards were used for calibration of the column. Omnisec software using refractive index and light scattering signals was applied to calculate M_n and Đ of polystyrene synthesized.

2.2. Membranes characterization

2.2.1. Atomic force microscopy (AFM)

Atomic force microscopy (AFM Nano-Observer, CSInstruments) was used in tapping mode to characterize the surface morphology of PS-*b*-P2VP-*b*-PNIPAM thick films. Silicon cantilevers (PPP-NCH, Nanosensors) with a typical tip radius of ~5 nm were used. The resonance frequency of the cantilevers was about 235 kHz.

2.2.2. Scanning electron microscopy (SEM)

Scanning electron microscopy (SEM, Hitachi S-4800) was used at an accelerating voltage of 5 kV to acquire top view and cross-section images of both asymmetric thick films and monoliths formed by PS-*b*-P2VP-*b*-PNIPAM chains.

3. Protocol: CHAPTER 2

3.1. Synthesis of PS macro-CTA by RAFT

In the following section, we will describe the synthesis procedure for the homopolymer **S7** presented in **Table 1** in **Chapter 2**.

A 100 mL round-bottomed flask was charged with 60 g of freshly purified styrene (0.57 mol), 0.26 g of CDPA (0.66 mmol) and 21 mg of AIBN (0.13 mmol). The sealed reaction vessel was purged with nitrogen and immersed in a preheated oil bath at 70 °C for 20h. The styrene bulk polymerization was stopped by cooling the reaction vessel in an ice bath. The styrene bulk polymerization was stopped by cooling the reaction vessel in an ice bath, then an aliquot was withdrawn from the solution to determine the monomer conversion by ^{1}H NMR. By comparing the integrated aliphatic proton signals due to the PS groups at 1.88 ppm to those due to the styrene monomer at 5.77–5.83 ppm, the conversion was found to be 39%. The resulting PS

macro-chain transfer agent (CTA) was precipitated three times in cold methanol and dried overnight in a vacuum oven at RT) to give a white-yellowish powder. The molecular weight of hPS was determined only by SEC since the CTA chain-end protons are not visible from the NMR spectrum.

3.2. Synthesis of PS-*b*-P2VP macro-CTA by RAFT

In this part, we will describe the synthesis procedure for the diblock copolymer **SV3** presented in **Table 1** in **Chapter 2**.

In 200 mL round flask, $hPS_{28.2k}$ (5 g, 0.17 mmol) was mixed with 2VP (28.82 g, 0.27 mol), AIBN (5.8 mg, 0.035 mmol) and 1,4-dioxane (54.9 ml). The solution was purged with nitrogen and then heated to 70°C by using a temperature controlled oil bath. Polymerization was allowed to proceed during 7h prior to stop the reaction by immersing the vessel into an ice bath. An aliquot was withdrawn from the solution, then the brown mixture was concentrated in heptane and dried overnight under vacuum at room temperature (RT) (5.45 g, yield = 16 %). The PS-*b*-P2VP macro-RAFT agent conversion was calculated by ^{1}H NMR to be 10.2 %, by comparing the integrated aromatic proton signals of the P2VP ring at 8.25 ppm to those of the 2VP monomer at 8.53 ppm. ^{1}H NMR (400MHz, CD_2Cl_2): δ = 8.25 (1H,m Ph), 6.61-7.06 (8H,m,Ph) and 1.27-2.30 (6H,m,CH-CH2). The PS-*b*-P2VP molecular weight and its PS volume fraction were determined by ^{1}H NMR to be 34.6 kg/mol and 0.83, respectively. SEC in THF using PS standard: M_n= 41.8 kg/mol, Đ = 1.14.

3.3. Synthesis of PS-*b*-P2VP-*b*-PNIPAM macro-CTA by RAFT

The synthesis procedure described in this part corresponds to the terpolymer **SVN7** in **Table 1** in **Chapter 2**.

The PS-*b*-$P2VP_{34.6k}$ macro-RAFT agent (4.5 g, 0.13 mmol), NIPAM (4.42 g, 0.03 mol) and AIBN (2.13 mg, 0.013 mmol) were dissolved in 23.4 ml of 1,4-dioxane. The solution was purged with nitrogen and then placed in preheated oil bath at 70°C for 5h. The polymerization was stopped by placing the reaction vessel into ice bath and an aliquot was afterwards

withdrawn. 1,4-dioxane was removed with a rotary evaporator after which the PS-*b*-P2VP-*b*-PNIPAM chains were dissolved in a small amount of THF. The ABC triblock terpolymer was precipitated once from cold diethyl ether, in order to eliminate the unreacted NIPAM monomer, and heptane. To properly eliminate the undesired PNIPAM dead chains, a Soxhlet extraction was carried out with ethanol at 95°C for 96h. The PS-*b*-P2VP-*b*-PNIPAM terpolymer was then concentrated, precipitated in heptane and dried in vaccum oven at RT. The conversion was calculated by ^{1}H NMR to be 56%, by comparing the integrated proton signals of the PNIPAM groups at 3.99 ppm to those of the NIPAM monomer at 4,01-4,13 ppm. ^{1}H NMR (400MHz, CD_2Cl_2): δ = 3,99 (1H, s, CH), 1.13 (6H,m,CH_3-). ^{1}H NMR spectrum revealed that PS-*b*-P2VP-*b*-PNIPAM chains consisted of PS (28.2 kg/mol, ϕ_{PS} = 0.68), P2VP (5.8 kg/mol, ϕ_{P2VP} = 0.13) and PNIPAM (8.5 kg/mol, ϕ_{PNIPAM} = 0.19). SEC in THF using PS standard: M_n= 26.4 kg/mol, Đ = 1.32.

3.4. Synthesis of PNIPAM macro-CTA by RAFT

A 100 mL round-bottomed flask was charged with 11 g of recrystallized NIPAM (0.09 mol), 0.35 g of DDMAT (0.97 mmol), 15.9 mg of AIBN (0.09 mmol) and 25.3 g of DMF. The sealed reaction vessel was purged with nitrogen and immersed in a preheated oil bath at 70 °C for 2h30. The NIPAM polymerization was stopped by cooling the reaction vessel in an ice bath, then an aliquot was withdrawn from the solution to determine the monomer conversion by 70%%. The resulting PNIPAM macro-chain transfer agent (CTA) was precipitated three times in cold diethyl ether dried overnight in a vacuum oven at RT to give a white-yellowish powder. The molecular weight of hPNIPAM was determined by NMR by comparing the integral peak of the amide group at 3.98 ppm to the one of the methyl group of end chain of DDMAT at 0.88pp. It was found to ~7 kg.mol^{-1} while the one established by SEC, $M_{n,SEC}$, in THF using PS standard was of ~4.9 kg.mol^{-1}, Đ = 1.02.

3.5. Synthesis of PNIPAM-*b*-P2VP macro-CTA by RAFT

A 50 mL round flask was charged with 2.66 g of the previously synthesized PNIPAM macro-CTA (0.38 mmol), 7.59g of 2VP (72.2 mmol) and 62.4 mg of AIBN (0.38mmol). The reaction

was performed in mass for 5h at 70°C prior to precipitate the PNIPAM-*b*-P2VP chains twice in hexane, followed by rinsing with cold water to eliminate the unattached PNIPAM chains and then lyophilization to eliminate all the water traces. The conversion was determined by ^{1}H NMR to be 36% by comparing the integrated aromatic proton signals of the P2VP ring at 8.25 ppm to those of the 2VP monomer at 8.53 ppm. ^{1}H NMR (400MHz, CD_2Cl_2): δ = 8.25 (1H,m Ph), 6.61-7.06 (8H,m,Ph) and 1.27-2.30 (6H,m,CH-CH2). The PS-*b*-P2VP molecular weight was determined by ^{1}H NMR to be 20.5 kg/mol. SEC in THF using PS standard: M_n= 19.8 kg/mol, Đ = 1.30

3.6. Synthesis of PNIPAM-*b*-P2VP-*b*-PNIPAM macro-CTA by RAFT

Here, 2.10 g of PNIPAM-*b*-P2VP macro-CTA (0.06 mmol) was mixed with 6 g of styrene (0.05 mol), 2.18 mg of AIBN (0.01 mmol) and 11.4 g of 1,4-dioxane. After degassing the reaction was plunged in preheated oil bath at 70°C for 48h, with addition of same initial amount of AIBN each 24h to reinitiate the reaction. the final terpolymer was precipitated twice in diethyl ether and then once in heptane. SEC trace was bimodal presenting high dispersity Đ = 2.10

3.7. Synthesis of PNIPAM-*b*-P2VP-*b*-PNIPAM by surfactant-free emulsion RAFT polymerization

In typical experiment, a 50 Ml round flask was charged with 1.57 g of PNIPAM-*b*-P2VP macro-CTA (0.07mmol), and 60 g of water. 4.8 g of styrene (46 mmol) and 0.6 mg of AIBN (0.03 mmol) were dissolved in DMF and added to the aqueous solution. After purging the solution mixture with nitrogen, the reaction was allowed to proceed overnight under stirring at 800 rpm. After removing the DMF/H_2O mixture, the resulting PISA-latex was dissolved in THF and subsequently precipitated twice in diethyl ether prior to be washed in heptane.

^{1}H NMR (400MHz, CD_2Cl_2): δ = 3,99 (1H, s, CH), 1.13 (6H,m,CH_3-). ^{1}H NMR spectrum revealed that PS-*b*-P2VP-*b*-PNIPAM chains consisted of PNIPAM (7.0 kg/mol, ϕ_{PNIPAM} = 0.13), P2VP (18.4 kg/mol, ϕ_{P2VP} = 0.35) and PS (26.7 kg/mol, ϕ_{PNIPAM} = 0.51). SEC in THF using PS standard: M_n= 115.1 kg/mol, Đ = 1.17.

4. Protocol: CHAPTER 3

4.1. Membrane preparation by Non-solvent induced phase separation (NIPS)

The terpolymer synthesized by RAFT polymerization (**SVN7** from **Chapter 2**) was dissolved in solvent mixture of DOX/THF (50/50 by weight). The polymer solution (18 wt.%) was casted onto (3x3 cm) silicon substrates by using a tape casting technique with 250 μm gap. DOX and THF were allowed to evaporate during 30 s at room temperature, forming a dense air surface layer with a kinetically trapped nanoporous structure. The polymer film was then immersed into a coagulation bath of water for 5 min to induce the polymer precipitation. In this step, the miscible solvent mixture and water exchange to give rise to an integral-asymmetric membrane. The solid film was then deposited on high permeable hydrophilic polyvinylidene fluoride (PVDF) for further use.

4.2. Membrane preparation by solvent vapor annealing (SVA)

In this study, the self-assembly of PS-*b*-P2VP-*b*-PNIPAM terpolymers was stimulated by exposing films for different times (ranging from 0h to 7h) to a continuous stream of chloroform ($CHCl_3$). The vapor was produced by bubbling nitrogen gas through the liquid solvent. The continuous flow system was used to control the $CHCl_3$ vapor pressure in the chamber by dilution with a separate stream so that a solvent vapor consisted of 32 sccm $CHCl_3$ vapor and 8 sccm N_2 (total 40 sccm). The morphology of the solvent-annealed PS-*b*-P2VP-*b*-PNIPAM thick film was frozen by fast removal of the chamber lid.

4.3. Water permeability measurements

The water permeability of the different PS-*b*-P2VP-*b*-PNIPAM thick films was studied using a dead-end filtration set-up by measuring the flux of Milli-Q pure water at different pressures (0–2 bar). The membrane was cut into a round shape with a diameter of 2.5 cm supported by a high permeable hydrophilic PVDF material. It was subsequently placed in an Amicon type filter cell (Amicon 8010 stirred cell) with a volume of 10 mL. The cell was connected to a pressure vessel filled with Milli-Q pure water, where pressure was applied using compressed air line. The cell

and the vessel were heated to specific temperatures ranging from 23 °C to °C by placing them inside a stainless steel electronic bath filled with water. To ensure a stable temperature, the cell was stored at a specific temperature for half an hour before the measurement.

5. Protocol: CHAPTER 4

5.1. Synthesis of PS-*b*-PNIPAM by RAFT

In 50 mL round flask, hPS_{22k} (2.7 g, 0.12 mmol) was mixed with NIPAM (4 g, 0.03 mol), AIBN (4.05 mg, 0.02 mmol) and 1,4-dioxane (10 g). The solution was purged with nitrogen and then heated to 70°C by using a temperature controlled oil bath. Polymerization was allowed to proceed during 1h prior to stop the reaction by immersing the vessel into an ice bath. An aliquot was withdrawn from the solution. The white-yellowish product was concentrated and precipitated twice in cold diethyl ether, then rinsed with hot water and filtrated

^{1}H NMR (400MHz, CD_2Cl_2): δ = 8.25 (1H,m Ph), 6.61-7.06 (8H,m,Ph) and 1.27-2.30 (6H,m,CH-CH2). The PS-*b*-PNIPAM molecular weight and its PS volume fraction were determined by ^{1}H NMR to be 22 kg/mol and 0.81, respectively. SEC in THF using PS standard: M_n= 21.1 kg/mol, Đ = 1.10.

General conclusion

The aim of this PhD thesis was to develop original smart nanostructures formed by linear ABC triblock terpolymer membranes having stimuli-responsive pores to facilitate the removal of fouling, which is considered as one of the biggest challenges in membrane technology. To this end, the strategy proposed in this work was based on the synthesis and self-assembly of double stimuli-responsive linear ABC terpolymers in membrane configuration.

The first part of this work was devoted to the synthesis of pH and thermo-responsive linear ABC triblock terpolymers. Reversible addition−fragmentation chain-transfer (RAFT) polymerization was used to prepare, for the first time, a series of well-defined polystyrene-*block*-poly(2-vinylpyridine)-*block*-poly(*N*-isopropylacrylamide) (PS-*b*-P2VP-*b*-PNIPAM) terpolymers able to self-assemble into smart nanostructures comprising a mechanically robust PS matrix and dual responsive P2VP/PNIPAM pores. This kind of materials are highly desirable for the manufacture of fouling resistant membranes since the formation of nanopores showing both pH- and thermo-sensitive behavior is an optimum strategy to effectively prevent the common problem of fouling.

The second section of this work was focused on the study of the self-assembly of the PS-*b*-P2VP-*b*-PNIPAM chains into asymmetric smart membranes. For that purpose, a non-solvent induced phase separation (NIPS) technique was first used to produce an asymmetric PS-*b*-P2VP-*b*-PNIPAM thick film composed of a dense top layer having a poorly defined phase and a macroporous substructure. The thick film was then exposed to chloroform vapors *via* the use of a solvent vapor annealing (SVA) treatment that allows for the membrane surface reconstruction from a NIPS made poorly defined phase into a well-ordered perforated lamellar structure. The thermo/pH dual responsive behavior of the prepared films was therefore evaluated by water permeability measurements.

In the last part of this work, to improve the membrane hydrophilicity, blended double stimuli-responsive terpolymer thick films with amphiphilic copolymers were also manufactured. Here we selected two poly(ethylene oxide) (PEO)-based linear ABC terpolymers and a PNIPAM-based diblock copolymer to study the effect of polymer type, molecular weight as well as blend percentage on the membrane water permeability performances. We observed that the load of PS-*b*-P2VP-*b*-PEO chains with a specific amount within the PS-*b*-P2VP-*b*-PNIPAM membrane

can lead to a full reconstruction of the material top surface into a highly ordered lamellar phase, accompanied with an increase of both the hydrophilicity and thermo-responsiveness of the blended membrane. An important increase of the membrane water permeability (~80 $L.h^{-1}.m^{-2}.bar^{-1}$ at 46°C) was also demonstrated by using blends of PS-*b*-P2VP-*b*-PNIPAM and PS-*b*-PNIPAM chains. Finally, the full compatibility between the PNIPAM blocks makes that an important increase of the thermo-responsive character of the PS-*b*-P2VP-*b*-PNIPAM/PS-*b*-PNIPAM thick films is observed, which is one of the desired properties in the manufacture of fouling-resistant membranes.

Outlook

Since the aim of this work was to manufacture fouling-resistant membranes, logically, the next step would be to evaluate this property. To this end, the self-cleaning efficiency can be evaluated by filtering suspensions of dextran or bovine serum albumin (BSA) for example. The rejection of the feed solution of this kind of particle suspensions as a response to the change of the pH and temperature can be measured. If the water permeability values of the smart membrane are restored after filtration of the particles, that would confirm the self-cleaning and fouling-resistance of the membrane.

The same type of experiments can also be performed on blended membranes, more precisely on the PS-*b*-P2VP-*b*-PNIPAM/PS-*b*-PNIPAM thick films. As demonstrated in **Chapter 4**, the wettability of this blended membrane was higher than that of its unblended homolog. In addition, the thermo-responsive character was also increased, so that an improvement of self-cleaning properties would be expected.

To push the system one-step further, the PS-*b*-P2VP-*b*-PNIPAM membrane surface can be post-functionalized with grafted hydrophilic PEO homopolymers to decrease the hydrophobic-hydrophobic interactions between foulants and the membrane surface. This grafting approach can be based on the exploitation of the different affinities of metallic precursors. To this end, metallic salts such as gold salt (Au^{3+}) can be added to interact with the mid-block P2VP prior to be reduced to Au^0 by ultra-violet (UV) irradiations or by a reactive ion etch (RIE) plasma treatment. Thiol-terminated hydrophilic homopolymers such as PEO can be attached on the metallic nanorings surrounding the membrane pores to protect them against foulants by forming a hydrophilic barrier. The membrane post-functionalization methodology would be as follow: the double stimuli-responsive thick film will be immersed into an aqueous $HAuCl_4$ solution then subsequently treated by an oxygen RIE plasma to complete the Au^{3+} to Au^0 reduction. The gold nanorings will ultimately be functionalized with thiol-terminated fouling-resistant homopolymers, such as commercially available poly(ethylene oxide) (PEO) by deep-coating procedure that consists on immersing the membrane inside a PEO-SH solution and subsequent rinsing in water. The thiol-gold chemistry is an effective methodology to achieve a high-grafting density in different media.

In order to improve the double stimuli-responsiveness of the prepared membrane, another strategy based on the change of the terpolymer architecture can be envisaged. The synthesis of

well-defined linear PNIPAM-*b*-PS-*b*-P2VP terpolymers having the thermo-sensitive block and pH-sensitive one at the ends of the terpolymer will generate decoupling of pH and temperature effects and increase in membrane wettability in response to both stimuli.

The change of terpolymer architecture as well as its composition is a promising strategy to reach other morphologies such as cylindrical or gyroid that are highly desirable in membrane technology to increase permeability and selectivity by reducing the pore dimensionality.

Scientific contributions

➢ Publications

1. Karim Aissou, Muhammad Mumtaz, **Hana Bouzit**, Gilles Pécastaings, Giuseppe Portale, Guillaume Fleury and Georges Hsziioannou. Bicontinuous Network Nanostructure with Tunable Thickness Formed on Asymmetric Triblock Terpolymer Thick Films. Macromolecules 52, 4413–4420 (2019).

2. Karim Aissou, **Hana Bouzit**, Felix Krusch, Jean Pierre Méricq, Didier Cot, Nathalie Masquelez, Stéphanie Roualdes and Damien Quémener. Asymmetric Solvent-Annealed Triblock Terpolymer Thick Films Topped by a Hexagonal Perforated Lamellar Nanostructure. *Macromol.Rapid Commun*. 2100585 (2021).

3. **Hana Bouzit**, Felix Krusch, Daniel Hermida-Merino, Didier Cot, Jean Pierre Méricq, Stéphanie Roualdes, Mona Semsarilar, Damien Quémener and Karim Aissou. Double Stimuli-Responsive Perforated Lamellar Structure Formed by Linear ABC Triblock Terpolymer Monoliths. *J.Polym.Sci.2022,1.*

➢ Oral communications

1. Hana Bouzit, Mona Semsarilar, Damen Quémener and Karim Aissou. Synthesis and Self-assembly of Double Stimuli-Responsive Polystyrene-block-poly(2-vinylpyridine)-*block*-poly(*N*-isopropylacrylamide) Triblock Terpolymers. Balard Chemistry Conférences. 15-18th June 2021. Montpellier, France

2. Hana Bouzit, Mona Semsarilar, Damen Quémener and Karim Aissou. Synthesis and Self-assembly of Amphiphilic Double Stimuli-Responsive Polystyrene-block-poly(2-vinylpyridine)-*block*- poly(*N*-isopropylacrylamide) Triblock Terpolymers. CopamphiChemistry Conférences. 16-18th June 2021.Nancy, France